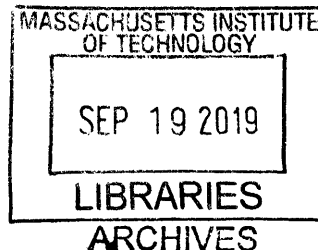# Ion-exchanged Metal–Organic Frameworks for Industrially Relevant Catalysis Applications

by

Hoyoung Daniel Park

M.S. in Chemical Engineering Practice,
Massachusetts Institute of Technology (2015)

B.S. in Chemical and Biological Engineering,
Seoul National University (2013)

Submitted to the Department of Chemical Engineering
in Partial Fulfillment of the Requirements for the Degree of

Doctor of Philosophy

at the

MASSACHUSETTS INSTITUTE OF TECHNOLOGY

September 2019

Signature redacted

Signature of Author: ....
Department of Chemical Engineering

Signature redacted July 19, 2019

Certified by: ....
Yuriy Román-Leshkov
Thesis Supervisor, Associate Professor of Chemical Engineering

Signature redacted.

Certified by: ....
Mircea Dincă
Thesis Supervisor, Associate Professor of Chemistry

Signature redacted

Accepted by: ....
Patrick S. Doyle
Robert T. Haslam (1911) Professor of Chemical Engineering
Chairman, Committee for Graduate Students

1

MITLibraries

DISCLAIMER NOTICE

Due to the condition of the original material, there are unavoidable flaws in this reproduction. We have made every effort possible to provide you with the best copy available.

Thank you.

The images contained in this document are of the best quality available.

Ion-exchanged Metal–Organic Frameworks for Industrially Relevant Catalysis Applications

by

Hoyoung Daniel Park

Abstract

The inorganic clusters of metal–organic frameworks (MOFs) offer a unique combination of synthetic tunability, structural uniformity, and site accessibility uncommon in conventional heterogeneous catalysts. As such, the inorganic nodes of MOFs provide a promising platform that can be engineered to promote challenging chemical transformations for which no adequate solid catalysts exist. This thesis focuses on the postsynthetic ion exchange behavior of the inorganic nodes in MOFs and its use in the preparation of ion-exchanged MOF catalysts for industrially relevant chemical transformations. Chapter 1 introduces the characteristics of MOFs relevant to heterogeneous catalysis and highlights their structural tunability with an emphasis on their node ion exchange behavior. Chapter 2 details the application of the postsynthetic ion exchange strategy in the preparation of $Co(CO)_4^-$-incorporated Cr-MIL-101 ($Co(CO)_4 \subset$ Cr-MIL-101, Cr-MIL-101 = $Cr_3O(BDC)_3F$, H_2BDC = 1,4-benzenedicarboxylic acid), the first heterogeneous catalyst for epoxide carbonylation. Chapters 3 and 4 outline the use of $Co(CO)_4 \subset$ Cr-MIL-101 in a fixed-bed reactor process for the continuous-flow carbonylative production of β-lactone and succinic anhydride, respectively. Chapter 5 describes the use of Cr^{3+}-exchanged MFU-4l (Cr-MFU-4l, MFU-4l = $Zn_5Cl_4(BTDD)_3$, H_2BTDD = bis(1H-1,2,3,-triazolo[4,5-b],[4',5'-i])dibenzo[1,4]dioxin)) as an exemplary system to demonstrate pre-reaction treatment with alkylaluminum species as a simple method to isolate a MOF catalyst for gas phase ethylene polymerization. The favorable performance of these MOF catalysts underscores the intrinsic advantages of their inorganic nodes, which support precise coordination geometries as isolated single sites within a porous scaffold for novel catalytic applications. Combined with the high structural tunability of the node metal sites, the inorganic clusters of MOFs hold tremendous potential for rational catalyst design.

This thesis is dedicated to Mr. John Price,

who sparked my interest in chemistry and chemical engineering

when our paths crossed in Ukarumpa, Papua New Guinea.

Table of Contents

Chapter 1

Inorganic Nodes of Metal–Organic Frameworks: Opportunities for Heterogeneous Catalysis

Metal–organic frameworks (MOFs) are coordination networks composed of inorganic clusters tethered together by organic ligands in a distinct periodic fashion (Figure 1.1). The metal nodes and the coordinating linkers often arrange themselves into a three-dimensional lattice structure, giving rise to the high porosity characteristic of numerous MOFs. This permanent porosity closely resembles that of zeolites, hence drawing natural comparisons of MOFs to zeolites in terms of their potential as heterogeneous catalysts. A distinguishing feature of MOFs that sets them apart from zeolites is the presence of organic

Metal Cluster
Trimeric Cr(III) Octahedral Cluster

Crystalline Framework

Organic Linker
Terephthalic Acid

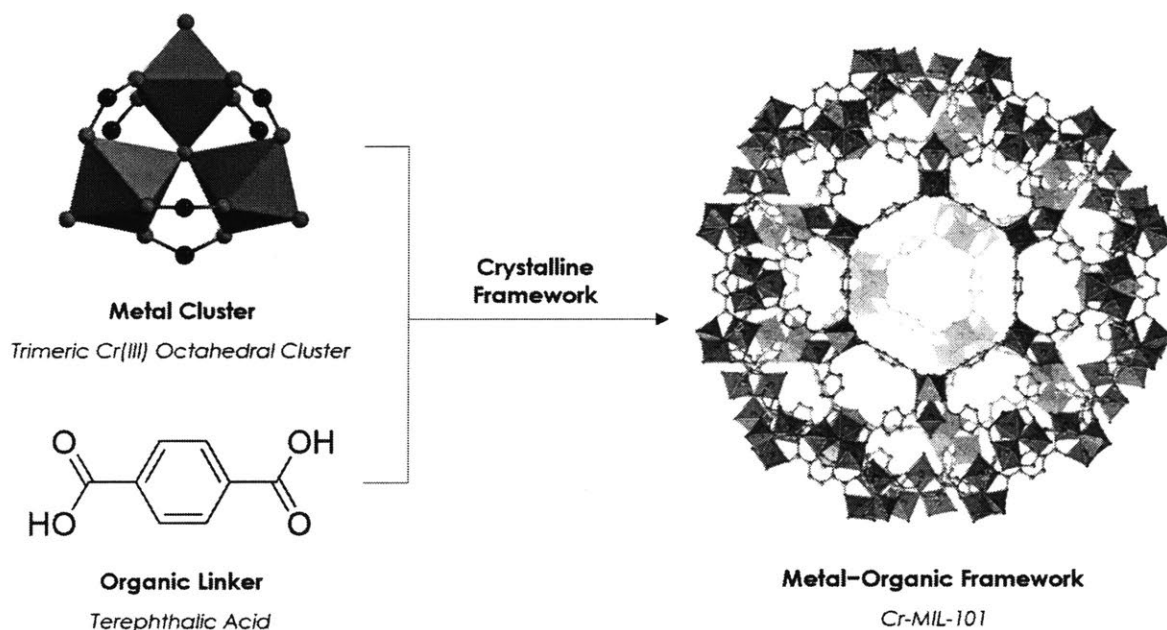**Metal–Organic Framework**
Cr-MIL-101

Figure 1.1: Illustrative structure of a metal–organic framework (Cr-MIL-101) with its constituent metal clusters (μ_3-O-bridged trimeric Cr(III) octahedral clusters) and organic linkers (terephthalic acid).

linkers as integral constituents of the framework structure. This can impose a limitation on the stability of MOFs, as the organic ligands and their coordinative bonds to the metal nodes are more prone to chemical or thermal degradation than the purely inorganic Si–O or Al–O bonds of a zeolite framework.[1] However, provided the MOF is maintained under conditions that do not irreversibly disrupt its framework structure, the presence of organic ligands enables a wide variety of functionalities to be imparted to MOFs through rational design. One way this is achieved is through direct inclusion of the functional organic linkers to MOFs, either by using the pre-functionalized linkers in MOF synthesis or by functionalizing the linkers subsequent to MOF synthesis.[2] Alternatively, the organic ligands can be used to tune the reactivity of the metal centers in the inorganic nodes, as the organic linkers directly ligate to the metal nodes and determine their coordination geometry.[3] In this way, a judicious choice of the linkers allows direct tuning of the electronic environment of the node metal centers that can then be utilized to promote certain metal-substrate interactions for catalysis.[4] This is, in effect, directly analogous to the strategies employed by inorganic chemists in the development of molecular metal complex catalysts. In this regard, the inorganic clusters of MOFs represent a unique platform where the centuries-old knowledge of molecular inorganic chemistry can be utilized directly for applications in heterogeneous catalysis.

Just as the organic ligands can be varied to impart catalytic activity to the inorganic clusters of MOFs, the metal ions themselves can be substituted for the same effect. This can be accomplished by using the desired metal precursors directly in MOF synthesis or by incorporating the metal ions into a pre-synthesized MOF. Of these, the postsynthetic metal

ion exchange route can be particularly attractive, as certain inorganic cluster structures in MOFs cannot be accessed through direct synthesis.[4] This can arise, for instance, when the desired metal ions induce excessive lattice strain for inclusion into the targeted node geometry or when the desired metal precursor decomposes under MOF synthesis conditions. In these cases, postsynthetic ion exchange strategies can reduce the lattice strain by partially substituting the metal ions into the framework, or maintain the integrity of the metal precursors by employing ion exchange conditions milder than those used in MOF synthesis.[5] In addition, the postsynthetic ion exchange route has an added advantage that it allows utilization of the favorable structural characteristics of a known MOF without necessitating the synthesis of the target MOF structure using a new set of metal precursors.[6] This can be particularly useful considering the complex nature of MOF crystallization, where a simple change in the identity of a metal precursor may entail laborious optimization of synthesis conditions.

Postsynthetic metal ion exchange has been widely used in the literature as a means to impart rationally-designed catalytic activity to the inorganic clusters of MOFs. This is commonly accomplished by soaking the MOF in a metal precursor solution over a period of time for the desired ion exchange to occur between the MOF nodes and the solution. Of those, the most common examples include cation exchange into the metal nodes of MOFs. This framework cation exchange is made possible by the dynamic nature of linker ligation to the metal nodes and solvent coordination to the metal cations that allow various metals to be incorporated into a wide range of node geometries (Figure 1.2).[7] It opens up exciting opportunities for catalysis, especially as the inorganic nodes of MOFs often exhibit unique
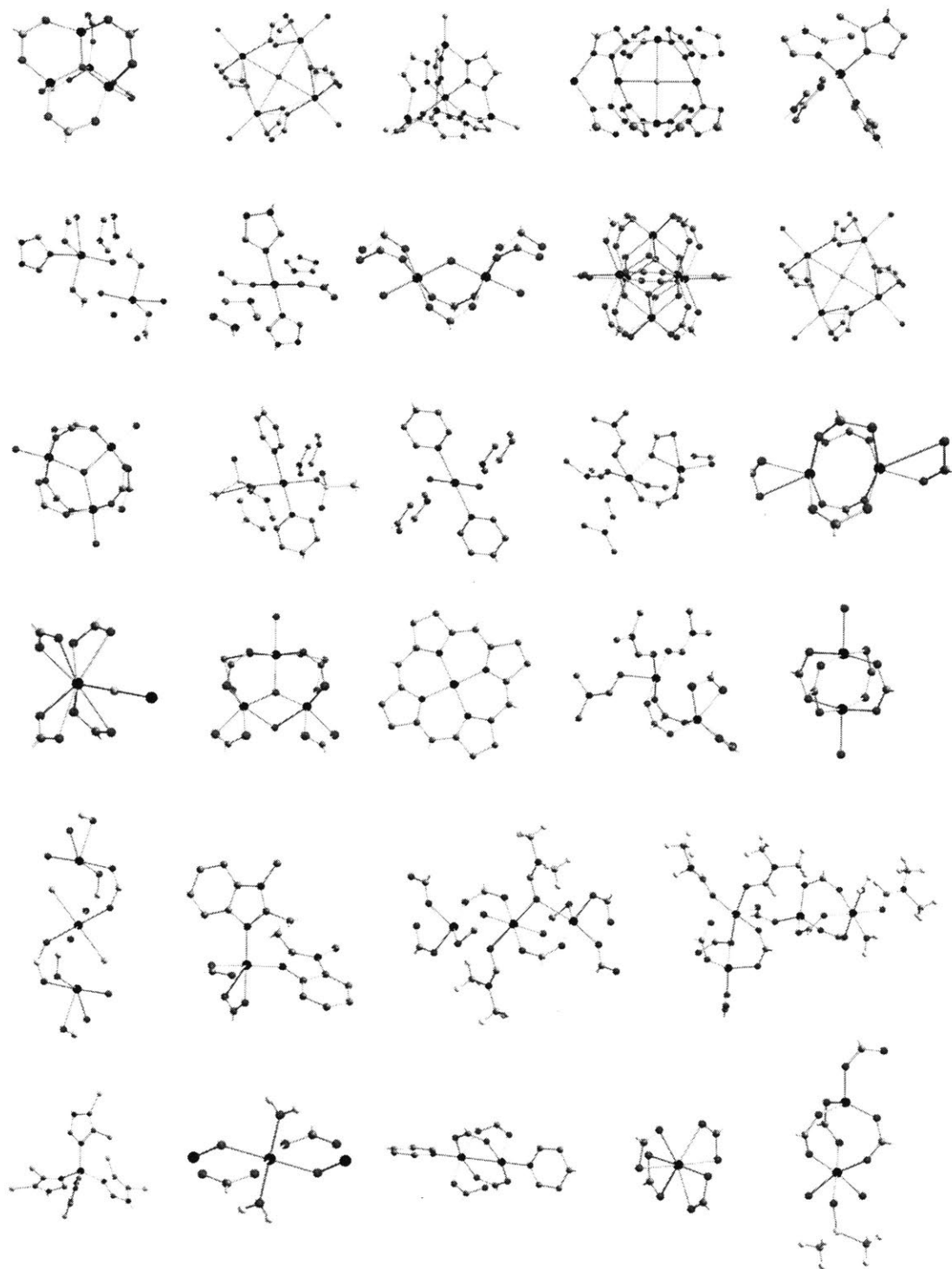
Figure 1.2: Examples of inorganic clusters in MOFs known to undergo node cation exchange. Black, green, red, blue, and gray spheres denote metal, chloride, oxygen, nitrogen, and carbon atoms, respectively.[4]

coordination geometries not found in molecular chemistry. Therefore, the pre-defined structure of the MOF nodes can be used to capture metal cations in an unusual ligand environment to promote unconventional reactivity. For example, the tripodal coordination environment provided by the inorganic nodes of MOF-5 (MOF-5 = $Zn_4O(BDC)_3$, H_2BDC = 1,4-benzenedicarboxylic acid) supports NO disproportion or olefin epoxidation activity subsequent to the exchange of its Zn^{2+} ions by Mn^{2+} or Fe^{2+}, respectively.[8,9] Likewise, Ni-MOF-74 (Ni-MOF-74 = $Ni_2(DOBDC)$, H_2DOBDC = 2,5-dioxido-1,4-benzenedicarboxylic acid) undergoes ion exchange with Co^{2+}, which then shows activity for aerobic oxidation of cyclohexene.[10] MFU-4*l* (MFU-4*l* = $Zn_5Cl_4(BTDD)_3$, H_2BTDD =bis(1*H*-1,2,3,-triazolo[4,5-*b*],[4',5'-*i*])dibenzo[1,4]dioxin)) is another example where the peripheral tetrahedral Zn^{2+} ions in the nodes can be replaced by Cu^{2+} ions for ethylbenzene oxidation activity;[11] by Co^{2+} ions for CO oxidation or stereoselective diene polymerization activity (Figure 1.3);[12,13] by Ni^{2+} ions for ethylene dimerization activity;[14] and by Cr^{3+}, Ti^{3+}, or V^{4+} ions for olefin polymerization activity.[15,16]

Postsynthetically exchanging the counter ions that balance the charge on the nodes is another strategy through which the catalytically active ions can be incorporated to the inorganic clusters of MOFs. Metal ions introduced in this way are then electrostatically bound to the charged inorganic nodes of the MOF and are able to participate in catalysis as heterogenized species. For a successful implementation of this strategy, the target MOF needs to maintain a permanent charge on its inorganic clusters for Coulombic interactions with the exchanged ions, and it also needs to have sufficiently large pores for inclusion of the guest ions. $(Et_4N)_3In_3(BTC)_4$ (H_3BTC = benzene-1,3,5-tricarboxylic acid) is a MOF that
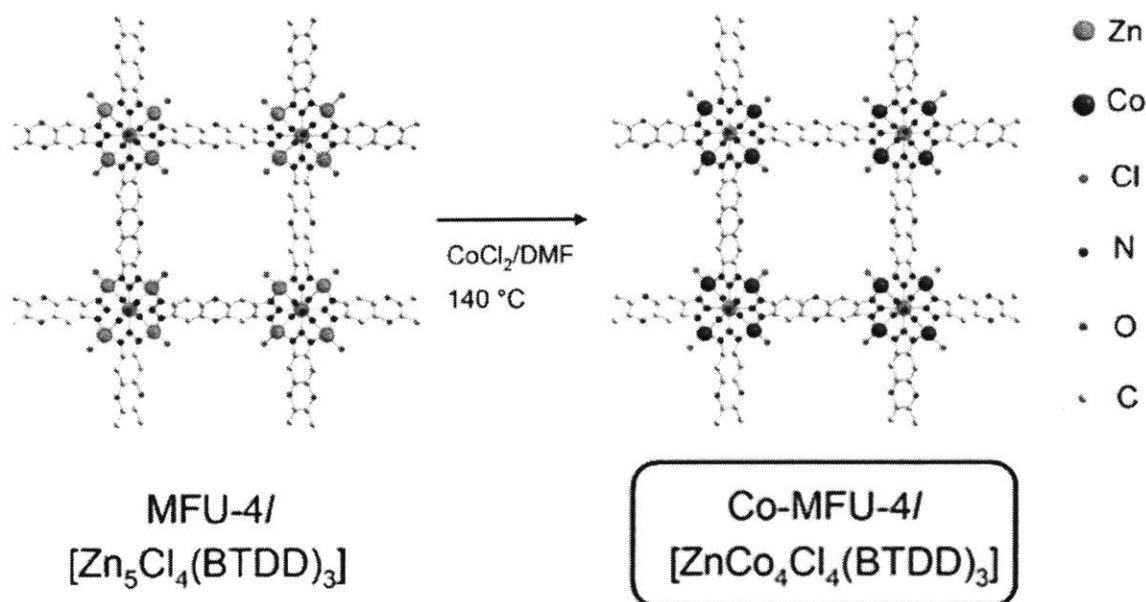
Figure 1.3: Inorganic node ion exchange of Co^{2+} into MFU-4*l*.[12]

meets these criteria, with anionic $[In_3(BTC)_4]^{3-}$ clusters charged-balanced by $(Et_4N)^+$ ions

in its pores with 7.0 Å by 7.6 Å windows.[17] Postsynthetic cation exchange with $[CpFe(CO)_2]^+$

ions led to their replacement of the $(Et_4N)^+$ ions in the framework and resulted in

heterogeneous Diels-Alder reactivity comparable to that of $[CpFe(CO)_2][BF_4]$ in solution.

Likewise, AMOF-1 (AMOF-1 = $(Me_2NH_2)_2Zn_3(L)_2$, HL = 5,5'-(1,4-phenylenebis(methylene))

bis(oxy)diisophthalic acid)) with its mobile $(Me_2NH_2)^+$ ions was reported to undergo ion

exchange with solvated Cu^{2+} ions to show heterogeneous catalytic activity for the coupling

of o-phenylenediamine and benzaldehydes to benzimidazoles.[18] In another example, a

much larger $[Rh(dppe)(COD)]^+$ (dppe = 1,2-bis(diphenylphosphino)ethane and COD = 1,5-

cyclooctadiene) complex was shown to replace $(Me_2NH_2)^+$ ions in ZJU-28 (ZJU-28 =

$(Me_2NH_2)_3[In_3(BTB)_4]$, H_3BTB = 4,4',4''-benzene-1,3,5-triyl-tribenzoic acid) owing to the

large 9 Å by 9 Å pore windows of ZJU-28 (Figure 1.4). The ion-exchanged ZJU-28 was able to perform heterogeneous hydrogenation of 1-octene to *n*-octane.[19,20]

While examples such as these showcase the potential of postsynthetic ion exchange schemes in the rational design of MOF catalysts, more work remains to be done to firmly establish their practical utility. To this end, it would be particularly valuable to have more examples of ion-exchanged MOFs that display catalytic performance unmatched by existing catalysts. This could be achieved by targeting more challenging reactions rather than resorting to "proof-of-concept" reactions that merely serve the purpose of verifying successful ion exchange in a MOF. In particular, the catalytic performance of ion-exchanged MOFs could be better distinguished from those of existing homogeneous catalysts by refraining from the overwhelmingly-popular liquid-phase batch reaction studies and targeting gas phase or continuous-flow reactions, for which heterogeneous catalysts, such as MOFs, hold unparalleled advantages. In addition, it would be helpful to have more reports of ion exchange schemes that take full advantage of the structural
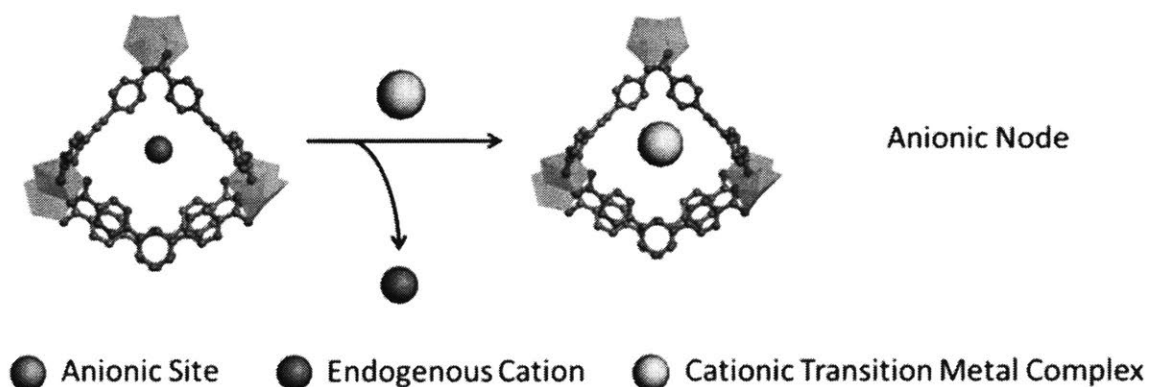

Figure 1.4: Charge-balancing ion exchange of [Rh(dppe)(COD)]⁺ (dppe = 1,2-bis(diphenylphosphino)ethane and COD = 1,5-cyclooctadiene) into ZJU-28.[20]

benefits of the MOF platform. For instance, the role of the MOF in the reported examples of charge-balancing ion exchanges is limited to providing a porous ion exchange matrix that can house catalytically active ions. The unique ability of the inorganic clusters of MOFs in promoting unconventional reactivity remains completely unexploited in these schemes.

This thesis aims to address these shortcomings and showcase the practical utility of the ion-exchanged MOFs in their applications to industrially-relevant chemical transformations. Chapter 2 details the design and synthesis of $Co(CO)_4^-$-incorporated Cr-MIL-101 ($Co(CO)_4 \subset$ Cr-MIL-101, Cr-MIL-101 = $Cr_3O(BDC)_3F$, H_2BDC = 1,4-benzenedicarboxylic acid) as the first heterogeneous catalyst for epoxide carbonylation, a reaction with high commercial value in the plastics and pharmaceuticals industries. The charge-balancing anion exchange employed for this catalyst is unique in that the postsynthetically introduced $Co(CO)_4^-$ ions participate in cooperative catalysis only in the presence of the coordinatively unsaturated Cr^{3+} sites provided by the MOF framework. Therefore, this scheme demonstrates a new charge-balancing ion exchange strategy that not only exploits the electrostatic attraction provided by the charged inorganic clusters, but also the unique coordination geometry of the node metal centers in catalyzing a challenging chemical transformation. Chapters 3 and 4 further explore the utility of $Co(CO)_4 \subset$ Cr-MIL-101 by demonstrating the first examples of the carbonylative production of β-lactone and succinic anhydride using a continuous-flow fixed-bed reactor. Chapter 5 describes the postsynthetic $AlMe_3$ treatment of Cr^{3+}-exchanged MFU-4l that enabled the first systematic investigation of gas phase ethylene polymerization by a MOF catalyst. The favorable performance of these ion-exchanged MOF catalysts in continuous-flow and gas

phase reactions highlights the practical advantages conferred by the heterogeneous MOF catalysts over existing homogeneous catalysts. It is hoped that the results provided herein will aid the future development of novel ion-exchanged MOF catalysts for applications in heterogeneous catalysis.

References

(1)   Yuan, S.; Feng, L.; Wang, K.; Pang, J.; Bosch, M.; Lollar, C.; Sun, Y.; Qin, J.; Yang, X.; Zhang, P.; Wang, Q.; Zou, L.; Zhang, Y.; Zhang, L.; Fang, Y.; Li, J.; Zhou, H. Stable Metal–Organic Frameworks: Design, Synthesis, and Applications. *Adv. Mater.* **2018**, *30*, 1704303.

(2)   Cohen, S. M. Postsynthetic Methods for the Functionalization of Metal–Organic Frameworks. *Chem. Rev.* **2012**, *112*, 970–1000.

(3)   Kalmutzki, M. J.; Hanikel, N.; Yaghi, O. M. Secondary Building Units as the Turning Point in the Development of the Reticular Chemistry of MOFs. *Sci. Adv.* **2018**, *4*, eaat9180.

(4)   Brozek, C. K.; Dincă, M. Cation Exchange at the Secondary Building Units of Metal–Organic Frameworks. *Chem. Soc. Rev.* **2014**, *43*, 5456–5467.

(5)   Wang, Z.; Cohen, S. M. Postsynthetic Modification of Metal–Organic Frameworks. *Chem. Soc. Rev.* **2009**, *38*, 1315–1319.

(6)   Lalonde, M.; Bury, W.; Karagiaridi, O.; Brown, Z; Hupp, J. T.; Farha, O. K. Transmetalation: Routes to Metal Exchange within Metal–Organic Frameworks. *J. Mater. Chem. A.* **2013**, *1*, 5453–5468.

(7)   Brozek, C. K.; Michaelis, V. K.; Ong, T; Bellarosa, L.; López, N.; Griffin, R. G.; Dincă, M. Dynamic DMF Binding in MOF-5 Enables the Formation of Metastable Cobalt-Substituted MOF-5 Analogues. *ACS Cent. Sci.* **2015**, *1*, 252–260.

(8)   Stubbs, A. W.; Braglia, L.; Borfecchia, E.; Meyer, R. J.; Román-Leshkov, Y; Dincă, M. Selective Catalytic Olefin Epoxidation with Mn^{II}-Exchanged MOF-5. *ACS Catal.* **2018**, *8*, 596–601.

(9)   Brozek, C. K.; Miller, J. T.; Stoian, S. A.; Dincă, M. NO Disproportionation at a Mononuclear Site-Isolated Fe^{2+} Center in Fe^{2+}-MOF-5. *J. Am. Chem. Soc.* **2015**, *137*, 7495–7501.

(10)   Sun, D.; Sun, F.; Deng, X.; Li, Z. Mixed-Metal Strategy on Metal–Organic Frameworks (MOFs) for Functionalities Expansion: Co Substitution Induces

Aerobic Oxidation of Cyclohexene over Inactive Ni-MOF-74. *Inorg. Chem.* **2015**, *54*, 8639–8643.

(11) Denysenko, D.; Jelic, J.; Reuter, K.; Volkmer, D. Postsynthetic Metal and Ligand Exchange in MFU-4*l*: A Screening Approach toward Functional Metal–Organic Frameworks Comprising Single-Site Active Centers. *Chem. Eur. J.* **2015**, *21*, 8188–8189.

(12) Denysenko, D.; Werner, T.; Grzywa, M.; Puls, A.; Hagen, V.; Eickerling, G; Jelic, J; Reuter, K.; Volkmer, D. Reversible Gas-phase Redox Processes Catalyzed by Co-exchanged MFU-4*l*(arge). *Chem. Commun.* **2012**, *48*, 1236–1238.

(13) Dubey, R. J. -C.; Comito, R. J.; Wu, Z; Zhang, G.; Rieth, A. J.; Hendon, C. H.; Miller, J. T.; Dincă, M. Highly Stereoselective Heterogeneous Diene Polymerization by Co-MFU-4*l*: A Single-Site Catalyst Prepared by Cation Exchange. *J. Am. Chem. Soc.* **2017**, *139*, 12664–12669.

(14) Metzger, E. D.; Brozek, C. K.; Comito, R. J.; Dincă, M. Selective Dimerization of Ethylene to 1-Butene with a Porous Catalyst. *ACS Cent. Sci.* **2016**, *2*, 148–153.

(15) Comito, R. J.; Fritzsching, K. J.; Sundell, B. J.; Schmidt-Rohr, K.; Dincă, M. Single-Site Heterogeneous Catalysts for Olefin Polymerization Enabled by Cation Exchange in a Metal–Organic Framework. *J. Am. Chem. Soc.* **2016**, *138*, 10232–10237.

(16) Comito, R. J.; Wu, Z.; Zhang, G.; Lawrence III, J. A.; Korzyński, M. D.; Kehl, J. A.; Miller, J. T.; Dincă, M. Stabilized Vanadium Catalyst for Olefin Polymerization by Site Isolation in a Metal–Organic Framework. *Angew. Chem. Int. Ed.* **2018**, *57*, 8135–8139.

(17) Grigoropoulos, A.; Whitehead, G. F. S.; Perret, N.; Katsoulidis, A. P.; Chadwick, F. M.; Davies, R. P.; Haynes, A.; Brammer, L.; Weller, A. S.; Xiao, J.; Rosseinsky, M. J. Encapsulation of an Organometallic Cationic Catalyst by Direct Exchange into an Anionic MOF. *Chem. Sci.* **2016**, *7*, 2037–2050.

(18) Chakraborty, A.; Bhattacharyya, S.; Hazra, A.; Ghosh, A. C.; Maji, T. K. Post-synthetic Metalation in an Anionic MOF for Efficient Catalytic Activity and Removal of Heavy Metal Ions from Aqueous Solution. *Chem. Commun.* **2016**, *52*, 2831–2834.

(19) Genna, D. T.; Wong-Foy, A. G.; Matzger, A. J.; Sanford, M. S. Heterogenization of Homogeneous Catalysts in Metal–Organic Frameworks via Cation Exchange. *J. Am. Chem. Soc.* **2013**, *135*, 10586–10589.

(20) Genna, D. T.; Pfund, L. Y.; Samblanet, D. C.; Wong-Foy, A. G.; Matzger, A. J.; Sanford, M. S. Rhodium Hydrogenation Catalysts Supported in Metal–Organic Frameworks: Influence of the Framework on Catalytic Activity and Selectivity. *ACS Catal.* **2016**, *6*, 3569–3574.

Chapter 2

Heterogeneous Epoxide Carbonylation by Cooperative Ion-Pair Catalysis in Co(CO)$_4^-$-Incorporated Cr-MIL-101

2.1. Abstract

Despite the commercial desirability of epoxide carbonylation to β-lactones, the reliance of this process on homogeneous catalysts makes its industrial application challenging. Here we report the preparation and use of a Co(CO)$_4^-$-incorporated Cr-MIL-101 (Co(CO)$_4$⊂Cr-MIL-101, Cr-MIL-101 = Cr$_3$O(BDC)$_3$F, H$_2$BDC = 1,4-benzenedicarboxylic acid) heterogeneous catalyst for the ring-expansion carbonylation of epoxides, whose activity, selectivity, and substrate scope are on par with those of the reported homogeneous catalysts. We ascribe the observed performance to the unique cooperativity between the post-synthetically introduced Co(CO)$_4^-$ and the site-isolated Lewis acidic Cr(III) centers of the metal–organic framework (MOF). The heterogeneous nature of Co(CO)$_4$⊂Cr-MIL-101 allows the first demonstration of gas-phase continuous-flow production of β-lactones from epoxides, attesting to the potential applicability of the heterogeneous epoxide carbonylation strategy.

2.2. Introduction

β-lactones have received considerable attention due to their prevalence as key intermediates in numerous synthetic pathways.[1,2] Their versatility stems from the inherent ring strain in the four-membered cycles, which renders β-lactones highly susceptible to a rich variety of ring-opening and ring-expanding transformations. The high commercial value of the resulting products, namely β-hydroxyacids,[3] biodegradable polyhydroxyalkanoates,[4] and succinic anhydrides,[5] further substantiates the industrial relevance of β-lactone chemistry. Despite their obvious utility, β-lactones have traditionally found comparatively little use industrially because their synthesis is challenging.[6] One particularly attractive solution to this challenge is the ring-expansion carbonylation of epoxides, which exploits the ready availability of epoxides and CO.[7–9] This route has become viable recently through the work of Alper et al. and Coates et al., who have demonstrated efficient carbonylation of epoxides by a series of homogeneous catalysts constituted of a Lewis acid and $Co(CO)_4^-$.[10–15] This discovery has prompted an ongoing effort in the private sector to commercialize an epoxide carbonylation process, despite the homogeneous nature of the catalyst.[16] At large scale, however, heterogeneous processes are clearly desirable, yet to date there are no competent heterogeneous catalysts for this process that can compete with the homogeneous systems. The development of an effective heterogeneous catalyst would undoubtedly aid the integration of the epoxide carbonylation process to industrial practice.

Herein, we report the synthesis and use of a $Co(CO)_4^-$-incorporated Cr-MIL-101 ($Co(CO)_4 \subset Cr$-MIL-101, Cr-MIL-101 = $Cr_3O(BDC)_3F$, H_2BDC = 1,4-benzenedicarboxylic acid) as the first heterogeneous catalyst for the carbonylation of epoxides to β-lactones that is competitive with the homogeneous process. The activity and selectivity profiles of $Co(CO)_4 \subset Cr$-MIL-101 compare favorably with those of the most-active homogeneous catalysts for the liquid-phase batch carbonylation of a range of epoxide substrates. Enabled by the heterogeneous nature of our catalyst, we also report the first proof-of-concept demonstration of gas-phase continuous-flow production of β-butyrolactone from propylene oxide and CO.

2.3. Results and Discussion

In designing a heterogeneous epoxide carbonylation catalyst, we focused our attention on the proposed catalytic cycle for the carbonylation of epoxides by [Lewis acid]$^+$[$Co(CO)_4$]$^-$: (1) epoxide activation by [Lewis acid]$^+$, (2) attack by $Co(CO)_4^-$, (3) migratory insertion and uptake of CO, and (4) ring closing and extrusion (Figure 2.1A).[17] In view of the irreplaceable role of $Co(CO)_4^-$ in the proposed CO insertion steps, we identified [Lewis acid]$^+$ as the modifiable component and investigated its structure in various [Lewis acid]$^+$[$Co(CO)_4$]$^-$ catalysts. One recurring motif found in the homogeneous catalysts was the pseudo-octahedral Cr(III) center, in which the metal ion is coordinated equatorially by the nitrogen or oxygen atoms of a tetradentate macrocyclic ligand and axially by the oxygen atoms of the solvent molecules (Figures 2.1B and 2.1C).[14,15] We reasoned that such coordination environment favors the activation of epoxides for carbonylation and searched for a
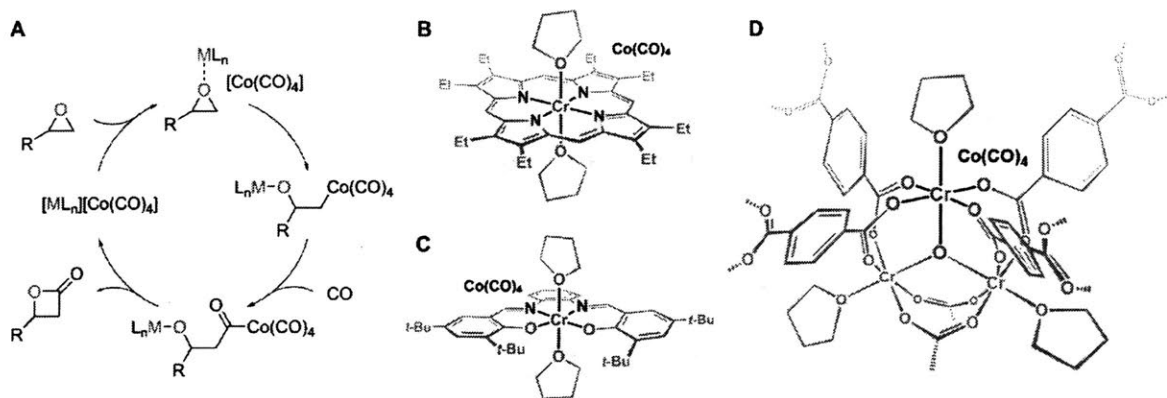
Figure 2.1: (A) Proposed catalytic cycle for the ring-expansion carbonylation of epoxides by [Lewis acid]$^+$[Co(CO)$_4$]$^-$.[17] (B) Illustration of the structure of [(OEP)Cr(THF)$_2$]$^+$ [Co(CO)$_4$]$^-$ (OEP = 2,3,7,8,12,13,17,18-octaethylporphyrinato, THF = tetrahydrofuran).[14] (C) Illustration of the structure of [(salph)Cr(THF)$_2$]$^+$[Co(CO)$_4$]$^-$ (salph = *N,N'*-o-phenylenebis(3,5-di-*tert*-butylsalicylideneimine)).[15] (D) Illustration of the metal cluster structure of Co(CO)$_4$⊂Cr-MIL-101 with coordinated THF molecules.

heterogeneous analogue. The MOF Cr-MIL-101 was a promising candidate as its metal clusters contain structurally similar octahedral Cr(III) ions that are coordinated equatorially by the oxygen atoms of the bridging terephthalate ligands and axially by a μ_3-oxygen atom and a solvent molecule (Figure 2.1D).[18] Crucially, Cr-MIL-101 has a cationic framework with ion-exchangeable F$^-$.[19,20] We surmised that exchanging F$^-$with Co(CO)$_4$$^-$ would lead to the isolation of a heterogeneous catalyst of the general formula [Lewis acid]$^+$[Co(CO)$_4$]$^-$, mimicking that of the homogeneous species. Other innate properties of Cr-MIL-101 that we deemed favorable for catalysis were its high hydrothermal and chemical stability, large surface area (4100 m^2/g as measured by N$_2$ adsorption), large windows (12 Å and 16 Å) and pores (29 Å and 34 Å) for ready diffusion of reaction species, site-isolation of the Lewis acidic Cr(III) centers for robust catalysis, and facile synthesis using inexpensive chromium and terephthalic acid precursors.[21] Similar strategies to leverage the intrinsic

stability,[22,23] porosity,[24,25] and site-isolation[26–28] of MOFs have proven to be effective in their applications to heterogeneous catalysis. Therefore, post-synthetic ion exchange of $Co(CO)_4^-$ into Cr-MIL-101 was sought for the formation of a heterogeneous [Lewis acid]$^+$[$Co(CO)_4$]$^-$ system.

The charge-balancing F$^-$ anions in the as-synthesized Cr-MIL-101 are directly coordinated to the Cr(III) sites of the framework.[8] To replace these framework-bound anions with uncoordinated $Co(CO)_4^-$, anion exchange was performed in two discrete steps: (1) exchange of the bound F$^-$ with mobile Cl$^-$ using $AlCl_3$ and (2) exchange of the mobile Cl$^-$ with $Co(CO)_4^-$ using $Na[Co(CO)_4]$. In the initial anion exchange, Al^{3+} shows greater affinity to F$^-$ than the framework Cr(III) sites, resulting in the abstraction of F$^-$ from the MOF.[19] The consequent charge imbalance is compensated by the inclusion of Cl$^-$ into the framework. This sequence of events was tracked by energy dispersive X-ray spectroscopy (EDX) analysis of the Cr-MIL-101 sample before (Cr-MIL-101-F) and after (Cr-MIL-101-Cl) soaking in a solution of $AlCl_3$ (Figure 2.2A). In the EDX spectra, the F Kα peak observed at 0.68 keV for Cr-MIL-101-F was replaced by the Cl Kα peak at 2.62 keV for Cr-MIL-101-Cl upon $AlCl_3$ treatment and extensive washing. The absence of the F Kα and Al Kα peaks in the spectrum of Cr-MIL-101-Cl implies complete exchange of F$^-$ by Cl$^-$ and negligible retention of [$AlCl_3F$]$^-$ or any potentially unreacted $AlCl_3$. The structure of the MOF remained intact after the ion exchange as evidenced by the retention of crystallinity in the powder X-ray diffraction (PXRD) analysis of Cr-MIL-101-Cl (Figure 2.S1).
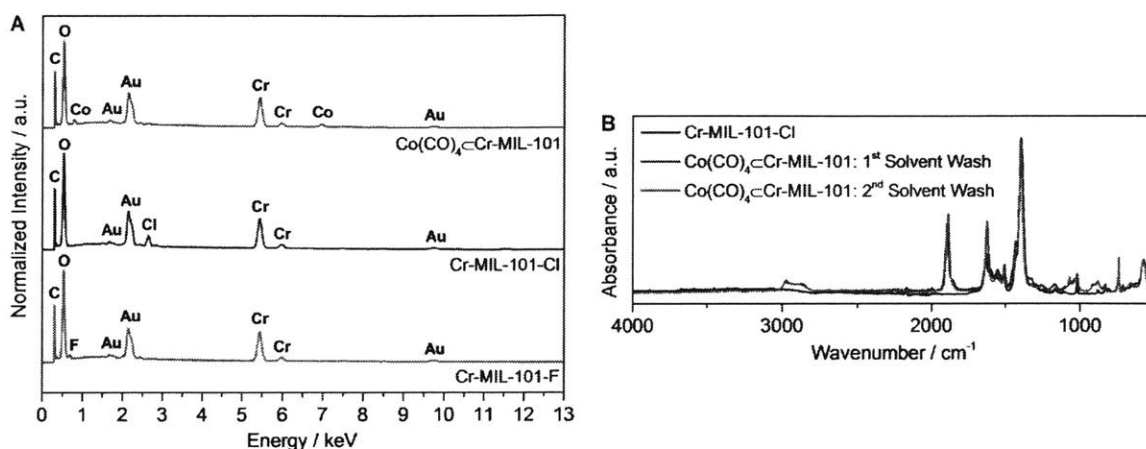
Figure 2.2. (A) EDX spectra of Cr-MIL-101-F, Cr-MIL-101-Cl, and Co(CO)$_4$⊂Cr-MIL-101. Au peaks from the pre-analysis Au coating of samples. (B) ATR-IR absorption spectra of Cr-MIL-101-Cl and Co(CO)$_4$⊂Cr-MIL-101.

Subsequent anion exchange between Cr-MIL-101-Cl and Na[Co(CO)$_4$] was analyzed by EDX and attenuated total reflectance infrared spectroscopy (ATR-IR), both of which confirmed the elimination of Cl$^-$ and inclusion of Co(CO)$_4^-$ into the framework. Upon soaking Cr-MIL-101-Cl in a Na[Co(CO)$_4$] solution, the Cl Kα peak in the EDX spectrum of the former was replaced by Co Kα and Lα peaks at 6.92 keV and 0.78 keV, respectively (Figure 2.2A). The Co peaks persisted even after repeatedly washing Co(CO)$_4$ ⊂ Cr-MIL-101 in tetrahydrofuran (THF), which readily solubilizes Na[Co(CO)$_4$], suggesting that Co(CO)$_4^-$ is immobilized electrostatically in the MOF through ion-pairing with the Cr(III) Lewis acid sites.[29] The EDX spectrum also evidences the near-absence of the Cl Kα peak at 2.62 keV and the Na Kα peak at 1.04 keV, which are prominent in the spectra of Cr-MIL-101-Cl and Na[Co(CO)$_4$], respectively (Figure 2.S2). These observations suggest that the observed Co signal for Co(CO)$_4$⊂Cr-MIL-101 does not stem from residual Na[Co(CO)$_4$] adsorbed on the surface of the MOF, but rather from substitution of Cl$^-$ by Co(CO)$_4^-$. The ion exchange and

inclusion of Co(CO)$_4$$^-$ in Cr-MIL-101 are further corroborated by the attenuated total reflectance infrared (ATR-IR) spectrum of Co(CO)$_4$⊂Cr-MIL-101, which clearly shows the emergence of a single peak at 1888 cm^{-1} after the exchange procedure (Figure 2.2B). This band is in line with the characteristic carbonyl stretching mode of the tetrahedral Co(CO)$_4$$^-$ ion in various metal complexes, including those reported for the homogeneous [Lewis acid]$^+$[Co(CO)$_4$]$^-$ epoxide carbonylation catalysts.[12–15,30,31] Finally, the structure and porosity of the MOF was retained after this final ion exchange step as evident in the unchanged PXRD pattern for Co(CO)$_4$⊂Cr-MIL-101 (Figure 2.S1).

The catalytic activity demonstrated by Co(CO)$_4$⊂Cr-MIL-101 for the ring-expanding carbonylation of epoxides is competitive with that of the homogeneous catalysts. When using neat 1,2-epoxyhexane as a substrate, Co(CO)$_4$⊂Cr-MIL-101 loaded with 0.5 mol % of cobalt produced the corresponding β-lactone in 86% yield after 5 h under 60 bar of CO at 60 °C (Table 2.1, entry 6). This corresponds to a calculated site time yield (STY) of 34 h^{-1}, which is comparable to the values reported for a series of homogeneous catalysts under similar reaction conditions (Table 2.1, entries 1–5).

The solvent dependence of the carbonylation activity in Co(CO)$_4$⊂Cr-MIL-101 also mimicked that of the reported homogeneous systems. When a range of solvents was screened for optimizing activity with Co(CO)$_4$⊂Cr-MIL-101, reactions in weakly coordinating ethers such as 1,2-dimethoxyethane (DME) showed the highest activity. In other solvents, especially the more strongly coordinating solvents such as THF, the reactions proceeded at a much slower rate. Identical solvent dependence has been reported

Table 2.1. Catalysts for the Ring-expansion Carbonylation of Epoxides

Entry	Catalyst	R	Solvent	P_{CO} (bar)	T (°C)	t (h)	[Epoxide]/[Co][a]	Yield (%)	STY (h^{-1})[b]	Ref.
1	$BF_3 \cdot Et_2O$ + $[PPN]^+[Co(CO)_4]^-$[c]	n-Bu	DME[h]	62	80	24	50	66	1.4	(10)
2	$[(Cp)_2Ti(THF)_2]^+[Co(CO)_4]^-$[d]	$(CH_2)_2HC=CH_2$	DME[h]	62	60	4	20	90	4.5	(11)
3	$[(salph)Al(THF)_2]^+[Co(CO)_4]^-$[e]	n-Bu	neat	62	60	6	350	40	23	(13)
4	$[(TPP)Cr(THF)_2]^+[Co(CO)_4]^-$[f]	n-Bu	neat	62	60	6	350	>99	58	(13)
5	$[(OEP)Cr(THF)_2]^+[Co(CO)_4]^-$[g]	n-Bu	neat	62	60	6	4500	>99	740	(14)
6	$Co(CO)_4 \subset Cr\text{-}MIL\text{-}101$	n-Bu	neat	60	60	5	200[i]	86[i]	34	this work
7	$Co(CO)_4 \subset Cr\text{-}MIL\text{-}101$	n-Bu	DME[h]	60	60	1	200[i]	88[j]	180	this work
8	$Co(CO)_4 \subset Cr\text{-}MIL\text{-}101$	$(CH_2)_2HC=CH_2$	DME[h]	60	60	1.5	200[i]	93[j]	120	this work
9	$Co(CO)_4 \subset Cr\text{-}MIL\text{-}101$	CH_2OEt	DME[h]	60	60	4	200[i]	92[j]	46	this work
10	$Co(CO)_4 \subset Cr\text{-}MIL\text{-}101$	CH_2Cl	DME[h]	60	60	4	200[i]	56[j, k]	28	this work

[a] [Epoxide]/[Co] = moles of epoxide per mole of cobalt in catalyst. [b] Site Time Yield = moles of β-lactone produced per mole of cobalt in catalyst per hour throughout overall reaction time t. [c] PPN = bis(triphenylphosphine)iminium. [d] Cp = Cyclopentadienyl. [e] salph = N,N'-o-phenylenebis(3,5-di-tert-butylsalicylideneimine). [f] TPP = 5,10,15,20-tetraphenylporphyrinato. [g] OEP = 2,3,7,8,12,13,17,18-octaethylporphyrinato. [h] DME = 1,2-dimethoxyethane. [i] As determined from an inductively coupled plasma mass spectrometry (ICP-MS) derived cobalt content of the catalyst. [j] As determined by ^{1}H-NMR analysis with mesitylene as an internal standard. [k] 32% of the substrate epoxide remained unreacted.

for the Cr(III)-based $[(salph)Cr(THF)_2]^+[Co(CO)_4]^-$ (salph = N,N'-o-phenylenebis-(3,5-di-tert-butylsalicylideneimine)), a homogeneous catalyst that most closely resembles $Co(CO)_4 \subset Cr\text{-}MIL\text{-}101$ structurally (Figure 2.1C).[15]

Importantly, $Co(CO)_4 \subset Cr\text{-}MIL\text{-}101$ displays the broad functional group tolerance of the homogeneous catalysts as evidenced by its activity toward an array of aliphatic epoxides as well as glycidyl ether and epichlorohydrin (Table 2.1, entries 7–10). It is also noteworthy that the observed catalytic activity of $Co(CO)_4 \subset Cr\text{-}MIL\text{-}101$ is orders of magnitude higher than that of an immobilized homogeneous catalyst under similar reaction conditions.[32]

To validate the heterogeneous nature of the observed catalytic activity, $Co(CO)_4 \subset Cr$-MIL-101 was isolated from a portion of the epoxide carbonylation reaction mixture by filtration at ~15% conversion (Figure 2.S3). When the acquired filtrate and the unfiltered mixture were both subjected to the standard reaction conditions again, the filtrate did not show any increase in β-lactone yield whereas the unfiltered portion resumed its epoxide carbonylation activity. The structural integrity of $Co(CO)_4 \subset Cr$-MIL-101 was also retained after all epoxide carbonylation reactions as confirmed by PXRD analysis of spent $Co(CO)_4 \subset Cr$-MIL-101 (Figure 2.S1).

To verify the catalytic cooperativity between the Cr(III) sites and $Co(CO)_4^-$ in $Co(CO)_4 \subset Cr$-MIL-101, Cr-MIL-101-F, Cr-MIL-101-Cl, and $Na[Co(CO)_4]$ were tested for epoxide carbonylation activity (Table 2.S1). All systems displayed negligible product formation when subjected to a 5 h reaction with neat 1,2-epoxyhexane at 0.5 mol % loading, 60 bar CO, and 60 °C. In addition, no substantial catalytic activity was observed when HKUST-1 (Cu_3BTC_2, H_3BTC = benzene-1,3,5-tricarboxylic acid) (Figure 2.S4), a representative Lewis acidic MOF with Cu(II) sites,[33] was subjected to the same reaction conditions along with an equimolar amount of $Na[Co(CO)_4]$ (Table 2.S1). These results show that the epoxide carbonylation activity is specific to $Co(CO)_4 \subset Cr$-MIL-101, where the unique combination of $Co(CO)_4^-$ and the strong Lewis acidic Cr(III) sites of the Cr-MIL-101 framework is required for cooperative catalysis. It is interesting to note that an equimolar mixture of the as-synthesized Cr-MIL-101 and $Na[Co(CO)_4]$ also showed β-lactone formation under reaction conditions, presumably due to partial formation of the Cr/Co sites *in situ* (Table

2.S1). The observed catalytic activity, however, was lower than that of $Co(CO)_4 \subset Cr$-MIL-101, which has pre-assembled Cr/Co sites installed within the framework prior to reaction.

Encouraged by the observed heterogeneous epoxide carbonylation activity in liquid-phase batch reactions, we subjected $Co(CO)_4 \subset Cr$-MIL-101 to a gas-phase continuous-flow reaction using propylene oxide and CO. Uniquely among all known catalysts for this reaction, $Co(CO)_4 \subset Cr$-MIL-101 showed catalytic epoxide carbonylation activity to form β-butyrolactone under unoptimized reaction conditions: holding $Co(CO)_4 \subset Cr$-MIL-101 at 70 °C and subjecting it to 20 bar of 0.02 mol % propylene oxide and balance CO flowing at 125 mL/min (at standard temperature and pressure, STP) resulted in STYs of approximately 6 $mol_{\beta\text{-Butyrolactone}} \cdot mol_{Co}^{-1} \cdot h^{-1}$ and a turnover number of 60 $mol_{\beta\text{-Butyrolactone}} \cdot mol_{Co}^{-1}$ after 24 h on stream (Figures 2.S5 and 2.S6). Notably, catalytic activity ensued only after *in situ* removal of the pore-filling THF solvent left-over from catalyst synthesis, which presumably block substrate access to the Cr/Co active sites. We expect optimization of the reaction conditions to further enhance catalytic performance for a more efficient continuous production of β-lactones. Nonetheless, the ability to perform reactions in the gas phase is a unique feature of our heterogeneous catalyst that is inaccessible to the homogeneous catalysts developed to date.

2.4. Conclusion

In summary, we have demonstrated the successful preparation of $Co(CO)_4 \subset Cr$-MIL-101 and its catalytic activity in the heterogeneous ring-expansion carbonylation of epoxides. We

attribute this activity to the cooperativity between the Lewis acidic Cr(III) sites and the post-synthetically incorporated $Co(CO)_4^-$. The favorable catalytic performance exemplified by this heterogeneous system and its proof-of-concept application in the first gas-phase continuous production of β-lactone highlight the effectiveness of the heterogeneous epoxide carbonylation pathway and warrant further evaluation of its industrial applicability.

2.5. Experimental Information

General Considerations

All manipulations of air/water-sensitive compounds were conducted using standard inert-atmosphere glove box and Schlenk line techniques.

Powder X-ray diffraction (PXRD) patterns were recorded on a Bruker Advance II diffractometer equipped with θ/2θ Bragg-Brentano geometry and Ni-filtered Cu Kα radiation (Kα₁ = 1.5406 Å). The tube voltage and current were 40 kV and 40 mA, respectively.

Energy dispersive X-ray spectroscopy (EDX) analysis was conducted using a JEOL 6010LA analytical scanning electron microscope at 15 keV and a working distance of 10 mm.

Attenuated total reflectance infrared (ATR-IR) absorption spectra were acquired using a Bruker Alpha ATR Fourier transform IR spectrometer under an inert atmosphere.

Cobalt quantifications of $Co(CO)_4 \subset Cr$-MIL-101 samples were conducted using an Agilent 7900 inductively coupled plasma mass spectrometer (ICP-MS). Weighed $Co(CO)_4 \subset Cr$-MIL-101 samples were digested in concentrated nitric acid (67~70% w/v %, BDH Aristar) using a microwave digestion system (Milestone, UltraWAVE) and the cobalt content was determined from calibration curves constructed from standard solutions (VWR, ICP/MS certified reference standards).

Epoxide carbonylation reactions were analyzed using ^{1}H-NMR (Bruker Avance 400 MHz) and a gas chromatograph equipped with a mass selective detector for identification (Agilent Technologies, model 5975C) and a flame ionization detector for quantification (Agilent Technologies, model 7890A). The gas chromatograph was fitted with a DB-5ms column (Agilent, 30 m × 0.25 mm ID × 0.25 μm). Identification of the product β-lactones was supplemented by comparing their ^{1}H-NMR spectra with the published spectra.

Materials

Chromium(III) nitrate nonahydrate (98.5%, Alfa Aesar), terephthalic acid (≥98%, Alfa Aesar), hydrofluoric acid (48~51 w/v %, BDH Aristar), ammonium fluoride (≥98%, Sigma-Aldrich), aluminum(III) chloride hexahydrate (99%, Alfa Aesar), dicobalt octacarbonyl (stabilized with 1~5% hexanes, Strem), sodium hydroxide (≥98%, Macron), copper(II) nitrate trihydrate (99%, Sigma-Aldrich), trimesic acid (95%, Sigma-Aldrich), mesitylene (≥99.8% analytical standard, Sigma-Aldrich), ethanol (99.5%, VWR), N,N'-dimethylformamide (99.5%, Sigma-Aldrich), and carbon monoxide (research grade 4.0, Airgas) were used as received. Silicon carbide powder (320 grit, Alfa Aesar) was dried in a

convection oven at 120 °C overnight prior to use. Methanol (99.9%, VWR), tetrahydrofuran

(ACS grade, BDH), and 1,2-dimethoxyethane (99.5%, Sigma-Aldrich) were passed through

two silica columns in a Glass Contour solvent system and degassed with a flow of argon gas

for 30 min followed by three freeze-pump-thaw cycles prior to use. Propylene oxide (≥99%,

Sigma-Aldrich), 1,2-epoxybutane (99%, Sigma-Aldrich), 1,2-epoxyhexane (97%, Sigma-

Aldrich), 1,2-epoxy-5-hexene (97%, Sigma-Aldrich), ethyl glycidyl ether (≥98%, TCI) and

epichlorohydrin (≥99%, Sigma-Aldrich) were stirred over >5 w/v % calcium hydride for a

minimum of three days, vacuum transferred, and degassed by three freeze-pump-thaw

cycles prior to use.

Experimental Details

Synthesis of Cr-MIL-101: Cr-MIL-101 was prepared according to the procedures reported

by Férey et al.[21,33] A typical synthesis involved a mixture of $Cr(NO_3)_3 \cdot 9H_2O$ (800 mg, 2.00

mmol) and terephthalic acid (332 mg, 2.00 mmol) in 10.0 mL of water with 2.0 mmol of HF.

The mixture was introduced to a Parr pressure vessel, which was placed in a convection

oven held at 220 °C for 8 h. After natural cooling, the mixture was first passed through a

large-pore fritted glass filter to remove the residual terephthalic acid. The filtrate was then

passed through a fine-pore filter paper to collect the Cr-MIL-101 product. The obtained Cr-

MIL-101 was further purified by two solvent treatments using ethanol and aqueous NH_4F.

The first solvent treatment involved introducing the solid sample to refluxing ethanol until

no detection of colored impurities in the mother liquor. The sample was then subjected to

an aqueous solution of 30 mM NH_4F at 60 °C for 10 h. After natural cooling, Cr-MIL-101 was

filtered and washed several times with hot water at 60 °C to remove residual NH_4F. The filtered sample was then desolvated by heating under vacuum at 150 °C for 18 h.

Anion Exchange of Cr-MIL-101 with AlCl$_3$: Anion exchange between Cr-MIL-101 and AlCl$_3$ was conducted according to the procedures reported by Feng et al.[19] A typical procedure involved subjecting Cr-MIL-101 to an aqueous solution of 30 mM AlCl$_3$·6H$_2$O at 90 °C for 18 h (1 g of Cr-MIL-101 per 1 L of solution). The solid sample was filtered and washed several times with hot water at 90 °C to remove residual AlCl$_3$. The filtered sample was then desolvated by heating under vacuum at 150 °C for 18 h. The obtained final product was labeled as Cr-MIL-101-Cl.

Synthesis of Na[Co(CO)$_4$]: Na[Co(CO)$_4$] was prepared according to the procedures reported by Edgell and Lyford.[34] A typical synthesis involved charging a Schlenk flask with Co$_2$(CO)$_8$ (5.00 g, 14.6 mmol) and a magnetic stir bar under an inert atmosphere. Freshly ground NaOH (6.00 g, 150 mmol) and tetrahydrofuran (50 mL) were then transferred to the flask and the reaction mixture was left to stir in an ice bath for 6 h while wrapped in aluminum foil. The product mixture was then passed through a Celite pad and washed several times with tetrahydrofuran. The collected filtrate was pumped down and dried overnight to obtain the final product.

Anion Exchange of Cr-MIL-101-Cl with Na[Co(CO)$_4$]: A typical procedure involved subjecting Cr-MIL-101-Cl to a methanol solution of 30 mM Na[Co(CO)$_4$] and stirring overnight (20 mg of Cr-MIL-101-Cl per 20 mL of solution). The solid sample was then

filtered and washed by suspending the sample in fresh tetrahydrofuran and stirring overnight. The washing procedure was repeated several times. The obtained final product was labeled as $Co(CO)_4 \subset Cr\text{-}MIL\text{-}101$.

Synthesis of HKUST-1: HKUST-1 was prepared according to the procedures reported by Zhu et al.[35] A typical procedure involved dissolving trimesic acid (500 mg, 2.38 mmol) in a 15 mL solution of a 1:1 mixture of ethanol and N,N'-dimethylformamide. $Cu(NO_3)_2 \cdot 3H_2O$ (1.03 g, 4.26 mmol) was dissolved separately in 7.5 mL of water and added to the solution of trimesic acid. The mixture was left to stir for 10 min and transferred to a Parr pressure vessel, which was introduced to a convection oven held at 100 °C for 12 h. After natural cooling, the mixture was passed through a fine-pore fritted glass filter to isolate the solid product. The obtained solids were washed three times with fresh N,N'-dimethylformamide and then submerged in 100 mL of methanol for solvent exchange. The supernatant was replenished with fresh methanol every ~3 h for a total of 16 times over a period of a few days to ensure complete exchange of the solvent. The solvent-exchanged solids were isolated by filtration and introduced to a vacuum oven held at 60 °C for 6 h. The dried product was then further desolvated by heating under vacuum at 150 °C for 18 h. PXRD analysis of the prepared sample verified the final product as HKUST-1 (Figure 2.S4).

Liquid-phase Epoxide Carbonylation with $Co(CO)_4 \subset Cr\text{-}MIL\text{-}101$: A typical procedure involved charging a glass vial with epoxide, 1,2-dimethoxyethane (1 mL per 1 mmol of epoxide), $Co(CO)_4 \subset Cr\text{-}MIL\text{-}101$ (0.5 cobalt mol % loading with respect to the epoxide, based on an ICP-MS derived cobalt content of $Co(CO)_4 \subset Cr\text{-}MIL\text{-}101$), and a magnetic stir

bar. The vial was then immediately transferred to a stainless steel Parr reactor, and the reactor was sealed in an inert-atmosphere glove box. The reactor was then taken out of the glove box, placed in a hood, pressurized with CO, and heated to 60 °C (CO pressure of 60 bar at 60 °C) with a temperature controller (Digi-Sense, 68900) and an internal thermocouple probe (Omega, KQXL-18). The temperature was held constant while stirring for the specified time on a magnetic stir plate, after which the reactor was cooled in an ice bath until the pressure reached a minimum. After careful venting of CO to atmospheric pressure, the glass vial was removed, and the product mixture was filtered through a polytetrafluoroethylene syringe filter (Millex, 0.20 μm). A small sample of the filtrate was analyzed via ^{1}H-NMR with added mesitylene as a standard. All control reactions were conducted in an analogous manner as described above for $Co(CO)_4 \subset Cr\text{-}MIL\text{-}101$.

Catalyst Heterogeneity Test with $Co(CO)_4 \subset Cr\text{-}MIL\text{-}101$: A typical procedure involved conducting a standard epoxide carbonylation reaction as outlined above for a sufficient time to reach the desired conversion of the substrate epoxide. After careful venting of CO to atmospheric pressure, the Parr reactor was refilled with nitrogen, and brought into an inert-atmosphere glove box. The glass vial holding the reaction mixture was then taken out of the reactor and the reaction mixture was divided into two equal aliquots. One of the aliquots was passed through a polytetrafluoroethylene syringe filter (Millex, 0.20 μm) to collect the filtrate in a separate vial and a small fraction of the filtrate was analyzed via gas chromatography. The two glass vials, one holding the collected filtrate and the other holding the unfiltered reaction mixture, were then transferred to separate stainless steel Parr reactors, and the reactors were sealed in the glove box. The two reactors were taken

out of the glove box, placed in a hood, and again subjected to standard reaction conditions. After the specified time, the product mixtures from both reactors were recovered and analyzed via gas chromatography in a manner analogous to the procedure outlined above.

Gas-phase Epoxide Carbonylation with Co(CO)₄⊂Cr-MIL-101: A typical procedure involved mixing 40 mg of Co(CO)₄⊂Cr-MIL-101 with 300 mg of silicon carbide powder in an inert-atmosphere glove box and packing the mixture between two inert layers of silicon carbide/glass wool plugs in a stainless-steel tube reactor (OD 6.35 mm, wall thickness 0.89 mm). A thermocouple probe (Omega, KQXL-116) was mounted downstream in direct contact with the end of the catalyst bed for reactor temperature monitoring. The packed reactor was isolated in an inert atmosphere using valves prior to transfer out of the glove box. Dry and degassed propylene oxide was also charged into a custom-made stainless-steel saturator in the glove box and isolated using valves. The saturator and the reactor were then taken into a hood and connected to a carbon monoxide flow reaction setup with a CO mass flow controller (Brooks instruments, 5850E), custom-made oxygen/water traps, a back pressure regulator (Swagelok, KPB1L), and a heated gas line carrying the reactor effluent to a gas chromatograph for analysis. The saturator was held in an acetone bath with an immersion cooler (Thermo Scientific, EK90) for sustained delivery of the reactant epoxide while the reactor was placed in a single-zone furnace (Carbolite, GTF 11/50/150B) and connected to a temperature controller (Digi-Sense, 68900). The reactor was first pressurized to 20 bar of CO using a back-pressure regulator while bypassing the saturator. When the reactor reached the desired pressure, the reactor was bypassed using valves and rest of the reaction setup was pressurized again to 20 bar while flowing CO through the

saturator holding the epoxide substrate. After the desired pressure was reached, flow was stabilized to 125 mL/min and was directed through the reactor maintained at 70 °C, upon which periodic gas chromatograph injections were made. Separate gas chromatograph injections were also taken while bypassing the reactor and the obtained results were averaged to acquire a baseline feed level prior to entering the reactor.
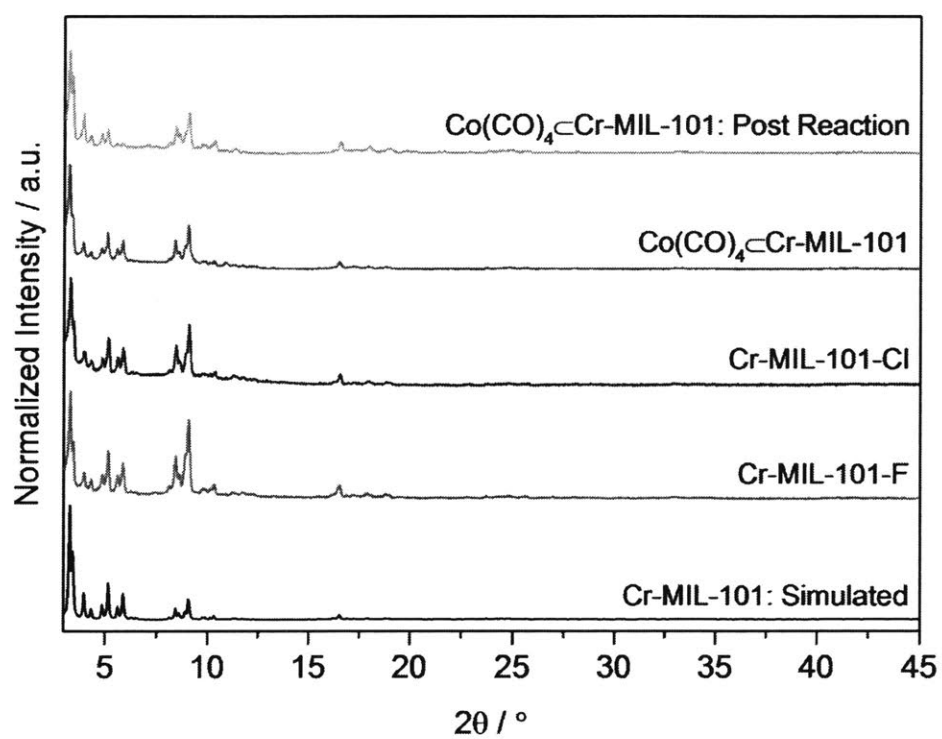
2.6. Supporting Information

Figure 2.S1: PXRD patterns of simulated Cr-MIL-101, Cr-MIL-101-F, Cr-MIL-101-Cl, Co(CO)₄⊂Cr-MIL-101, and post-reaction Co(CO)₄⊂Cr-MIL-101.
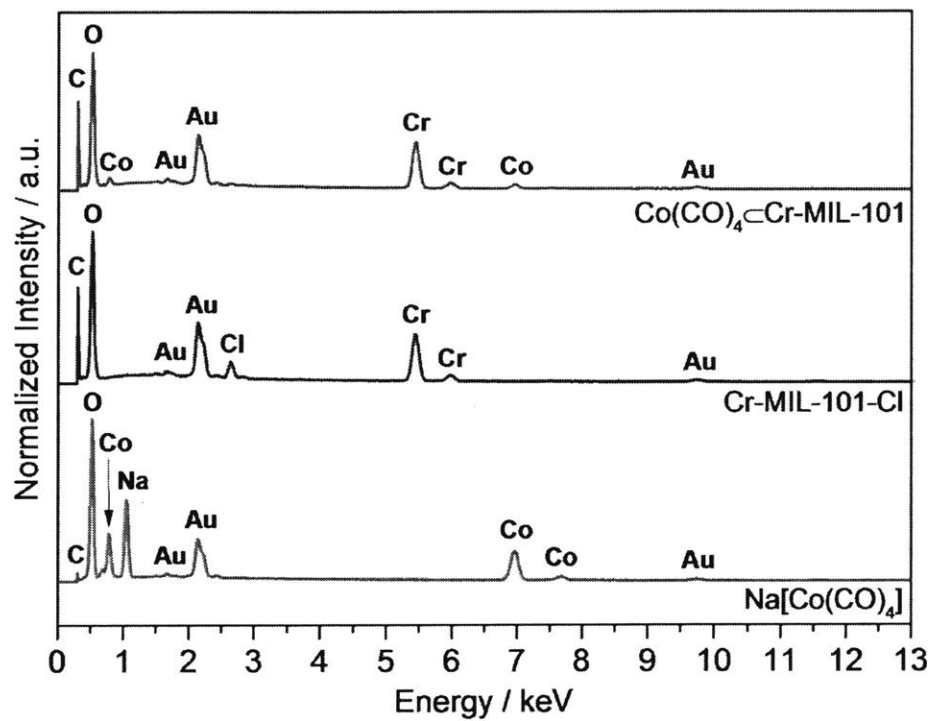
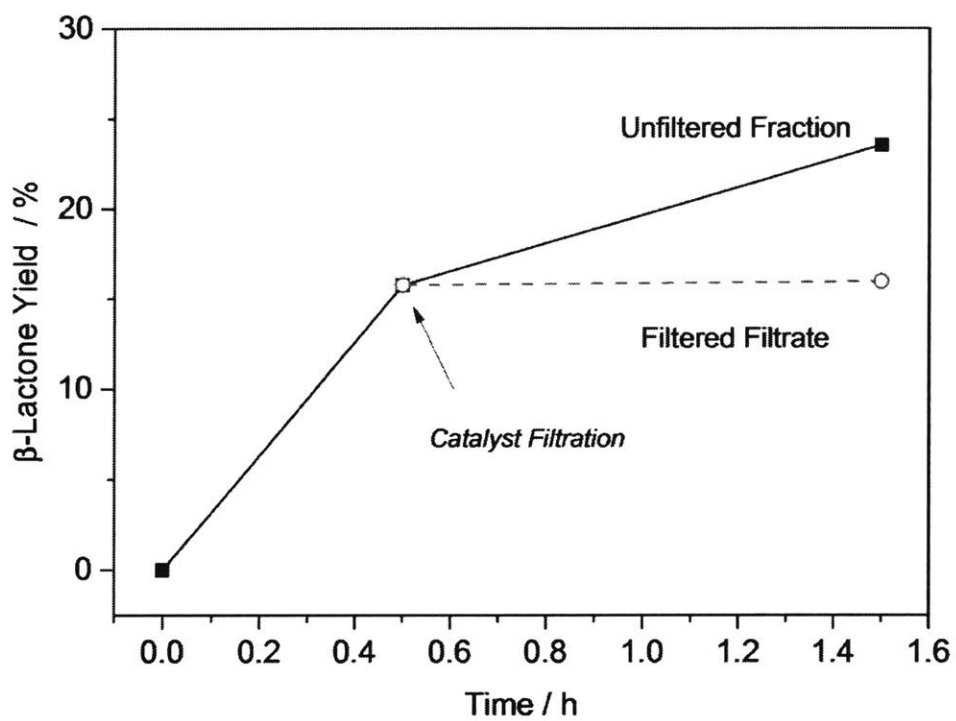**Figure 2.S2:** EDX spectra of Na[Co(CO)$_4$], Cr-MIL-101-Cl, and Co(CO)$_4$⊂Cr-MIL-101.

Figure 2.S3: Catalyst heterogeneity test for $Co(CO)_4 \subset Cr\text{-MIL-101}$. Reaction conditions: 1,2-epoxybutane substrate, 0.1 cobalt mol % catalyst in DME, 60 bar of CO at 60 °C, and catalyst filtration conducted at 0.5 h. Lines are meant as a guide to the eye.
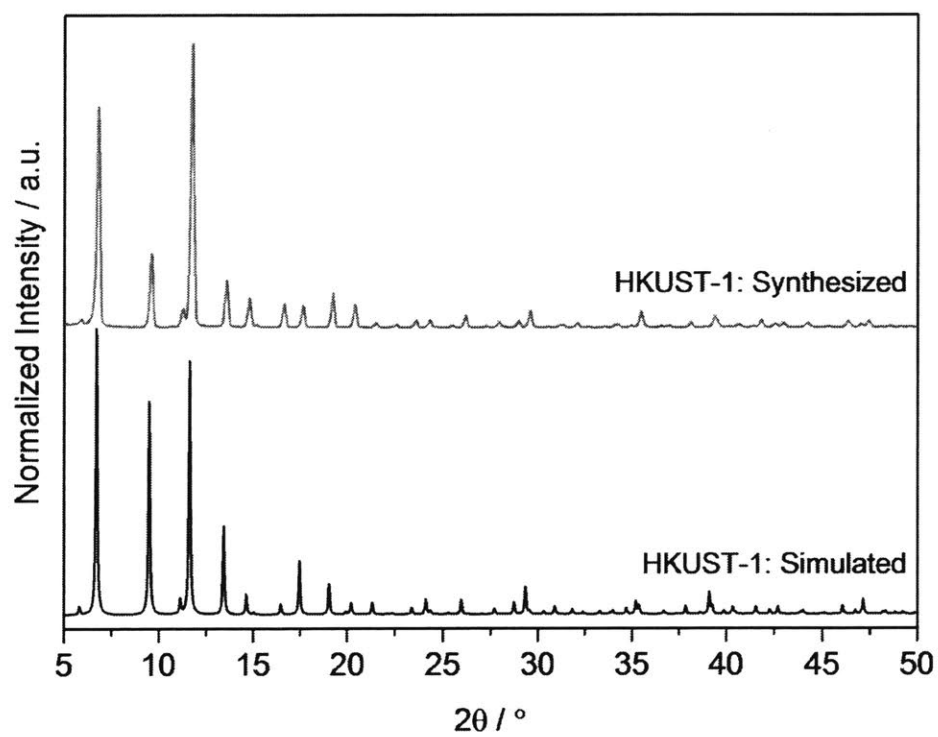
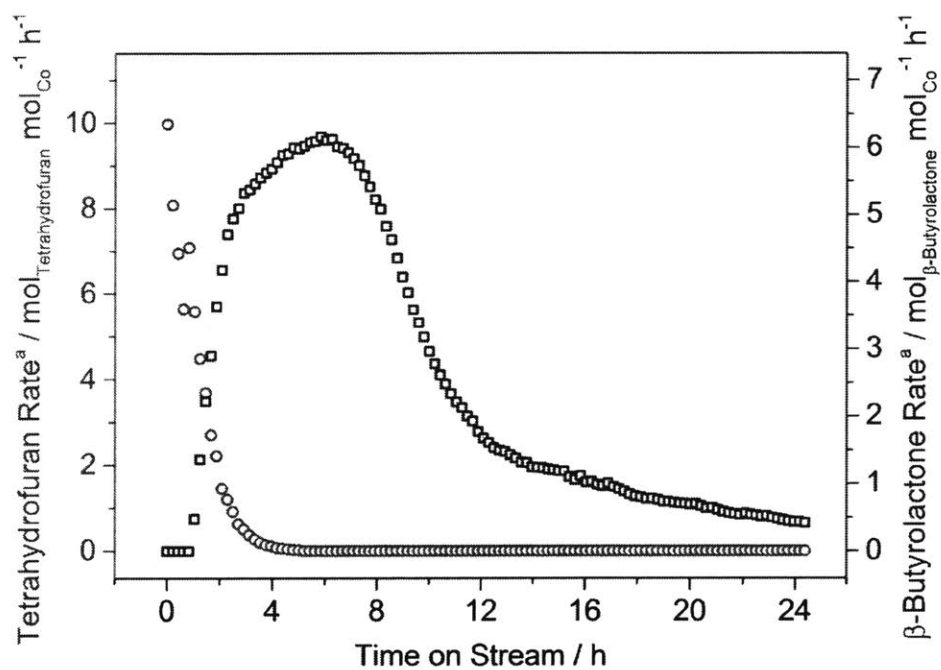**Figure 2.S4:** PXRD patterns of simulated HKUST-1 and synthesized HKUST-1.

Figure 2.S5: Gas-phase continuous-flow production of β-butyrolactone from propylene oxide and CO with Co(CO)₄⊂Cr-MIL-101. Reaction conditions: propylene oxide (0.02%) / CO (balance) (mol %) at 20 bar of total pressure and 70 °C; total flow rate of 125 mL/min (STP).

Figure 2.S6: Gas-phase continuous-flow production of β-butyrolactone from propylene oxide and CO with $Co(CO)_4 \subset Cr$-MIL-101. Reaction conditions: propylene oxide (0.02%) / CO (balance) (mol %) at 20 bar of to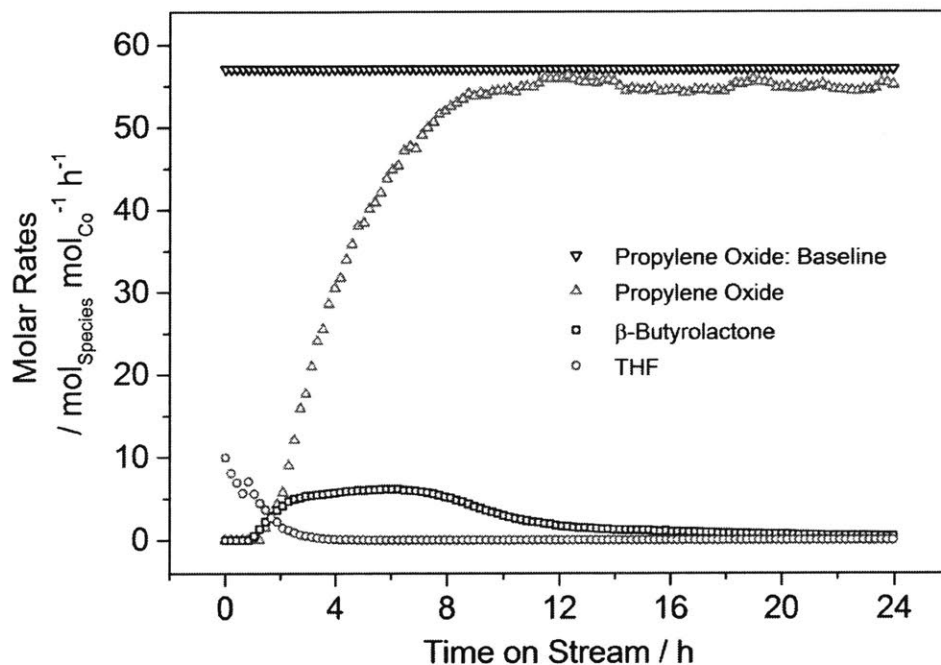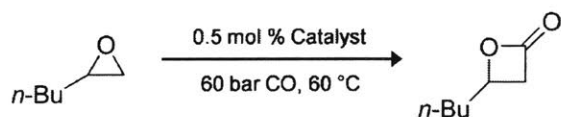tal pressure and 70 °C; total flow rate of 125 mL/min (STP). Baseline propylene oxide level was acquired by flowing the reactant under reaction conditions while bypassing the reactor.

Table 2.S1. Catalysts for the Ring-expansion Carbonylation of 1,2-Epoxyhexane

Entry	Catalyst	Yield (%)
1	Cr-MIL-101-F	0[a]
2	Cr-MIL-101-Cl	0[a]
3	Na[Co(CO)$_4$]	<2[a]
4	HKUST-1 + Na[Co(CO)$_4$]	<2[a]
5	Cr-MIL-101 + Na[Co(CO)$_4$]	34[b,c]
6	Co(CO)$_4$⊂Cr-MIL-101	86[a], 88[b]

[a] Neat substrate, 5 h, yields determined by GC analysis. [b] 1,2-Dimethoxyethane solvent (1 mL / 1 mmol of substrate), 1 h, yields determined by ^{1}H-NMR analysis with mesitylene as an internal standard. [c] 58% of the substrate epoxide remained unreacted.

43

2.7. References

(1)   Pommier, A.; Pons, J. M. Recent Advances in β-Lactone Chemistry. *Synthesis* **1993**, 5, 441–459.

(2)   Schneider, C. Catalytic, Enantioselective Syntheses of β-Lactones – Versatile Synthetic Building Blocks in Organic Chemistry. *Angew. Chem. Int. Ed.* **2002**, 41, 744–746.

(3)   Wang, Y.; Tennyson, R. L.; Romo, D. β-Lactones: intermediates for natural product total synthesis and new transformations. *Heterocycles* **2004**, 64, 605–658.

(4)   Müller, H. M.; Seebach, D. Poly(hydroxyalkanoates): A Fifth Class of Physiologically Important Organic Biopolymers? *Angew. Chem. Int. Ed.* **1993**, 32, 477–502.

(5)   Mori, Y.; Tsuji, J. Organic Syntheses by Means of Metal Complexes. III. Cobalt Carbonyl-catalyzed Carbonylation of β-Propiolactone. *Bull. Chem. Soc. Jpn.* **1969**, 42, 777–779.

(6)   Yang, H. W.; Romo, D. Methods for the Synthesis of Optically Active β-Lactones (2-Oxetanones). *Tetrahedron* **1999**, 55, 6403–6434.

(7)   Khumtaveeporn, K.; Alper, H. Transition Metal Mediated Carbonylative Ring Expansion of Heterocyclic Compounds. *Acc. Chem. Res.* **1995**, 28, 414–422.

(8)   Church, T. L.; Getzler, Y. D. Y. L.; Byrne, C. M.; Coates, G. W. Carbonylation of Heterocycles by Homogeneous Catalysts. *Chem. Commun.* **2007**, 7, 657–674.

(9)   Kramer, J. W.; Rowley, J. M.; Coates, G. W. Ring-expanding Carbonylation of Epoxides. In *Organic Reactions*; Denmark, S. E. et al., Eds.; John Wiley & Sons, Inc.: Hoboken, 2015; pp 1–104.

(10)   Lee, J. T.; Thomas, P. J.; Alper, H. Synthesis of β-Lactones by the Regioselective, Cobalt and Lewis Acid Catalyzed Carbonylation of Simple and Functionalized Epoxides. *J. Org. Chem.* **2001**, 66, 5424–5426.

(11)   Mahadevan, V.; Getzler, Y. D. Y. L.; Coates, G. W. [Lewis Acid]$^+$[Co(CO)$_4$]$^-$ Complexes: A Versatile Class of Catalysts for Carbonylative Ring Expansion of Epoxides and Aziridines. *Angew. Chem. Int. Ed.* **2002**, 41, 2781–2784.

(12)   Getzler, Y. D. Y. L.; Mahadevan, V.; Lobkovsky, E. B.; Coates, G. W. Synthesis of β-Lactones: A Highly Active and Selective Catalyst for Epoxide Carbonylation. *J. Am. Chem. Soc.* **2002**, 124, 1174–1175.

(13)   Schmidt, J. A. R.; Mahadevan, V.; Getzler, Y. D. Y. L.; Coates, G. W. A Readily Synthesized and Highly Active Epoxide Carbonylation Catalyst Based on a Chromium Porphyrin Framework: Expanding the Range of Available β-Lactones. *Org. Lett.* **2004**, 6, 373–376.

(14)   Schmidt, J. A. R.; Lobkovsky, E. B.; Coates, G. W. Chromium(III)

Octaethylporphyrinato Tetracarbonylcobaltate: A Highly Active, Selective, and Versatile Catalyst for Epoxide Carbonylation. *J. Am. Chem. Soc.* **2005**, *127*, 11426–11435.

(15) Kramer, J. W.; Lobkovsky, E. B.; Coates, G. W. Practical β-Lactone Synthesis: Epoxide Carbonylation at 1 atm. *Org. Lett.* **2006**, *8*, 3709–3712.

(16) Allen, S. D.; Valente, R. R.; Lee, H.; Cherian, A. E.; Bunning, D. L.; Clinton, N. A.; Fruchey, O. S.; Dombek, B. D. Process for Beta-Lactone Production. U.S. Patent 8,796,475, 2014.

(17) Church, T. L.; Getzler, Y. D. Y. L.; Coates, G. W. The Mechanism of Epoxide Carbonylation by [Lewis Acid]$^+$[Co(CO)$_4$]$^-$ Catalysts. *J. Am. Chem. Soc.* **2006**, *128*, 10125–10133.

(18) Férey, G.; Mellot-Draznieks, C.; Serre, C.; Millange, F.; Dutour, J.; Surblé, S.; Margiolaki, I. A Chromium Terephthalate-based Solid with Unusually Large Pore Volumes and Surface Area. *Science* **2005**, *309*, 2040–2042.

(19) Mao, C.; Kudla, R. A.; Zuo, F.; Zhao, X.; Mueller, L. J.; Bu, X.; Feng, P. Anion Stripping as a General Method to Create Cationic Porous Framework with Mobile Anions. *J. Am. Chem. Soc.* **2014**, *136*, 7579–7582.

(20) Berdonosova, E. A.; Kovalenko, K. A.; Polyakova, E. V; Klyamkin, S. N.; Fedin, V. P. Influence of Anion Composition on Gas Sorption Features of Cr-MIL-101 Metal–Organic Framework. *J. Phys. Chem. C* **2015**, *119*, 13098–13104.

(21) Cr-MIL-101 is stable up to 275 °C in air and retains its original crystallinity and porosity after refluxing in water for a week. Hong, D. Y.; Hwang, Y. K.; Serre, C.; Férey, G.; Chang, J. S. Porous Chromium Terephthalate MIL-101 with Coordinatively Unsaturated Sites: Surface Functionalization, Encapsulation, Sorption and Catalysis. *Adv. Funct. Mater.* **2009**, *19*, 1537–1552.

(22) Noh, H.; Cui, Y.; Peters, A. W.; Pahls, D. R.; Ortuño, M. A.; Vermeulen, N. A.; Cramer, C. J.; Gagliardi, L.; Hupp, J. T.; Farha, O. K. An Exceptionally Stable Metal–Organic Framework Supported Molybdenum(VI) Oxide Catalyst for Cyclohexene Epoxidation. *J. Am. Chem. Soc.* **2016**, *138*, 14720–14726.

(23) Thacker, N. C.; Lin, Z.; Zhang, T.; Gilhula, J. C.; Abney, C. W.; Lin, W. Robust and Porous β-Diketiminate-functionalized Metal–Organic Frameworks for Earth-Abundant-metal-catalyzed C–H Amination and Hydrogenation. *J. Am. Chem. Soc.* **2016**, *138*, 3501–3509.

(24) Fracaroli, A. M.; Siman, P.; Nagib, D. A.; Suzuki, M.; Furukawa, H.; Toste, F. D.; Yaghi, O. M. Seven Post-synthetic Covalent Reactions in Tandem Leading to Enzyme-like Complexity within Metal–Organic Framework Crystals. *J. Am. Chem. Soc.* **2016**, *138*, 8352–8355.

(25) Na, K.; Choi, K. M.; Yaghi, O. M.; Somorjai, G. A. Metal Nanocrystals Embedded in Single Nanocrystal of MOFs Give Unusual Selectivity as Heterogeneous Catalysts.

Nano Lett. **2014**, *14*, 5979–5983.

(26) Li, Z.; Peters, A. W.; Bernales, V.; Ortuño, M. A.; Schweitzer, N. M.; DeStefano, M. R.; Gallington, L. C.; Platero-Prats, A. E.; Chapman, K. W.; Cramer, C. J.; Gagliardi, L.; Hupp, J. T.; Farha, O. K. Metal–Organic Framework Supported Cobalt Catalysts for the Oxidative Dehydrogenation of Propane at Low Temperature. *ACS Cent. Sci.* **2017**, *3*, 31–38.

(27) Burgun, A.; Coghlan, C. J.; Huang, D. M.; Chen, W.; Horike, S.; Kitagawa, S.; Alvino, J. F.; Metha, G. F.; Sumby, C. J.; Doonan, C. J. Mapping-out Catalytic Processes in a Metal–Organic Framework with Single-crystal X-ray Crystallography. *Angew. Chem. Int. Ed.* **2017**, DOI: 10.1002/anie.201611254

(28) Ji, P.; Manna, K.; Lin, Z.; Urban, A.; Greene, F. X.; Lan, G.; Lin, W. Single-site Cobalt Catalysts at New $Zr_8(\mu_2-O)_8(\mu_2-OH)_4$ Metal–Organic Framework Nodes for Highly Active Hydrogenation of Alkenes, Imines, Carbonyls, and Heterocycles. *J. Am. Chem. Soc.* **2016**, *138*, 12234–12242.

(29) Edgell, W. F.; Lyford, J. Studies of Some Aspects of Solution Character by Molecular Spectroscopy. V. Identification, Population, and Equilibrium of the Anion Sites for $NaCo(CO)_4$ in Tetrahydrofuran. *J. Am. Chem. Soc.* **1971**, *93*, 6407–6414.

(30) Edgell, W. F.; Yang, M. T.; Koizumi, N. The Nature of the Solution of Sodium Tetracarbonylcobaltate(–I) in Various Solvents. *J. Am. Chem. Soc.* **1965**, *87*, 2563–2567.

(31) Edgell, W. F.; Lyford, J.; Barbetta, A.; Jose, C. I. Studies of Some Aspects of Solution Character by Molecular Spectroscopy. IV. Multiplicity and Nature of the $Co(CO)_4^-$ Environments in Certain Solvents. *J. Am. Chem. Soc.* **1971**, *93*, 6403–6406.

(32) Rajendiran, S.; Natarajan, P.; Yoon, S. A Covalent Triazine Framework-based Heterogenized Al–Co Bimetallic Catalyst for the RIng-expansion Carbonylation of Epoxide to β-Lactone. *RSC Adv.* **2017**, *7*, 4635–4638.

(33) Chui, S. S. Y.; Lo, S. M. F.; Charmant, J. P. H.; Orpen, A. G.; Williams, I. D. A Chemically Functionalizable Nanoporous Material $[Cu_3(TMA)_2(H_2O)_3]_n$. *Science* **1999**, *283*, 1148–1150.

(34) Edgell, W. F.; Lyford, J. Preparation of Sodium Cobalt Tetracarbonyl. *Inorg. Chem.* **1970**, *9*, 1932–1933.

(35) Yang, Y.; Shukla, P.; Wang, S.; Rudolph, V.; Chen, X. M.; Zhu, Z. Significant Improvement of Surface Area and CO_2 Adsorption of Cu-BTC via Solvent Exchange Activation. *RSC Adv.* **2013**, *3*, 17065–17072.

Chapter 3

Continuous-flow Production of β-Butyrolactone via Catalytic Propylene Oxide Carbonylation by $Co(CO)_4 \subset Cr\text{-MIL-101}$

3.1. Abstract

Despite being recognized as an outstanding precursor to biodegradable poly(3-hydroxybutyrate) plastics, β-butyrolactone remains vastly underutilized owing to its difficult synthesis. Here we demonstrate continuous-flow carbonylation of propylene oxide by $Co(CO)_4{}^-$-incorporated Cr-MIL-101 ($Co(CO)_4 \subset Cr\text{-MIL-101}$, Cr-MIL-101 = $Cr_3O(BDC)_3F$, H_2BDC = 1,4-benzenedicarboxylic acid) as a cost-effective route to β-butyrolactone from industrially-accessible substrates. The porous nature of the metal–organic framework catalyst enables its direct use in a fixed bed carbonylation process, which yields β-butyrolactone from a concurrent gas-liquid flow of CO and propylene oxide. Optimization of liquid-phase conditions led to enhanced stability of the carbonylation activity, resulting in the first report of sustained β-butyrolactone production using a fixed bed reactor process.

3.2. Introduction

With an annual global production of 68 million metric tons in 2015, polypropylene remains the second highest-volume plastic produced in the world, trailing only polyethylene.[1] Starkly contrasting its high production rate, however, is its meager 0.9% recycle rate, which

has raised societal concerns over worldwide accumulation of polypropylene waste.[2] Consequently, sustainable alternatives to polypropylene have gained much attention, of which poly(3-hydroxybutyrate) (PHB) shows particular promise.[3] PHB, a biopolymer synthesized by microbes as an energy storage medium, exhibits not only outstanding biodegradability, but also favorable mechanical properties resembling those of polypropylene.[4] PHB derivatives have thus found uses in packaging and cosmetics products as greener polypropylene substitutes,[5] and also in advanced medical applications as biocompatible implants.[6] Yet, its widespread adoption has been hampered by the high cost of its microbial production. Commercial fermentation processes for PHB synthesis typically require expensive substrates, such as sugars or fatty acids, costly PHB extraction from the cell, and challenging product separation from the fermentation broth.[7] These factors ultimately lead to a high market price for PHB, which, for example, was placed at $4.96 per kilogram in 2009, representing more than three times the price of polypropylene it seeks to displace.[8]

An alternate pathway to PHB that is free of aforementioned complications is through the polymerization of β-butyrolactone. The release of ring strain stored in the four-membered cyclic ester of β-butyrolactone allows ring-opening polymerization to proceed under mild conditions with various organometallic catalysts.[9] This circumvents the need for microbial polymerization, effectively replacing the costly PHB recovery from the cell and the fermentation broth for a much simpler separation from the catalyst and the solvent. In addition, the living nature of numerous β-butyrolactone polymerization systems allows precise control over the final structure of PHB, including its molecular weight,

polydispersity, tacticity, and comonomer inclusion.[10] While the challenging synthesis of β-butyrolactone has traditionally precluded its use as a commercial precursor to PHB, a recently-developed ring-expansion carbonylation of epoxides by homogeneous [Lewis acid]$^+$[Co(CO)$_4$]$^-$ ion-pair catalysts offers an intriguing cost-effective route to β-butyrolactone starting from industrially-available propylene oxide and CO.[11]

Herein, we report a catalytic strategy for the continuous synthesis of β-butyrolactone via propylene oxide carbonylation by a heterogeneous Co(CO)$_4$$^-$-incorporated Cr-MIL-101 (Co(CO)$_4$⊂Cr-MIL-101, Cr-MIL-101 = Cr$_3$O(BDC)$_3$F, H$_2$BDC = 1,4-benzenedicarboxylic acid) catalyst. Specifically, gas-liquid flow of CO and propylene oxide solution through the solid metal–organic framework (MOF) catalyst bed affords a three-phase reactive system, in which easily separable β-butyrolactone is obtained with superb selectivity at room temperature. Optimization of the liquid-phase medium resulted in improved stability and product separability for the continuous-flow propylene oxide carbonylation process, constituting the first example of sustained β-butyrolactone synthesis using a fixed bed reactor.

3.3. Results and Discussion

Epoxide carbonylation by [Lewis acid]$^+$[Co(CO)$_4$]$^-$ catalysts has been postulated to follow a cooperative ion-pair mechanism shown in Figure 3.1A: (1) substrate activation by [Lewis acid]$^+$, (2) ring opening by Co(CO)$_4$$^-$, (3) CO insertion, and (4) product displacement upon ring closure.[12] Based on this mechanistic understanding, we designed and reported
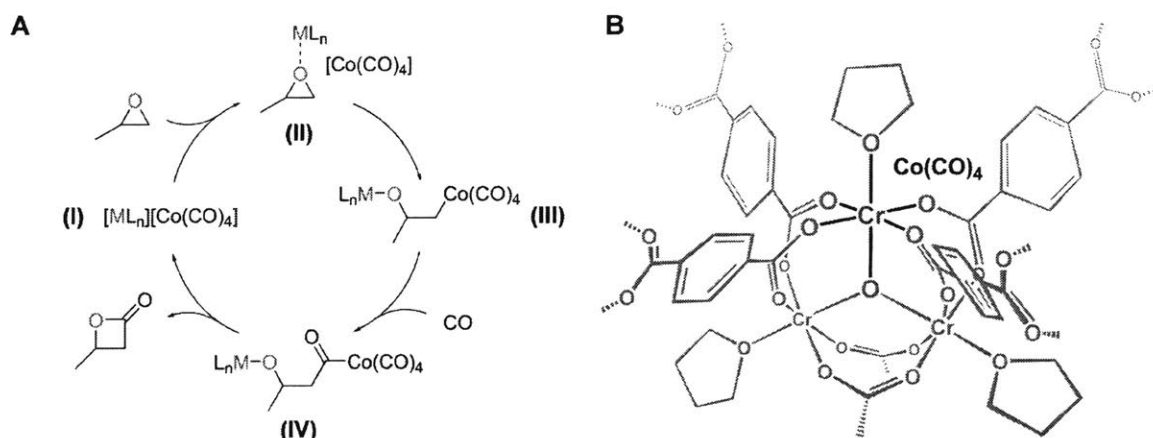
Figure 3.1. (A) Proposed catalytic cycle for the ring-expansion carbonylation of propylene oxide by [Lewis acid]$^+$[Co(CO)$_4$]$^-$. (B) Illustration of the inorganic node structure of Co(CO)$_4$⊂Cr-MIL-101 with coordinated tetrahydrofuran molecules.

Co(CO)$_4$⊂Cr-MIL-101 as a MOF-based heterogeneous catalyst with favorable batch-wise epoxide carbonylation activity comparable to those of other homogeneous [Lewis acid]$^+$[Co(CO)$_4$]$^-$ catalysts (Figures 3.1B and 3.S1–S5, Table 3.S1).[13] When Co(CO)$_4$⊂Cr-101 was applied to a gas phase flow carbonylation reaction, however, only a spike in activity was observed at a drastically lower rate (Figure 3.S6). Also observed was a concomitant loss in carbon balance with carbonylation activity, devoid of any detectable side products to account for the deficit (Figure 3.S7).

In an attempt to reconcile this discrepancy between batch and flow reactivity trends, we hypothesized that poor flow carbonylation activity could be attributed to the condensation of product β-lactone on the catalyst bed. Addition of a polar carbonyl moiety to propylene oxide greatly suppresses its vapor pressure, causing nearly a hundred-fold decrease upon carbonylation to β-butyrolactone (Figure 3.S8). Furthermore, the porous structure of Cr-MIL-101 with its exceptionally high volumetric density of open metal sites (~2 mmol$_{Cr}$/cm^3)

50

available for product binding, is disposed to favor condensation of non-volatile β-

butyrolactone in the pores.[14] Such condensation is particularly detrimental for the epoxide

carbonylation process, as $Co(CO)_4 \subset$ Cr-MIL-101 is known to further convert β-

butyrolactone to methylsuccinic anhydride through sequential carbonylation or to PHB via

in situ polymerization under reaction conditions (Figures 3.2 and 3.S9).[15] Both of these side

products have even lower vapor pressures than β-butyrolactone, which would promote

further clogging of the catalyst pores and subsequent deactivation of the catalyst under

mild gas-phase conditions. In fact, when the spent $Co(CO)_4 \subset$Cr-MIL-101 catalyst bed from

a gas-phase flow propylene oxide carbonylation reaction was isolated, there was noticeable

amount of generated liquids mixed with the catalyst particles. Observed loss in carbon

balance with carbonylation activity is also in line with the proposed formation of less-

volatile side products, such as methylsuccinic anhydride or PHB, that are difficult to detect

with an on-line gas chromatograph.

While the condensation of reaction products could be prevented by elevating the

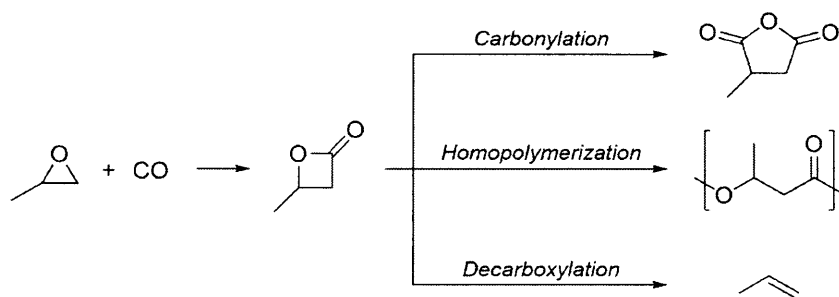temperature of the catalyst bed and the product stream, this simple solution is not

Figure 3.2. Carbonylation of propylene oxide to β-butyrolactone and its subsequent conversion to relevant byproducts: carbonylation to methylsuccinic anhydride, homopolymerization to poly(3-hydroxybutyrate), and decarboxylation to propylene.

51

applicable for the epoxide carbonylation process as the highly strained β-butyrolactone is known to undergo spontaneous decarboxylation at >80 °C to form propylene (Figure 3.2).[16] Accordingly, we instead sought to resolve this product condensation issue by transitioning from a gas-phase flow to a concurrent gas-liquid flow carbonylation process (Figure 3.S10). We reasoned that the presence of a constant flow of liquid through the catalyst bed would maintain a steady displacement of the produced β-lactone through the reactor, regardless of its low volatility. Consequent control over the retention time of the product β-butyrolactone was expected to prevent its further conversion to undesirable side products.

To test this hypothesis, we subjected 25 mg of Co(CO)$_4$⊂Cr-MIL-101 to a gas-liquid flow carbonylation reaction at room temperature with 0.02 mL/min of 0.1 M propylene oxide in toluene and an excess 30 mL/min (at STP) flow of CO at 30 or 60 bar. Under these conditions, β-butyrolactone was obtained as the sole detectable product and collected in the liquid stream with initial yields of ~90% and site time yield (STY) of ~8 mol$_{β\text{-Butyrolactone}}$·mol$_{Co}^{-1}$·h^{-1} (Figure 3.3). Remarkably, the observed yield and STY for gas-liquid flow carbonylation of propylene oxide were considerably higher than those observed in the gas-phase flow carbonylation (~11% yield with a STY of ~6 mol$_{β\text{-Butyrolactone}}$·mol$_{Co}^{-1}$·h^{-1}) at a much higher temperature of 70 °C (Figure 3.S7). More importantly, the stability of the observed carbonylation activity was significantly improved for the gas-liquid flow carbonylation process, especially when higher CO pressure was employed. Specifically, the turnover number (TON) increased from 105 mol$_{β\text{-Butyrolactone}}$·mol$_{Co}^{-1}$ to 160 mol$_{β\text{-Butyrolactone}}$·mol$_{Co}^{-1}$ when the CO pressure was increased from 30 to 60 bar, respectively, over a period of 20 h on stream.

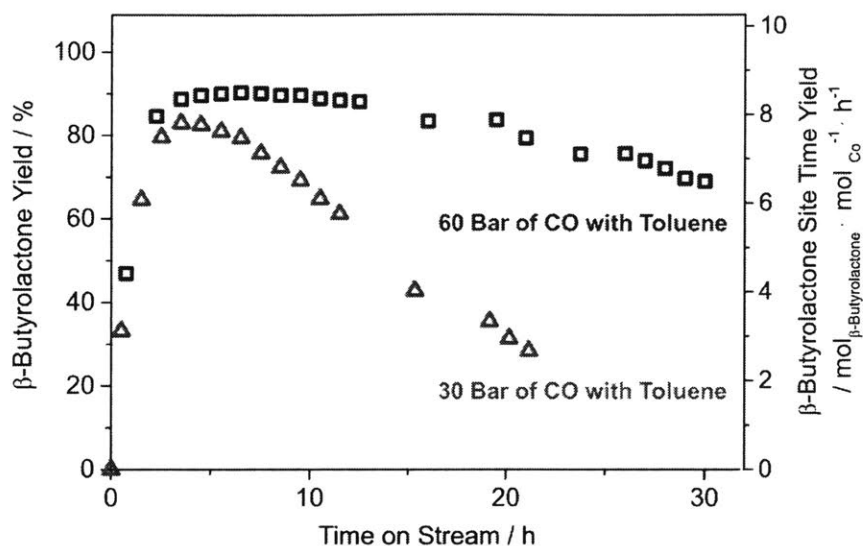**Figure 3.3.** Gas-liquid flow carbonylation of propylene oxide by $Co(CO)_4 \subset Cr$-MIL-101. Reaction conditions: 0.02 mL/min of 0.1 M propylene oxide in toluene, 30 mL/min (at STP) of CO at 60 or 30 bar, and 25 mg of catalyst at 22 °C.

To better understand the observed loss in activity over time, we recovered and analyzed the spent $Co(CO)_4 \subset Cr$-MIL-101 catalyst after 20 h of standard operation at 30 bar of CO with toluene (Figure 3.3). While the spent catalyst retained its original crystal structure as confirmed by the powder X-ray diffraction analysis (Figure 3.S1), attenuated total reflectance infrared spectroscopy (ATR-IR) characterization revealed substantial changes in the carbonyl region of the spectrum (Figure 3.4). Apart from the peak at 1826 cm^{-1} that could be assigned to the product β-butyrolactone ($v_{CO} = 1827$ cm^{-1})[12], we failed to detect the initial carbonyl band of $Co(CO)_4 \subset Cr$-MIL-101 and instead observed new carbonyl bands that were absent in the spectrum of the fresh catalyst. Similar results were obtained for a separate $Co(CO)_4 \subset Cr$-MIL-101 sample that was briefly exposed to the reactant epoxide, which showed the loss of the initial $Co(CO)_4^{-1}$ band at 1890 cm^{-1} and the emergence of new bands at 2050 cm^{-1}, 1980 cm^{-1}, and 1720 cm^{-1}. These observations parallel what has been
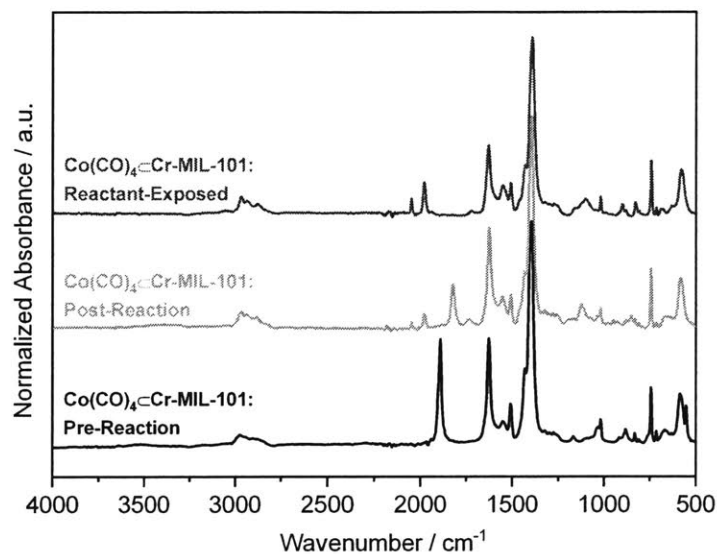
Figure 3.4. Attenuated total reflectance infrared spectra of Co(CO)$_4$⊂Cr-MIL-101. Spectra are normalized with respect to the peak at 744 cm^{-1} from the terephthalate ligand (ν$_{C-H}$) of Cr-MIL-101.[17]

reported for the homogeneous [Lewis acid]$^+$[Co(CO)$_4$]$^-$ catalysts, where *in situ* IR studies revealed a complete disappearance of the Co(CO)$_4$$^{-1}$ band at 1885 cm^{-1} upon addition of the reactant epoxide to the catalyst solution. This behavior is attributed to the rapid ring-opening of the reactant epoxide by the [Lewis acid]$^+$[Co(CO)$_4$]$^-$ ion-pair to form the cobalt acyl intermediate (Figure 3.1A, species IV), the proposed resting state of the catalyst. The new bands observed in our catalyst also resemble those of the reported cobalt acyl species that feature stretching bands of the lower-symmetry terminal carbonyls in the 2130–1890 cm^{-1} range and the acyl group band at ~1717 cm^{-1}.[12,18,19] However, lower peak intensities observed for the spent catalyst in comparison to the reactant-exposed fresh Co(CO)$_4$⊂Cr-MIL-101 confirm the loss of the cobalt carbonyl species from the catalyst during the reaction.

54

Another notable observation from the gas-liquid flow carbonylation reaction was that higher CO pressure increased the stability of the reaction profile whereas its activity remained the same, as seen in the unchanged initial STY (Figure 3.3). This effect is consistent with the proposed mechanism for epoxide carbonylation by [Lewis acid]$^+$[Co(CO)$_4$]$^-$, in which the ring-closing and displacement of the product lactone (Figure 3.1, from IV to I) constitutes the rate determining step and the β-hydride elimination of the cobalt alkyl intermediate (Figure 3.1, species III) represents the undesired side reaction pathway.[12] Since CO insertion does not factor into the proposed rate-determining step, the overall reaction rate is independent of CO pressure. However, since CO insertion into the cobalt alkyl intermediate competes with its undesired β-hydride elimination, higher CO pressure effectively suppresses the exit pathway from the catalytic cycle and leads to stable carbonylation activity. We believe that this proposed β-hydride elimination pathway is responsible for the observed loss of the cobalt carbonyl species from the catalyst, as its neutrally-charged elimination product HCo(CO)$_4$ can be liberated into the liquid medium unlike the initial Co(CO)$_4^-$ that is electrostatically bound to the cationic nodes of the MOF.

The crucial role of CO pressure in the epoxide carbonylation mechanism led us to identify the concentration of CO in the liquid phase as a key variable in maintaining an active gas-liquid flow carbonylation process. We therefore hypothesized that an alternate strategy to enhance the stability of the process would be to use solvents with higher CO solubility. To this end, we sought to find an optimum liquid medium for epoxide carbonylation by simulating the concentration of CO in common solvents at various pressures using Aspen

Plus® software (Figure 3.S11). The results from the simulation clearly favored ethers as a class of solvents with relatively higher CO solubility, a conclusion that was further corroborated by the experimentally-derived CO solubility values.[20] We then specifically selected methyl *tert*-butyl ether (MTBE) as a test system based on its industrial applicability stemming from a lower tendency to generate peroxides.

When MTBE was used instead of toluene in the gas-liquid flow carbonylation of propylene oxide by $Co(CO)_4 \subset Cr\text{-}MIL\text{-}101$ at 30 bar of CO, further improvement in the stability of the carbonylation activity was observed (Figure 3.S12). Specifically, 62% of the initial activity was retained after 20 h on stream for a reaction in MTBE, whereas only 38% of the initial activity was maintained when the reaction was run using toluene under identical conditions. Derived carbon balances were also noticeably better than those obtained from a gas-phase flow carbonylation reaction, suggesting suppressed entrapment of carbon species in the catalyst bed for the gas-liquid flow carbonylation. A slight reduction in the activity of the catalyst was observed with the change in solvent from toluene to MTBE, as evident from the lower initial STY value of ~6 $_{\beta\text{-Butyrolactone}} \cdot mol_{Co}^{-1} \cdot h^{-1}$. β-Butyrolactone yield could nonetheless be easily increased by reducing the liquid space velocity, which led to sustained carbonylation activity of 210 $mol_{\beta\text{-Butyrolactone}} \cdot mol_{Co}^{-1}$ turnovers over 40 h at a CO pressure of 60 bar (Figure 3.5). In addition to the enhanced stability of the process, use of MTBE aids the downstream recovery of product β-butyrolactone by establishing a wider volatility difference between the product and the solvent. This difference is particularly advantageous given the thermal instability of β-butyrolactone that prevents the operation of product separations at elevated temperatures.
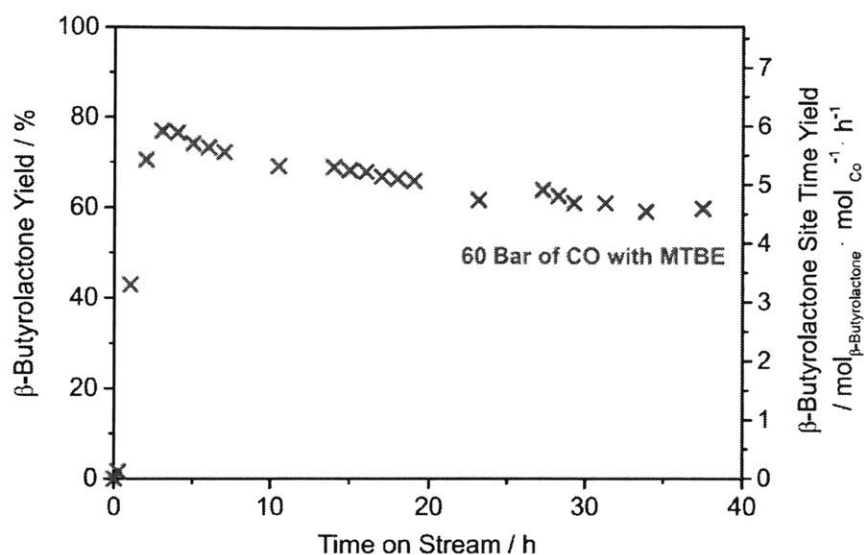
Figure 3.5. Gas-liquid flow carbonylation of propylene oxide by $Co(CO)_4 \subset Cr\text{-}MIL\text{-}101$. Reaction conditions: 0.015 mL/min of 0.1 M propylene oxide in methyl *tert*-butyl ether, 30 mL/min (at STP) of CO at 60 bar, and 25 mg of catalyst at 22 °C.

3.4. Conclusion

In summary, we demonstrated gas-liquid flow carbonylation of propylene oxide by $Co(CO)_4 \subset Cr\text{-}MIL\text{-}101$ as the first example of sustained synthesis of β-butyrolactone using a fixed bed reactor process. Utilization of industrially available substrates, ease of operation, and facile product recovery showcase the processing advantages conferred by this continuous-flow propylene oxide carbonylation pathway. At the core of the process is the heterogeneous epoxide carbonylation catalyst $Co(CO)_4 \subset Cr\text{-}MIL\text{-}101$, which utilizes the porosity,[21-23] synthetic tunability,[24-26] and site uniformity[27-31] intrinsic to its MOF platform to achieve a highly selective catalytic activity. Further optimization of the catalyst structure and process conditions is expected to lead to more efficient carbonylative production of β-butyrolactone, an important precursor to biodegradable PHB plastics.

3.5. Experimental Information

General Considerations

All manipulations of air/water-sensitive compounds were conducted using standard inert-atmosphere glove box and Schlenk line techniques.

Powder X-ray diffraction (PXRD) patterns were recorded on a Bruker Advance II diffractometer equipped with $\theta/2\theta$ Bragg-Brentano geometry and Ni-filtered Cu Kα radiation (Kα_1 = 1.5406 Å). The tube voltage and current were 40 kV and 40 mA, respectively. A thin layer of dry powdered sample was placed on a rotating zero-background silicon crystal plate for analysis.

Energy dispersive X-ray spectroscopy (EDX) analyses were conducted using a JEOL 6010LA analytical scanning electron microscope at 15 keV and a working distance of 10 mm. Dry powdered samples were mounted onto a stage using carbon tape and sputtered with Au prior to analysis.

Attenuated total reflectance infrared (ATR-IR) absorption spectra were acquired using a Bruker Alpha ATR Fourier transform IR spectrometer under an inert atmosphere.

Nitrogen adsorption isotherms were measured by a volumetric method using a Micromeritics ASAP 2020 gas sorption analyzer. ~30 mg of sample was pre-activated at 150°C under vacuum overnight to remove all residual solvent and transferred to a pre-weighed analysis tube in a glove box. The tube containing the sample was weighed again

to determine the mass of the sample, capped with a Micromeritics TranSeal, brought out of the glove box, and transferred to the analysis port of the gas sorption analyzer. Free space correction measurements were performed using an ultra-high purity helium gas (UHP grade, Airgas) and nitrogen isotherms were measured using an ultra-high purity grade nitrogen (UHP grade, Airgas). All nitrogen analyses were performed using a liquid nitrogen bath at 77 K.

Metal content of Cr-MIL-101 and $Co(CO)_4 \subset Cr\text{-}MIL\text{-}101$ samples was quantified using Agilent 7900 inductively coupled plasma mass spectrometer (ICP-MS). ~10 mg sample was weighed in a glove box, transferred to an acid digestion vessel (Model 4749, Parr Instrument Company), and digested in ~3 mL of concentrated nitric acid (67~70% w/v %, BDH Aristar) at 150 °C overnight. Metal concentrations of the resulting solution were determined using calibration curves constructed from standard solutions (ICP-MS certified reference standards, VWR).

Propylene oxide carbonylation reactions were analyzed using ^{1}H-NMR (AVANCE 400 MHz, Bruker) and a gas chromatograph (GC) equipped with a DB-5ms column (30 m × 0.25 mm ID × 0.25 μm, Agilent Technologies) and a flame ionization detector (FID) for quantification (Model 7890A, Agilent Technologies).

Materials

Toluene (99.8% Sigma-Aldrich), methanol (99.8%, Sigma-Aldrich), and tetrahydrofuran (ACS grade, BDH), were passed through two silica columns in a Glass Contour solvent

purification system, degassed with a flow of argon gas for 30 min, subjected to at least three freeze-pump-thaw cycles, and dried over activated molecular sieves prior to use. Propylene oxide (97%, Alfa Aesar) and mesitylene ($\geq$99.8% analytical standard, Sigma-Aldrich) were stirred over $\geq$5 w/v % calcium hydride for a minimum of three days, vacuum transferred, and degassed by at least three freeze-pump-thaw cycles prior to use. Methyl *tert*-butyl ether (anhydrous, 99.8%, Sigma-Aldrich) and 1,2,34-tetrahydronaphthalene (anhydrous, 99%, Sigma-Aldrich) were degassed by at least three freeze-pump-thaw cycles prior to use. Glass beads (1 mm diameter, EMD Millipore), Silicon carbide powder (320 grit, Alfa Aesar), and quartz wool (Fine, Chemglass Inc.) were dried in a convection oven overnight at 120 °C prior to use. β-Butyrolactone (98%, Sigma-Aldrich), carbon monoxide (Research grade 4.0, Airgas), and argon (Research grade 5.7, Airgas) were used as received. The following were prepared and characterized according to literature procedure[1,2]: Cr-MIL-101, Na[Co(CO)$_4$], and Co(CO)$_4$$\subset$Cr-MIL-101.

Experimental Details

Continuous-flow Propylene Carbonylation with Co(CO)$_4$$\subset$Cr-MIL-101: A typical procedure involved mixing the specified amount of Co(CO)$_4$$\subset$Cr-MIL-101 with ~800 mg of silicon carbide powder in an inert-atmosphere glove box and packing the solid mixture between two quartz wool plugs in a stainless-steel tubing segment (OD 6.35 mm, wall thickness 0.89 mm, Grainger). A thermocouple probe (KQXL-116, Omega) was mounted downstream in direct contact with the end of the catalyst bed for temperature monitoring. Void space within the tubing segment was filled with glass beads to minimize dead volume prior to isolating the packed tubing segment using valves. Propylene oxide substrate,

1,2,3,4-tetrahydronaphthalene standard, and solvent were also charged into a stainless-steel sample cylinder (304L-05SF4-150, Swagelok) in the glove box and isolated using valves. Packed tubing segment and liquid feed cylinder were then transferred out of the glove box and connected to a custom-built flow reaction setup (Figure 3.S10) equipped with a CO mass flow controller (5850E, Brooks Instruments), an oxygen trap (304L-HDF4-150, Swagelok) filled with pre-reduced Cu catalyst (8 x 14 mesh Q-5, Research Catalysts), a water trap filled with CaH_2 ($\geq$97%, Sigma-Aldrich), a liquid delivery pump (Series III, Scientific Systems), a single-zone furnace (Carbolite, GTF 11/50/150B) connected to a temperature controller (Digi-Sense, 68900), a single-stage gas/liquid separator (Series 20, Jerguson), a pressure gauge (PGI series, Swagelok), and a back-pressure regulator (KPB1L, Swagelok). Headspace of the liquid feed cylinder was blanketed by a continuous flow of argon through a bubbler to maintain an inert-atmosphere throughout the reaction. The reactor setup was first pressurized to the desired pressure of CO using a back-pressure regulator and allowed to stabilize to the specified flow of CO at the desired temperature. Liquid feed was then allowed to flow through the packed catalyst bed at the specified flowrate, upon which periodic liquid-phase samples were taken from the liquid-phase outlet of the gas/liquid separator. Quantification of collected samples was carried out based on GC-FID calibration curves constructed from calibration samples with weighed amounts of propylene oxide substrate, product β-butyrolactone, and mesitylene or 1,2,3,4-tetrahydronaphthalene standard in respective solvents (Figure 3.S6).

Characterization of Spent Co(CO)₄⊂Cr-MIL-101: A typical procedure involved recovering the spent catalyst from a continuous-flow carbonylation reaction after the

specified amount of time on stream by stopping the flow of reactants through the bed and isolating the packed tubing segment using valves. The isolated segment was then brought into the glove box, connected to a vacuum pump, and was opened to vacuum to remove the reactants and solvent occupying the packed tubing segment. The tubing segment was subsequently cut open to recover the catalyst bed and the catalyst was separated from the inert silicon carbide powder using sieves. The recovered catalyst was subjected to ATR-IR analysis in the glove box and PXRD analysis under ambient atmosphere. As a comparison, reactant-exposed catalyst was prepared by inserting a small open vial holding the fresh catalyst into a larger vial holding ~3 ml of the reactant epoxide in the glove box and sealing the larger vial with a cap. The fresh catalyst was thereby exposed to an atmosphere of the reactant epoxide for ~1 h, after which the catalyst was recovered and subjected to ATR-IR analysis in the glove box. A fresh sample of catalyst that was briefly washed with the reactant epoxide also showed an ATR-IR spectrum closely resembling that of the catalyst exposed to an atmosphere of the epoxide.
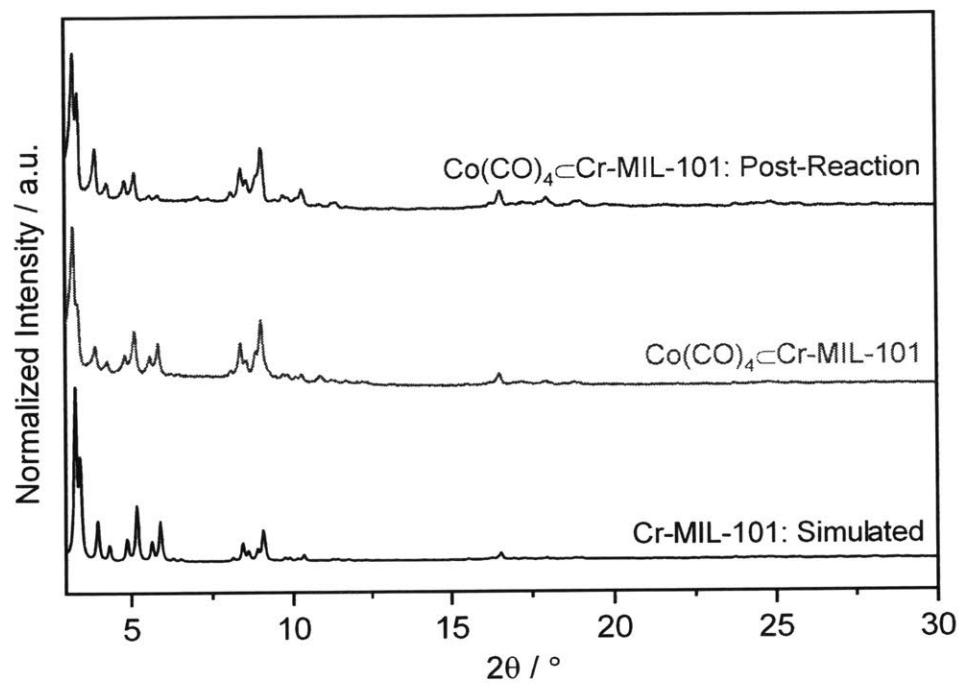
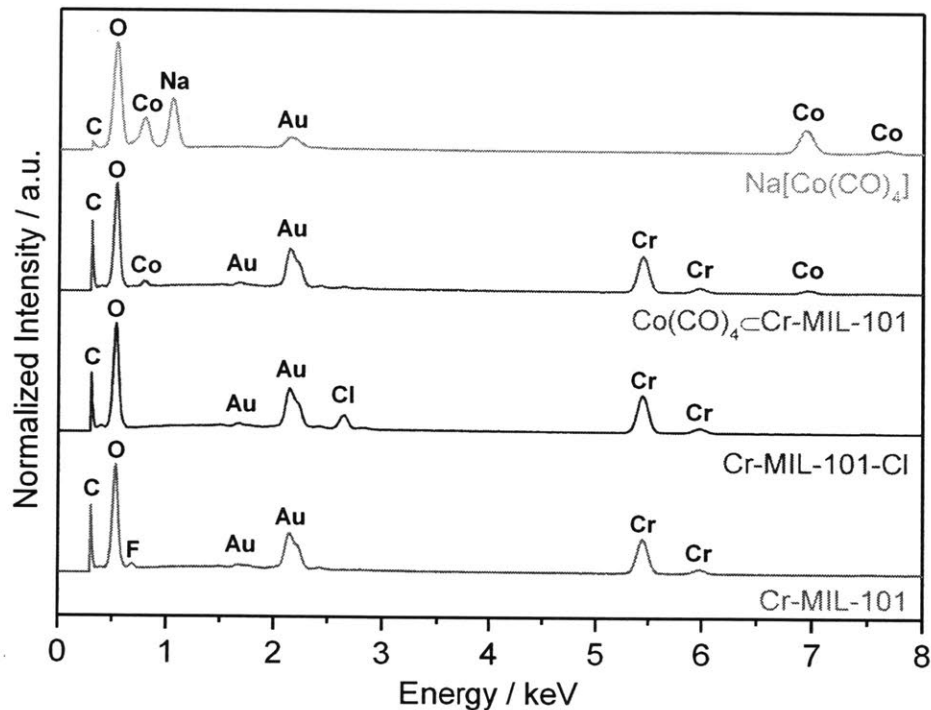**Figure 3.S1**. PXRD patterns of simulated Cr-MIL-101, Co(CO)₄⊂Cr-MIL-101, and post-reaction Co(CO)₄⊂Cr-MIL-101.

Figure 3.S2. EDX spectra of Cr-MIL-101, Cr-MIL-101-Cl, $Co(CO)_4 \subset Cr$-MIL-101, and $Na[Co(CO)_4]$. $Co(CO)_4 \subset Cr$-MIL-101 was prepared from $Na[Co(CO)_4]$ treatment of Cr-MIL-101-Cl, which was in turn obtained from $AlCl_3$ treatment of Cr-MIL-101. Incorporation of $Co(CO)_4^-$ into $Co(CO)_4 \subset Cr$-MIL-101 is evidenced by the presence of Co Kα (6.92 keV) and Co Lα (0.78 keV) peaks and the absence of Na Kα (1.04 keV), Cl Kα (2.62 keV), and F Kα (0.68 keV) peaks in the spectrum of $Co(CO)_4 \subset Cr$-MIL-101. All samples were sputtered with Au prior to analysis.

Figure 3.S3. ATR-IR spectra of Cr-MIL-101 and Co(CO)$_4$⊂Cr-MIL-101. Single band at 1890 cm^{-1} remained after repeated overnight washes with stirring in tetrahydrofuran (50 mL per 20 mg of Co(CO)$_4$⊂Cr-MIL-101), a solvent that readily solubilizes the Na[Co(CO)$_4$] salt. This band corresponds well to the characteristic carbonyl stretching mode of the tetrahedral Co(CO)$_4^-$ ion in various metal complexes, including those reported for the homogeneous [Lewis acid]$^+$[Co(CO)$_4$]$^-$ carbonylation catalysts.
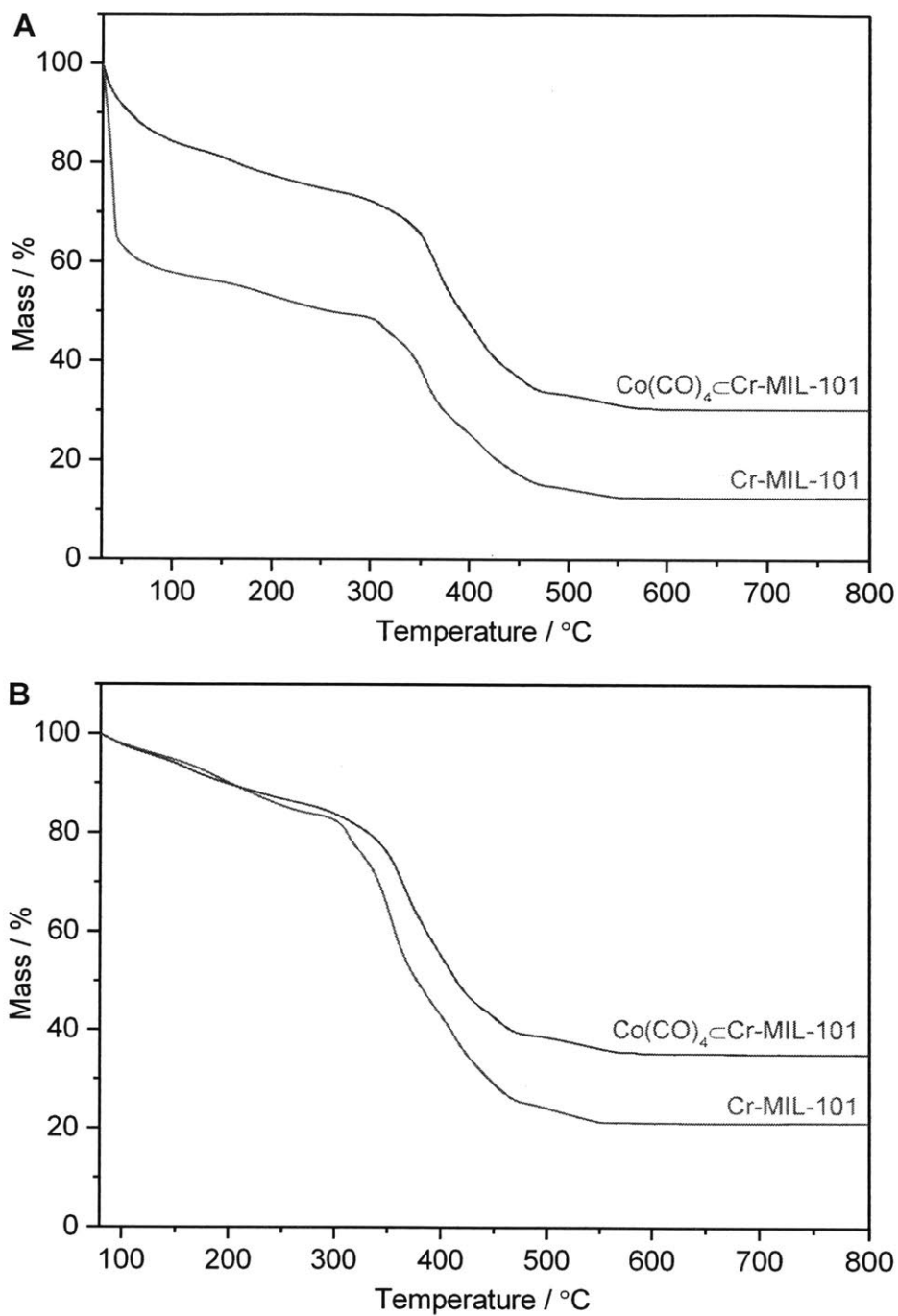
Figure 3.S4. TGA curves of Cr-MIL-101 and Co(CO)$_4$⊂Cr-MIL-101: (A) mass measurements normalized to initial mass at 30 °C and (B) mass measurements normalized to mass at 80 °C. Both samples were subjected to an overnight wash in tetrahydrofuran and subsequent filtration prior to analysis. Analysis was conducted at a heat ramp of 1 °C/min from 30 °C to 800 °C under a flow of nitrogen.
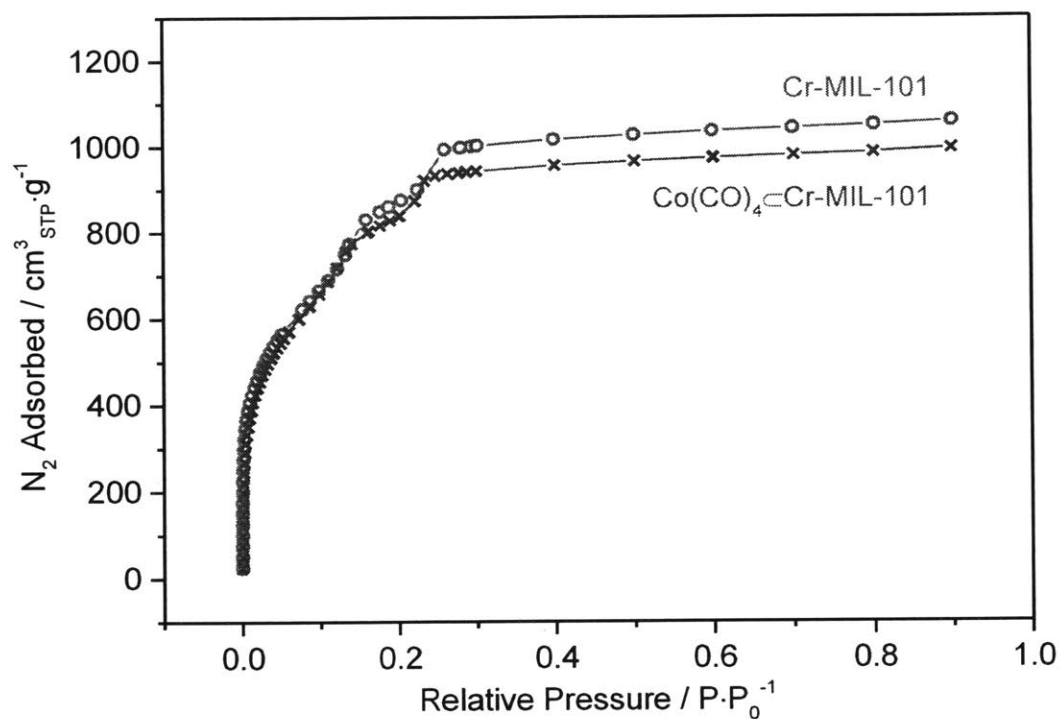
Figure 3.S5. Nitrogen adsorption isotherms of Cr-MIL-101 and Co(CO)$_4$⊂Cr-MIL-101 after outgassing under vacuum (10^{-5} torr) at 150 °C for 18 h. Calculated BET surface areas for Cr-MIL-101 and Co(CO)$_4$⊂Cr-MIL-101 were 3,450 ± 80 m²/g and 3,270 ± 46 m²/g, respectively. Surface areas were derived by fitting the BET equation to the acquired isotherm over the range of 0.05 ≤ P/P$_0$ ≤ 0.2.

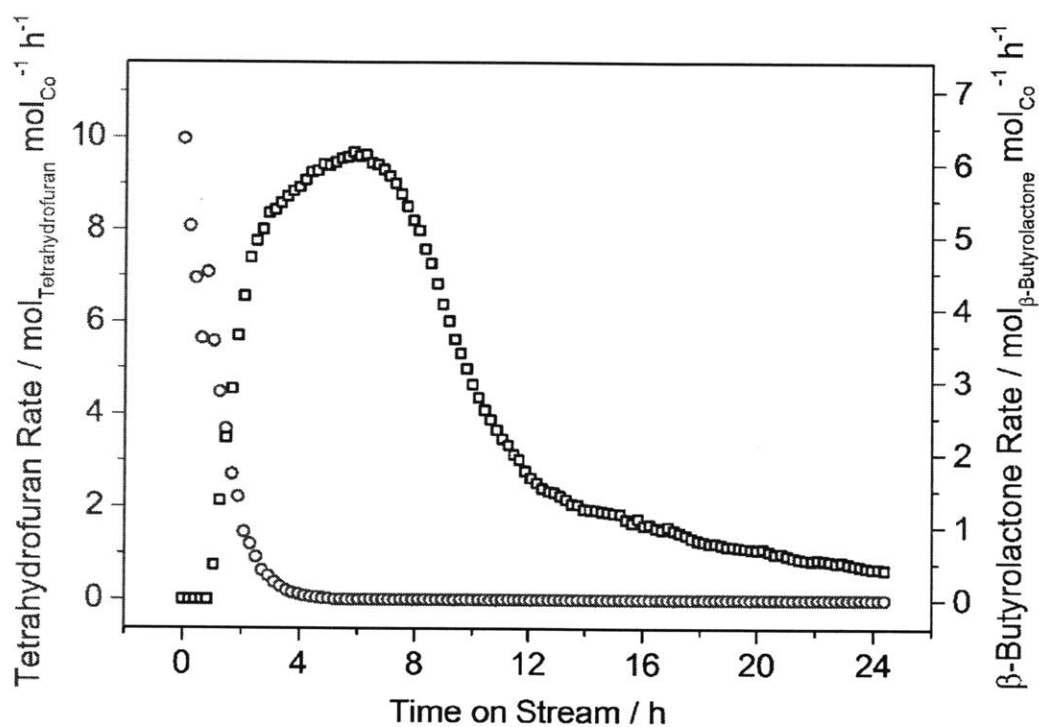**Figure 3.S6**. Gas-phase flow carbonylation of propylene oxide to β-butyrolactone with Co(CO)$_4$⊂Cr-MIL-101. Reaction conditions: propylene oxide (0.02%) / CO (balance) (mol %) at 20 bar of total pressure and 70 °C; total flow rate of 125 mL/min (at STP). Tetrahydrofuran was used to wash the catalyst prior to reaction.
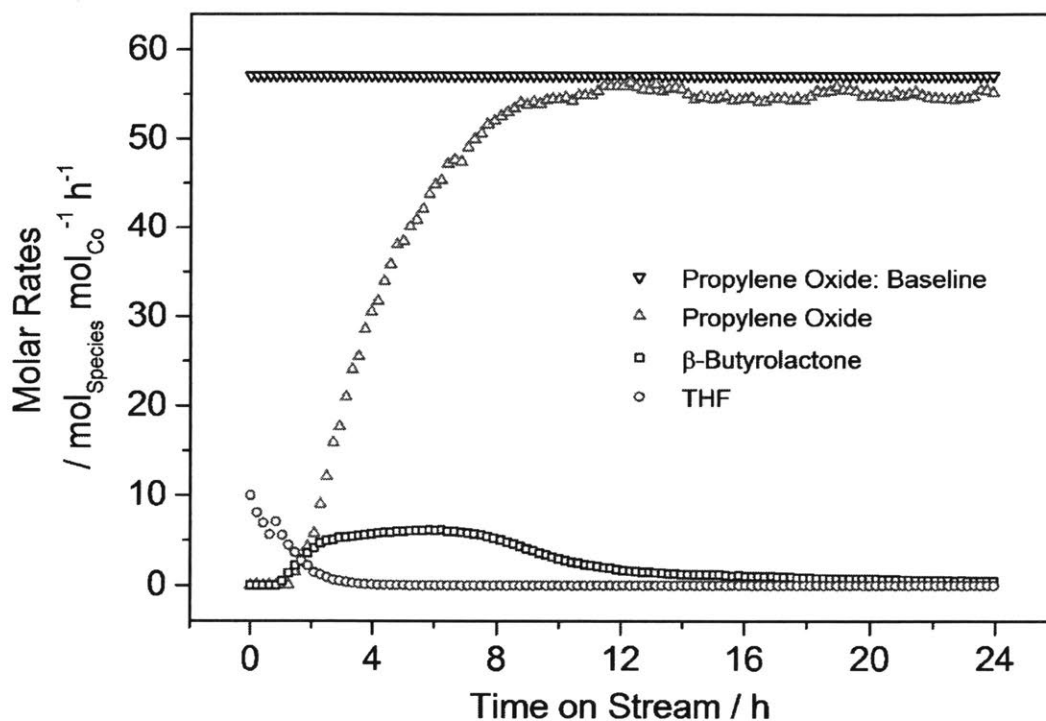
Figure 3.S7. Gas-phase flow carbonylation of propylene oxide to β-butyrolactone with $Co(CO)_4 \subset Cr$-MIL-101. Reaction conditions: propylene oxide (0.02%) / CO (balance) (mol %) at 20 bar of total pressure and 70 °C; total flow rate of 125 mL/min (at STP). Tetrahydrofuran was used to wash the catalyst prior to reaction. Noticeable deficit in carbon balance observed with appreciable propylene oxide carbonylation activity.
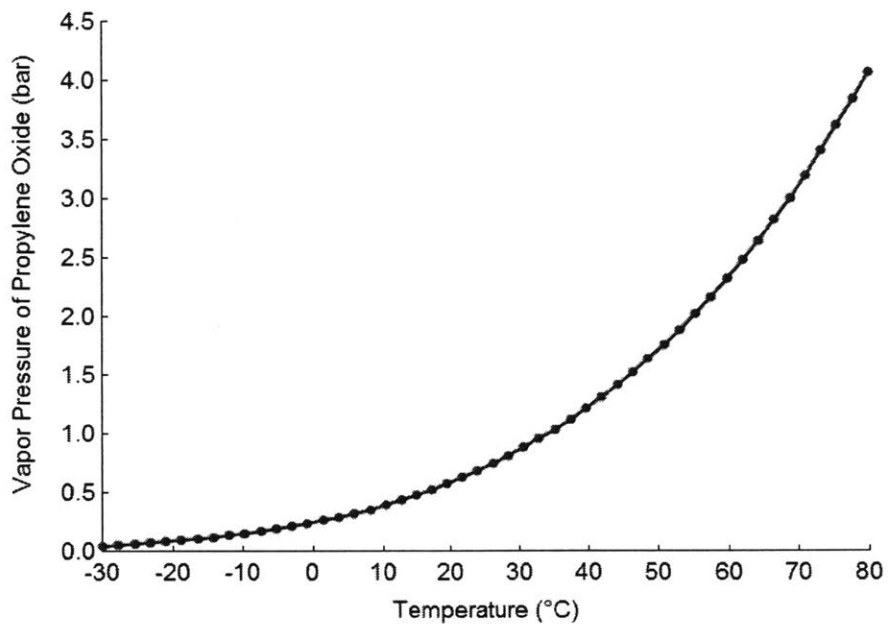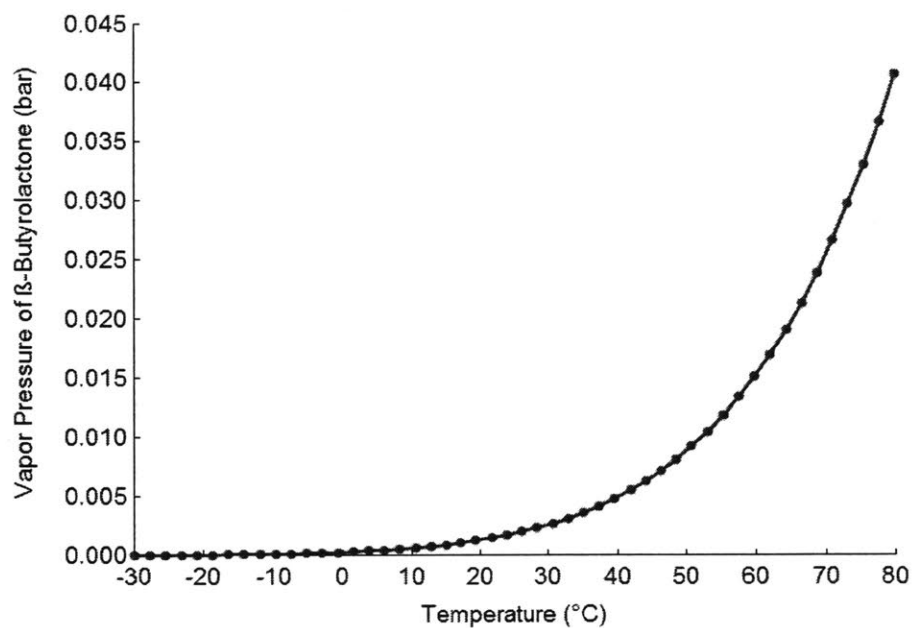
Figure 3.S8. Vapor pressure curves of β-butyrolactone and propylene oxide derived using physical properties analysis tool in Aspen Plus® software. Note the hundred-fold difference in the y-axis vapor pressure values.
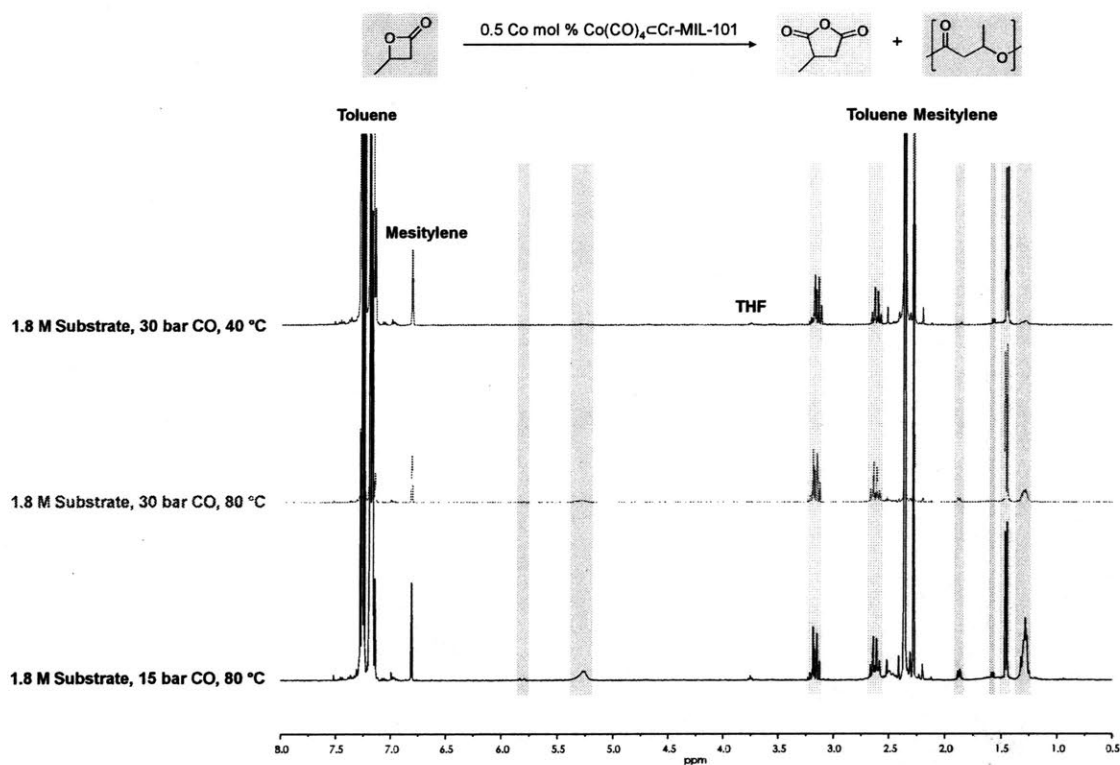
Figure 3.S9. ¹H-NMR spectra of product mixtures from batch carbonylation of β-butyrolactone by $Co(CO)_4 \subset Cr$-MIL-101 under various reaction conditions. Reaction times varied to reach >75% substrate conversion under all conditions. Mesitylene used as a standard for quantification.
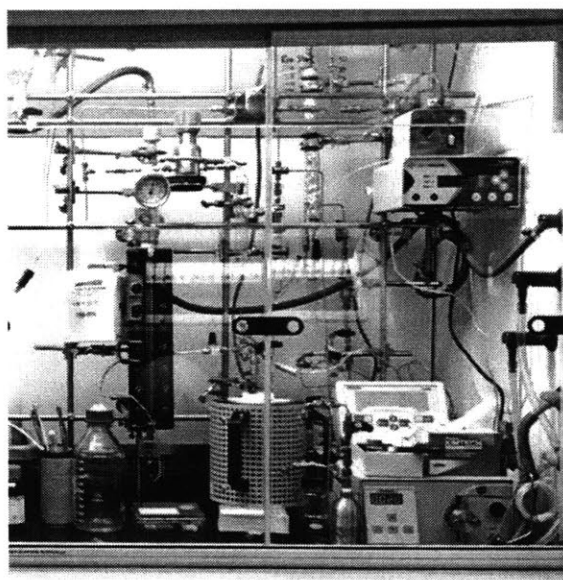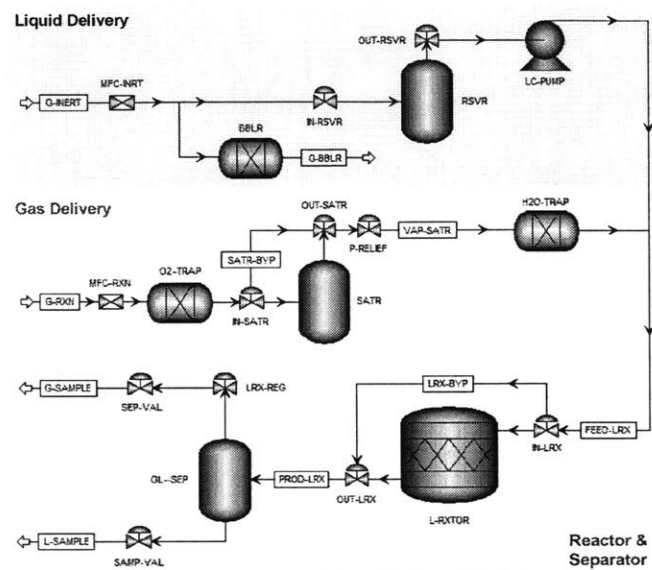
Figure 3.S10. Process flow diagram and experimental setup of the packed-bed reactor process for gas-liquid flow propylene oxide carbonylation.
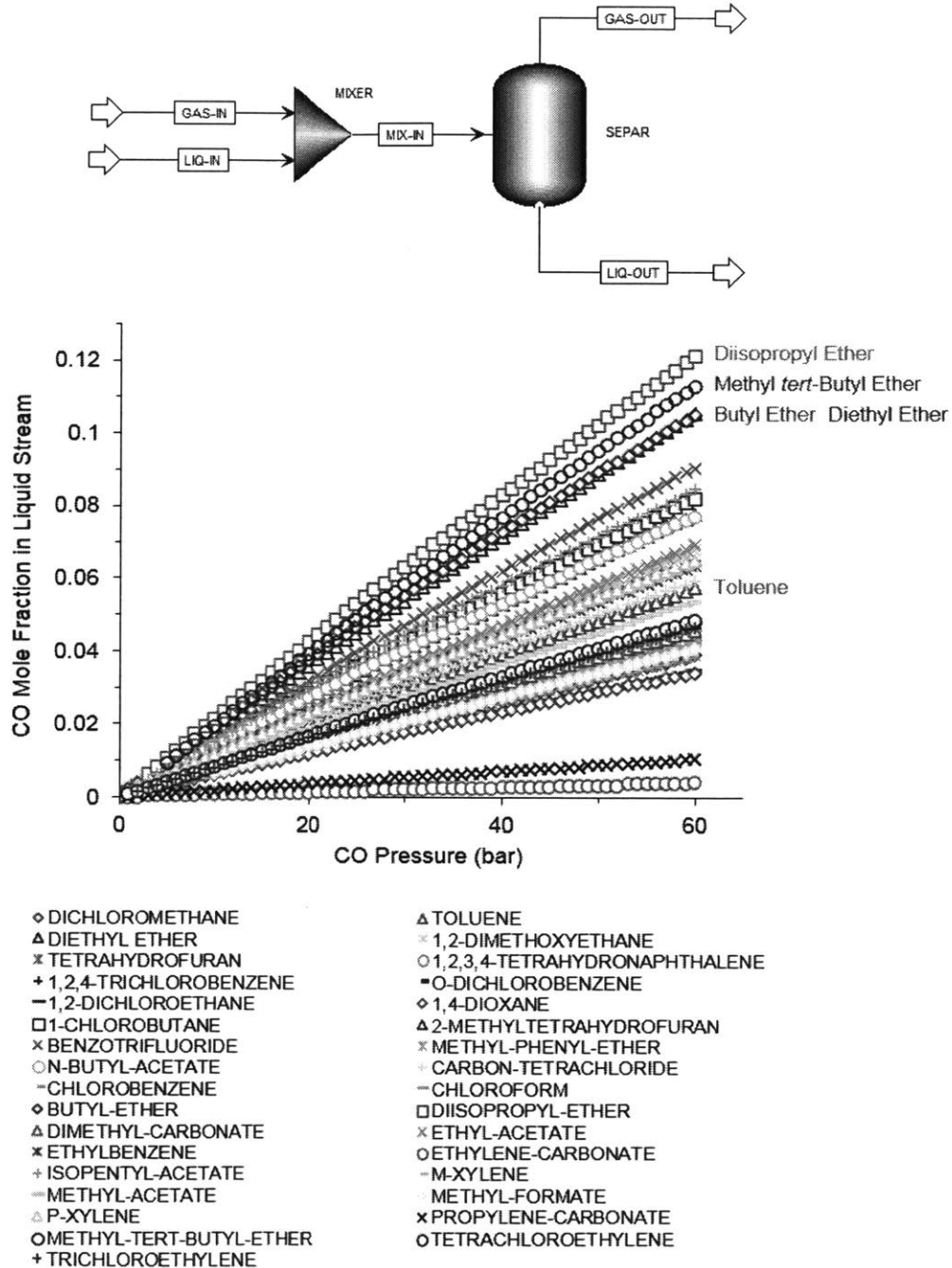
Figure 3.S11. Aspen Plus® software model for CO and solvent separations (above) and sensitivity analysis for CO mole fraction in the liquid stream against CO pressure of the SEPAR block (below). Model specifications: molar flowrate of CO/molar flowrate of solvent = 10, input streams and SEPAR block held at 25 °C, and calculations with Soave-Redlich-Kwong equation of state.
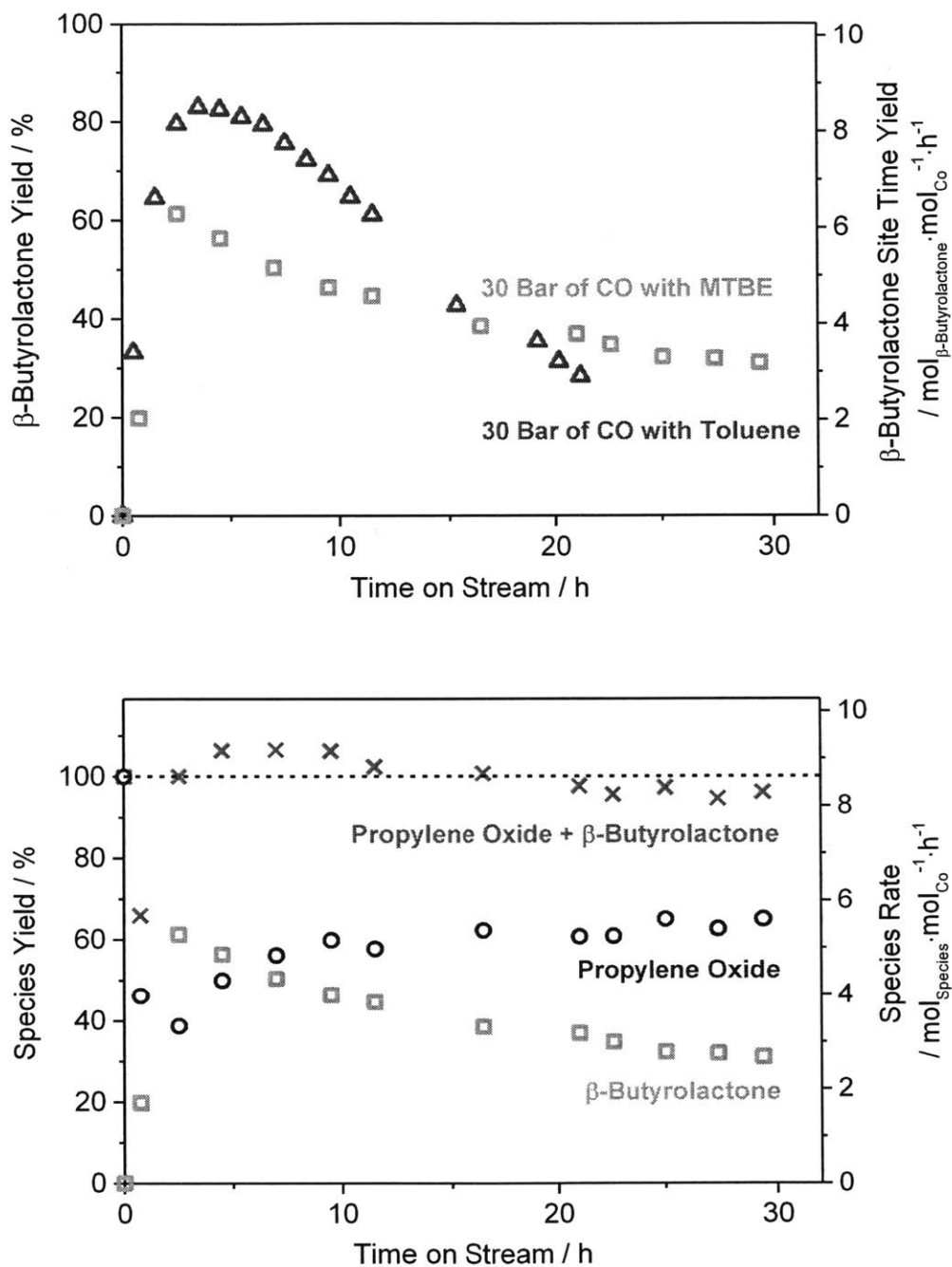
Figure 3.S12. Gas-liquid flow carbonylation of propylene oxide by $Co(CO)_4 \subset Cr\text{-}MIL\text{-}101$ with toluene or MTBE (above) and molar rates and yields of reaction species from a reaction in MTBE (below). Reaction conditions: 0.02 mL/min of 0.1 M propylene oxide in toluene or MTBE, 30 mL/min (at STP) of CO at 30 bar, and 25 mg of catalyst at 22 °C.

Table 3.S1. ICP-MS Analysis of Cr-MIL-101, Co(CO)$_4$⊂Cr-MIL-101, and Na[Co(CO)$_4$]

Sample	Cr (wt. %)	Co (wt. %)	Na (wt. %)
Cr-MIL-101[a]	22.1	Not detected	Not detected
Co(CO)$_4$⊂Cr-MIL-101[b]	14.8	3.0	0.02
Na[Co(CO)$_4$][b]	Not detected	30.4	12.2

[a] dried under vacuum at 150 °C. [b] dried under vacuum at ambient temperature.

3.7. References

(1) Geyer, R.; Jambeck, J. R.; Law, K. L. Production, Use, and Fate of All Plastics Ever Made. *Sci. Adv.* **2017**, *3*, 19–24.

(2) Recycle rate of polypropylene was derived from the United States municipal solid waste figures from 2015 as reported in *Advancing Sustainable Materials Management: 2015 Tables and Figures*; EPA530-F-18-004; U.S. Environmental Protection Agency, Office of Land and Emergency Management: Washington, DC, 2018.

(3) Poirier, Y.; Nawrath, C.; Somerville, C. Production of Polyhydroxyalkanoates, a Family of Biodegradable Plastics and Elastomers, in Bacteria and Plants. *Nat. Biotechnol.* **1995**, *13*, 142–150.

(4) Sim, S. J.; Snell, K. D.; Hogan, S. A.; Stubbe, J.; Rha, C.; Sinskey, A. J. PHA Synthase Activity Controls the Molecular Weight and Polydispersity of Polyhydroxybutyrate in vivo. *Nat. Biotechnol.* **1997**, *15*, 63–67.

(5) Chen, G. A Microbial Polyhydroxyalkanoates (PHA) Based Bio- and Materials Industry. *Chem. Soc. Rev.* **2009**, *38*, 2434–2446.

(6) Li, Z.; Loh, X. J. Water Soluble Polyhydroxyalkanoates: Future Materials for Therapeutic Applications. *Chem. Soc. Rev.* **2015**, *44*, 2865–2879.

(7) Wang, Y.; Yin, J.; Chen, G. Polyhydroxyalkanoates, Challenges and Opportunities. *Curr. Opin. Biotechnol.* **2014**, *30*, 59–65.

(8) DiGregorio, B. E. Biobased Performance Bioplastic: Mirel. *Chem. Biol.* **2009**, *16*, 1–2.

(9) Thomas, C. M. Stereocontrolled Ring-opening Polymerization of Cyclic Esters: Synthesis of New Polyester Microstructures. *Chem. Soc. Rev.* **2010**, *39*, 165–173.

(10) Ajellal, N.; Carpentier, J. F.; Guillaume, C.; Guillaume, S. M.; Helou, M.; Poirier, V.; Sarazin, Y.; Trifonov, A. Metal-catalyzed Immortal Ring-opening Polymerization of Lactones, Lactides and Cyclic Carbonates. *Dalt. Trans.* **2010**, *39*, 8363–8376.

(11) Church, T. L.; Getzler, Y. D. Y. L.; Byrne, C. M.; Coates, G. W. Carbonylation of Heterocycles by Homogeneous Catalysts. *Chem. Commun.* **2007**, *7*, 657–674.

(12) Church, T. L.; Getzler, Y. D. Y. L.; Coates, G. W. The Mechanism of Epoxide Carbonylation by [Lewis acid]$^+$[Co(CO)$_4$]$^-$ Catalysts. *J. Am. Chem. Soc.* **2006**, *128*, 10125–10133.

(13) Park, H. D.; Dincă, M.; Román-Leshkov, Y. Heterogeneous Epoxide Carbonylation by Cooperative Ion-pair Catalysis in Co(CO)$_4$$^-$-incorporated Cr-MIL-101. *ACS Cent. Sci.* **2017**, *3*, 444–448.

(14) Cr site density was calculated based on the formula weight (683.4 g/mol) and density (0.44 g/cm^3) of Cr-MIL-101 as reported in Furukawa, H; Cordova, K. E.; O'Keefe, M.; Yaghi, O. M. The Chemistry and Applications of Metal–Organic

Frameworks. *Science* **2013**, *341*, 123044–123057.

(15) Park, H. D.; Dincă, M.; Román-Leshkov, Y. Continuous-flow Production of Succinic Anhydrides via Catalytic β-Lactone Carbonylation by Co(CO)$_4$⊂Cr-MIL-101. *J. Am. Chem. Soc.* **2018**, *140*, 10669–10672.

(16) Pommier, A.; Pons, J. M. Recent Advances in β-Lactone Chemistry. *Synthesis* **1993**, *5*, 441–459.

(17) Liu, Q.; Ning, L.; Zheng, S.; Tao, M.; Shi, Y.; He, Y. Adsorption of Carbon Dioxide by MIL-101(Cr): Regeneration Conditions and Influence of Flue Gas Contaminants. *Sci. Rep.* **2013**, *3*, 2916.

(18) Kovács, I.; Ungváry, F. Synthesis, Characterization and Reactions of Acylcobalt Carbonyl Complexes, RC(O)Co(CO)$_{4-n}$L$_n$ (n = 0, 1, 2, 3). *Coord. Chem. Rev.* **1997**, *161*, 1–32.

(19) Massick, S. M.; Rabor, J. G.; Elbers, S.; Marhenke, J.; Bernhard, S.; Schoonover, J. R.; Ford, P. C. Time-Resolved Infrared Spectroscopic Study of Reactive Acyl Intermediates Relevant to Cobalt-Catalyzed Carbonylations. *Inorg. Chem.* **2000**, *39*, 3098–3106.

(20) International Union of Pure and Analytical Chemistry, Analytical Chemistry Division, Commision on Solubility Data. *Solubility Data Series*; Oxford, United Kingdom, 1990; Vol. 43.

(21) Li, Z.; Rayder, T. M.; Luo, L.; Byers, J. A.; Tsung, C. K. Aperture-opening Encapsulation of a Transition Metal Catalyst in a Metal–Organic Framework for CO$_2$ Hydrogenation. *J. Am. Chem. Soc.* **2018**, *140*, 8082–8085.

(22) Ji, P.; Song, Y.; Drake, T.; Veroneau, S. S.; Lin, Z.; Pan, X.; Lin, W. Titanium(III)-oxo Clusters in a Metal–Organic Framework Support Single-site Co(II)-hydride Catalysts for Arene Hydrogenation. *J. Am. Chem. Soc.* **2018**, *140*, 433–440.

(23) Zhang, Y.; Zhang, X.; Lyu, J.; Otake, K. I.; Wang, X.; Redfern, L. R.; Malliakas, C. D.; Li, Z.; Islamoglu, T.; Wang, B.; Farha, O. K. A Flexible Metal–Organic Framework with 4-connected Zr$_6$ Nodes. *J. Am. Chem. Soc.* **2018**, *140*, 11179–11183.

(24) Niu, Z.; Gunatilleke, W. D. C. B.; Sun, Q.; Lan, P. C.; Perman, J.; Ma, J.-G.; Cheng, Y.; Aguila, B.; Ma, S. Metal–Organic Framework Anchored with a Lewis Pair as a New Paradigm for Catalysis. *Chem* **2018**, *4*, 2587–2599.

(25) Chen, X.; Jiang, H.; Hou, B.; Gong, W.; Liu, Y.; Cui, Y. Boosting Chemical Stability, Catalytic Activity, and Enantioselectivity of Metal–Organic Frameworks for Batch and Flow Reactions. *J. Am. Chem. Soc.* **2017**, *139*, 13476–13482.

(26) Kalmutzki, M. J.; Hanikel, N.; Yaghi, O. M. Secondary Building Units as the Turning Point in the Development of the Reticular Chemistry of MOFs. *Sci. Adv.* **2018**, *4*, eaat9180

(27) Wright, A. M.; Wu, Z.; Zhang, G.; Mancuso, J. L.; Comito, R. J.; Day, R. W.; Hendon,

C. H.; Miller, J. T.; Dincă, M. A Structural Mimic of Carbonic Anhydrase in a Metal–Organic Framework. *Chem* **2018**, *4*, 2894–2901.

(28) Qin, J. S.; Yuan, S.; Lollar, C.; Pang, J.; Alsalme, A.; Zhou, H. C. Stable Metal–Organic Frameworks as a Host Platform for Catalysis and Biomimetics. *Chem. Commun.* **2018**, *54*, 4231–4249.

(29) Osadchii, D. Y.; Olivos-Suarez, A. I.; Szécsényi, Á.; Li, G.; Nasalevich, M. A.; Dugulan, I. A.; Crespo, P. S.; Hensen, E. J. M.; Veber, S. L.; Fedin, M. V.; Sankar, G.; Pidko, E. A.; Gascon, J. Isolated Fe sites in Metal Organic Frameworks Catalyze the Direct Conversion of Methane to Methanol. *ACS Catal.* **2018**, *8*, 5542–5548.

(30) Rojas-Buzo, S.; García-García, P.; Corma, A. Hf-based Metal–Organic Frameworks as Acid–base Catalysts for the Transformation of Biomass-derived Furanic Compounds into Chemicals. *Green Chem.* **2018**, *20*, 3081–3091.

(31) Sun, C.; Skorupskii, G.; Dou, J. H.; Wright, A. M.; Dincă, M. Reversible Metalation and Catalysis with a Scorpionate-like Metallo-Ligand in a Metal–Organic Framework. *J. Am. Chem. Soc.* **2018**, *140*, 17394–17398.

Chapter 4

Continuous-flow Production of Succinic Anhydride via
Catalytic β-Lactone Carbonylation by Co(CO)₄⊂Cr-MIL-101

4.1. Abstract

Industrial synthesis of succinic acid relies on hydrocarbon oxidation or biomass fermentation routes that suffer from energy-costly separation processes. Here we demonstrate an alternate route to succinic anhydrides via β-lactone carbonylation by heterogeneous bimetallic ion-pair catalysis in Co(CO)₄⁻-incorporated Cr-MIL-101 (Co(CO)₄⊂Cr-MIL-101, Cr-MIL-101 = Cr₃O(BDC)₃F, H₂BDC = 1,4-benzenedicarboxylic acid). Postsynthetically introduced Co(CO)₄⁻ facilitates CO insertion to β-lactone substrates activated by the Lewis acidic Cr(III) centers of the metal–organic framework (MOF), leading to catalytic carbonylation with activity and selectivity profiles that compare favorably to those reported for homogeneous ion-pair catalysts. Moreover, the heterogeneous nature of the MOF catalyst enables continuous production of succinic anhydride through a packed bed reactor, with room temperature β-propiolactone carbonylation activity of 1,300 mol$_{Anhydride}$·mol$_{Co}^{-1}$ over 6 h on stream. Simple evaporation of the fully converted product stream yields the desired anhydride as isolated solids,

highlighting the unique processing advantages conferred by this first example of heterogeneous β-lactone carbonylation pathway.

4.2. Introduction

As a representative four-carbon diacid, succinic acid is finding increasingly wide use as a precursor to high-value products in polymer,[1] food,[2] agriculture,[3] and pharmaceutical[4] industries. Its production, however, has traditionally depended on the energy-intensive benzene or n-butane oxidation pathway that features high operating temperatures,[5] limited yields of ~60% due to side oxidation reactions,[6] and incineration of waste gases owing to difficult separation of unreacted substrates.[7] To address this issue, the United States Department of Energy named succinic acid as the first chemical on its list of twelve "Top Value Added Chemicals From Biomass" and fostered the development of milder fermentative routes to succinic acids.[8] There has since been significant progress in the development of commercial-scale fermentation processes to succinates, giving rise to numerous processes with kilotonne-scale annual capacities.[9] Nonetheless, microbial fermentation processes present their own challenges, namely, undesired metabolic flux to byproducts[10] and costly product separation and purification from the fermentation broth that can account for up to 60–70% of the total production cost.[11]

Heterogeneous β-lactone carbonylation is a process that can potentially circumvent current limitations in hydrocarbon oxidation and microbial fermentation pathways. Due to their inherent ring strain, the four-membered β-lactone cycles undergo selective ring-

expanding carbonylation to succinic anhydrides under conditions much milder than those of the hydrocarbon oxidation process.[12] Facile recovery of the carbonylated product from the solid catalyst and solvent avoids energy-intensive separations from the fermentation broth required in fermentative processes. In addition, ready availability of β-lactone substrates from industrially accessible epoxides further underscores the intrinsic advantages of the heterogeneous β-lactone carbonylation strategy.[13]

Herein, we report $Co(CO)_4^-$-incorporated Cr-MIL-101 ($Co(CO)_4 \subset$Cr-MIL-101, Cr-MIL-101 = $Cr_3O(BDC)_3F$, H_2BDC = 1,4-benzenedicarboxylic acid) as the first heterogeneous catalyst for the selective ring-expansion carbonylation of β-lactones to succinic anhydrides. Competitive activity and selectivity profiles under mild conditions, along with ease of continuous-flow operation and product separations showcase the unique advantages of $Co(CO)_4 \subset$Cr-MIL-101. More importantly, these results stand to illustrate the potential of the heterogeneous β-lactone carbonylation pathway as a viable route to large-scale production of succinic anhydrides.

4.3. Results and Discussion

Our initial discovery of β-lactone carbonylation by $Co(CO)_4 \subset$Cr-MIL-101 was guided by mechanistic studies on heterocycle carbonylation by homogeneous [Lewis acid]$^+$[Co(CO)$_4$]$^-$ ion-pair catalysts. It has been proposed that β-lactone carbonylation by [Lewis acid]$^+$[Co(CO)$_4$]$^-$ follows a mechanism analogous to that of epoxide carbonylation: (1) substrate activation by [Lewis acid]$^+$, (2) ring opening by $Co(CO)_4^-$, (3) CO insertion,

and (4) product extrusion (Figure 4.1A).[14] Based on this mechanistic similarity, we hypothesized that our previously reported Co(CO)$_4$⊂Cr-MIL-101, a metal–organic framework (MOF)-based epoxide carbonylation catalyst featuring Lewis acidic Cr(III) secondary building units ion-paired with postsynthetically exchanged Co(CO)$_4^-$ (Figure 4.1B), would also be able to carbonylate β-lactones to succinic anhydrides.[15] We reasoned that the structural properties of Cr-MIL-101 found favorable for epoxide carbonylation would also be advantageous for β-lactone carbonylation: high surface area, large pore openings (12 Å and 16 Å) and pore diameters (29 Å and 34 Å) for low diffusional barrier to active sites, and high chemical and thermal stability for robust catalysis.[16] Synthetic accessibility of the catalyst through relatively inexpensive chromium, cobalt, and terephthalic acid precursors also distinguished Co(CO)$_4$⊂Cr-MIL-101 as an attractive candidate for use in the industrially-relevant β-lactone carbonylation.

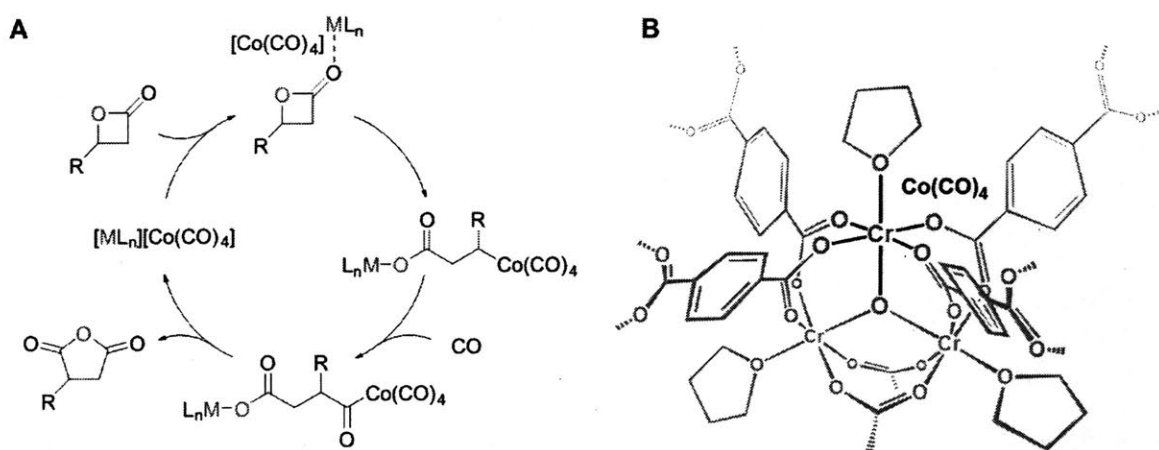**Figure 4.1.** (A) Proposed catalytic cycle for the ring-expansion carbonylation of β-lactones by [Lewis acid]$^+$[Co(CO)$_4$]$^-$.[14] (B) Illustration of the metal cluster structure of Co(CO)$_4$⊂Cr-MIL-101 with coordinated tetrahydrofuran molecules.[15]

Co(CO)$_4$⊂Cr-MIL-101 was prepared as previously reported (Figures 4.S1–S5 and Table 4.S1) and subjected to batch-wise carbonylation reactions with β-butyrolactone as a model substrate. When Co(CO)$_4$⊂Cr-MIL-101 loaded at 0.5 Co mol % with respect to the substrate was exposed to a 1.8 M solution of β-butyrolactone in toluene and 15 bar of CO at 80 °C for 24 h, full conversion of the substrate was observed, in line with what was reported for the homogenous catalyst [(salph)Al(THF)$_2$][Co(CO)$_4$] (salph = N,N'-o-phenylenebis(3,5-di-tert-butylsalicylideneimine), THF = tetrahydrofuran).[17] However, the product solution contained not only the desired methylsuccinic anhydride, but also poly(3-hydroxybutyrate) as a major side product (Figure 4.S6). Mixed formation of both the anhydride and the poly(lactone) has been reported for a number of [Lewis acid]$^+$[Co(CO)$_4$]$^-$ catalysts. It is the result of a competitive reaction where subsequent to substrate ring-opening, CO insertion leads to the desired carbonylation cycle while the alternative β-lactone insertion propagates the polymerization reaction (Figure 4.1A).[14] Given the competitive nature of the two parallel pathways, we sought to increase selectivity to the desired anhydride product by exploiting the differences in the reaction kinetics of the carbonylation and polymerization pathways. To this effect, reaction conditions were altered as follows: (1) substrate concentration was lowered to suppress β-lactone monomer propagation, (2) CO pressure was increased to promote CO insertion, and (3) reaction temperature was lowered to favor carbonylation featuring a presumably lower activation barrier (Figure 4.2).[14,18] These manipulations combined to promote a clear preference for the carbonylation pathway, with the selectivity for anhydride reaching ~87% under optimized conditions (Figures 4.2 and 4.S6).
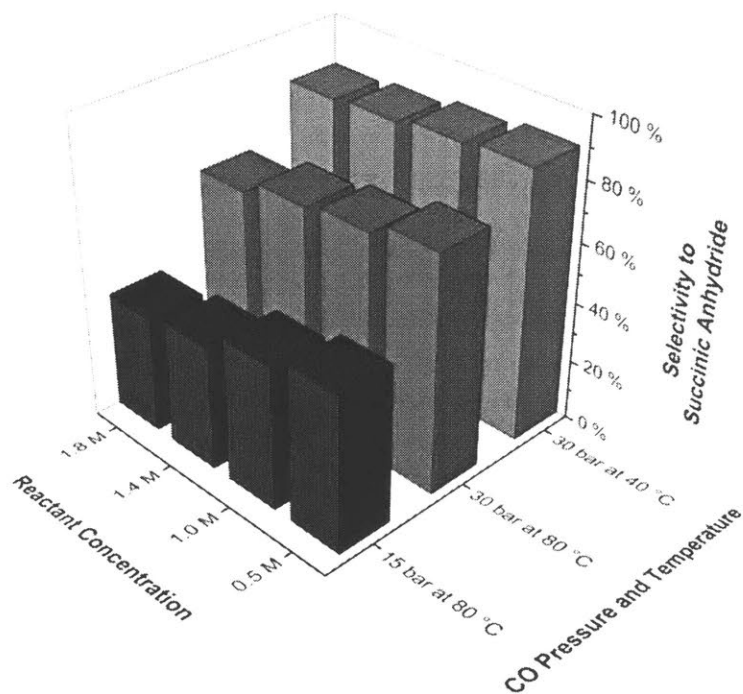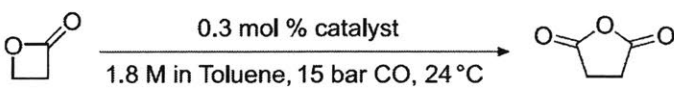
Figure 4.2. Selectivity to succinic anhydride as a function of the reaction conditions for batch carbonylation of β-butyrolactone by Co(CO)$_4$⊂Cr-MIL-101. Catalyst loaded at 0.5 Co mol % to the substrate in toluene and allowed to react for >75% conversion of the substrate under all conditions tested.

Selective carbonylation activity observed with the β-butyrolactone substrate led us to conduct subsequent studies using β-propiolactone to examine the applicability of Co(CO)$_4$⊂Cr-MIL-101 for the synthesis of the commercially-desirable unsubstituted succinic anhydride. Remarkably, when Co(CO)$_4$⊂Cr-MIL-101 loaded at 0.3 Co mol % with respect to the substrate was charged with a 1.8 M solution of β-propiolactone in toluene and 15 bar of CO for 18 h at room temperature, succinic anhydride was obtained as the sole reaction product in 92% yield without the poly(3-hydroxypropionate) byproduct (Table 4.1, entry 2 and Figure 4.S7). This corresponds to an overall site time yield of 16 h⁻¹, an

Table 4.1. Batch Carbonylation of β-Propiolactone.

$$\text{(β-propiolactone)} \xrightarrow[\text{1.8 M in Toluene, 15 bar CO, 24 °C}]{\text{0.3 mol \% catalyst}} \text{(succinic anhydride)}$$

Entry	Catalyst	t (h)	Yield (%)
1	[(salph)Al(THF)$_2$][Co(CO)$_4$][17]	24	98
2	Co(CO)$_4$⊂Cr-MIL-101	18	92[a]
3	Cr-MIL-101	18	0[a]
4	Na[Co(CO)$_4$]	18	12[a]
5	Cr-MIL-101 + Na[Co(CO)$_4$][b]	18	43[a]

[a] As determined by ^{1}H-NMR analysis against mesitylene as a standard. [b] Cr-MIL-101 + Na[Co(CO)$_4$] = equimolar mixture of the two species.

improvement over the value of 12 h^{-1} reported for the homogeneous [(salph)Al(THF)$_2$][Co(CO)$_4$] under analogous conditions (Table 4.1, entry 1).

To probe the catalytic cooperativity between the framework Cr(III) sites and the postsynthetically introduced Co(CO)$_4^-$ in Co(CO)$_4$⊂Cr-MIL-101, Cr-MIL-101 and Na[Co(CO)$_4$] were tested individually for β-propiolactone carbonylation activity (Table 4.1, entries 3 and 4). Expectedly, both Cr-MIL-101 and Na[Co(CO)$_4$] produced much lower yields, likely due to the absence of Co(CO)$_4^-$ needed for CO insertion and lack of strong Lewis acids needed for substrate activation, respectively. Although using an equimolar mixture of Cr-MIL-101 and Na[Co(CO)$_4$] as a catalyst led to significantly higher yields compared to using either precursor individually, the equimolar mixture was still inferior to Co(CO)$_4$⊂Cr-MIL-101 with pre-installed Cr/Co sites (Table 4.1, entry 5). We attribute this behavior to an incomplete *in-situ* formation of Cr/Co sites that leads to fractional carbonylation activity for the mixture of Cr-MIL-101 and Na[Co(CO)$_4$]. The need for the

coexistence of both the Lewis acidic Cr(III) and Co(CO)$_4^-$ for appreciable carbonylation activity suggests Cr/Co cooperative catalysis to be active for Co(CO)$_4$⊂Cr-MIL-101.

When several solvents were screened for optimizing β-propiolactone carbonylation activity with Co(CO)$_4$⊂Cr-MIL-101, the highest activities were observed with non-coordinating solvents such as toluene and dichloromethane (DCM) (Table 4.S2, entries 1 and 2). Reactions in coordinating solvents greatly reduced carbonylation activity, as exemplified by the low yields from reactions with 1,2-dimethoxyethane, tetrahydrofuran, and acetonitrile (Table 4.S2, entries 3–5). These results deviate from the solvent dependence observed for epoxide carbonylation by Co(CO)$_4$⊂Cr-MIL-101, in which mildly coordinating solvents, such as 1,2-dimethoxyethane, were found to be ideal. A similar discrepancy has been observed for various homogeneous catalysts of the general formula [Lewis acid]$^+$[Co(CO)$_4$]$^-$, where β-lactone carbonylation proceeded much faster in solvents that are less coordinating than those optimal for epoxide carbonylation. This behavior has been accredited to substrate activation and ring-opening being the rate limiting step for β-lactone carbonylation, where Lewis basic solvents more effectively compete for coordination to the Lewis acidic metal sites and hinder substrate ring-opening by Co(CO)$_4^-$ (Figure 4.1A).[14] Observation of an analogous solvent dependence with Co(CO)$_4$⊂Cr-MIL-101 lends credence that a similar mechanistic explanation may be applicable to β-lactone carbonylation by Co(CO)$_4$⊂Cr-MIL-101.

In order to confirm the heterogeneous nature of catalysis by Co(CO)$_4$⊂Cr-MIL-101, a β-propiolactone carbonylation reaction mixture at ~35% conversion was divided into two

aliquots, one of which was filtered (Figure 4.S8). When the filtrate and the unfiltered fraction were allowed to further react, the anhydride yield did not increase for the filtrate whereas the unfiltered portion resumed its carbonylation activity. The crystalline structure of Co(CO)$_4 \subset$Cr-MIL-101 was also maintained throughout all carbonylation reactions, as verified by powder X-ray diffraction analysis of spent Co(CO)$_4 \subset$Cr-MIL-101 (Figure 4.S9).

Having confirmed the heterogeneous β-lactone carbonylation activity by Co(CO)$_4 \subset$Cr-MIL-101, we designed a laboratory-scale packed-bed reactor process to study Co(CO)$_4 \subset$Cr-MIL-101 under continuous-flow conditions (Figure 4.S10). As a singular example among all β-lactone carbonylation catalysts developed to date, when Co(CO)$_4 \subset$Cr-MIL-101 at room temperature was subjected to a flow of 0.1 M β-propiolactone in DCM at 0.1 mL/min or a weight hourly space velocity (WHSV) of 1,200 h^{-1} and an excess CO flow of 30 mL/min at 45 bar, succinic anhydride was obtained as the sole product at 1,300 mol$_{Anhydride}$·mol$_{Co}^{-1}$ over 6 h on stream (Figures 4.3A and 4.S11). Co(CO)$_4 \subset$Cr-MIL-101 was also able to carbonylate β-butyrolactone cleanly to the respective methylsuccinic anhydride, with an activity of 360 mol$_{Anhydride}$·mol$_{Co}^{-1}$ over 60 h on stream at 40 °C when exposed to a flow of 0.5 M β-butyrolactone in toluene at 0.02 mL/min or a WHSV of 7.1 h^{-1} and an excess CO flow of 30 mL/min at 30 bar (Figures 4.3B and 4.S11). The dramatically higher activity observed with β-propiolactone is in line with the proposed S$_{N2}$ attack on the β-carbon of the lactone by Co(CO)$_4^-$ (Figure 4.1A), where decreased steric hindrance on the β-carbon leads to a significant increase in activity.[14] Carbonylation activity was also highly sensitive to CO pressure, where stability of the observed activity profiles was impaired at lower CO pressures for both β-propiolactone and β-butyrolactone substrates (Figure 4.3). This
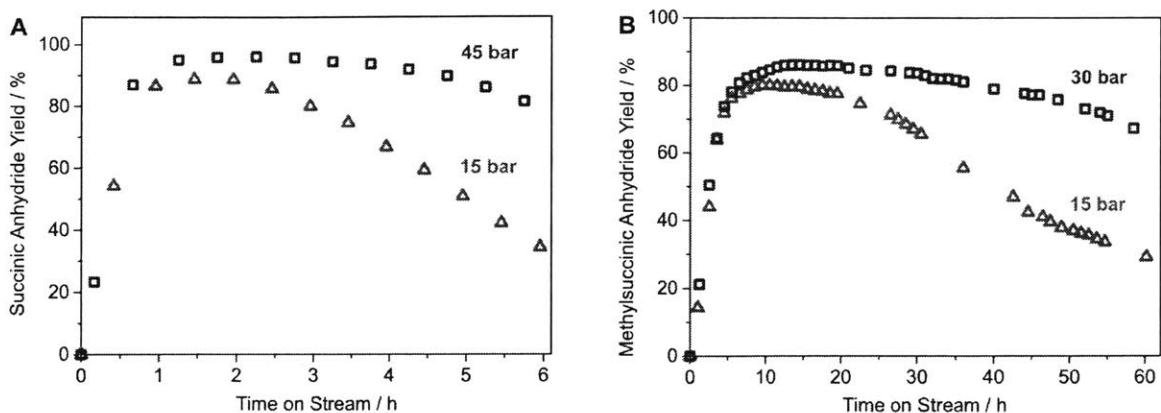
Figure 4.3. (A) Continuous-flow carbonylation of β-propiolactone by Co(CO)$_4$⊂Cr-MIL-101. Reaction conditions: 0.1 mL/min of 0.1 M β-propiolactone in DCM, 30 mL/min of CO at 45 bar or 15 bar, and 6.0 mg catalyst at 21 °C. (B) Continuous-flow carbonylation of β-butyrolactone by Co(CO)$_4$⊂Cr-MIL-101. Reaction conditions: 0.02 mL/min of 0.5 M β-butyrolactone in toluene, 30 mL/min of CO at 30 bar or 15 bar, and 130 mg catalyst at 40 °C.

behavior parallels the analogous CO pressure dependence observed in batch carbonylation studies, suggesting that competing side reactions, such as β-lactone homopolymerization, may be a major cause of deactivation.

A key feature of β-lactone carbonylation by Co(CO)$_4$⊂Cr-MIL-101 is the ease of product recovery from the heterogeneous catalyst. When catalyst loading was increased to fully convert the substrate in a continuous-flow β-propiolactone carbonylation, ambient evaporation of the volatile DCM from the product stream led to isolation of the desired succinic anhydride as a crystalline solid (Figure 4.S12). Similar results were obtained from batch-wise β-propiolactone carbonylation studies, where filtration of the solid catalyst and subsequent evaporation of the fully converted product mixture resulted in recovery of succinic anhydride crystals. These simple operations greatly contrast the complicated separations schemes required in hydrocarbon oxidation or microbial fermentation

processes (e.g., NH$_3$/H$_2$SO$_4$-assisted succinate precipitation, NaOH-assisted electrodialysis, amine-assisted reactive extraction, etc.[19]) and further corroborates the potential of our heterogeneous β-lactone carbonylation pathway for the industrial production of succinic anhydrides.

4.4. Conclusion

In summary, we report Co(CO)$_4$⊂Cr-MIL-101 as the first heterogeneous catalyst for the selective ring-expanding carbonylation of β-lactones to succinic anhydrides. Its facile application to a packed-bed reactor process for continuous production and recovery of succinic anhydrides substantiates the potential efficacy of the heterogeneous β-lactone carbonylation pathway. We ascribe the favorable performance of the catalyst to the intrinsic structural advantages of the MOF platform, which supports precise coordination geometries[20-22] as isolated single sites[23-25] within a robust porous scaffold[26-28] for novel catalytic applications. We believe these unique structural properties could be leveraged for the development of an improved class of heterogeneous catalysts. In addition, identification of an optimum flow reactor configuration through reaction kinetics studies is anticipated to further enhance the performance of the β-lactone carbonylation process.

4.5. Experimental Information

General Considerations

All manipulations of air/water-sensitive compounds were conducted using standard inert-atmosphere glove box and Schlenk line techniques.

Powder X-ray diffraction (PXRD) patterns were recorded on a Bruker Advance II diffractometer equipped with $\theta/2\theta$ Bragg-Brentano geometry and Ni-filtered Cu Kα radiation (Kα_1 = 1.5406 Å). The tube voltage and current were 40 kV and 40 mA, respectively. A thin layer of dry powdered sample was placed on a rotating zero-background silicon crystal plate for analysis.

Energy dispersive X-ray spectroscopy (EDX) analyses were conducted using a JEOL 6010LA analytical scanning electron microscope at 15 keV and a working distance of 10 mm. Dry powdered samples were mounted onto a stage using carbon tape and sputtered with Au prior to analysis.

Attenuated total reflectance infrared (ATR-IR) absorption spectra were acquired using a Bruker Alpha ATR Fourier transform IR spectrometer inside a glove box.

Thermal gravimetric (TGA) analyses were conducted using a TA Instruments Q500 analyzer equipped with a standard furnace (953032.901, TA Instruments) and a platinum pan (952018.906, TA Instruments). ~10 mg of sample was subjected to an equilibration step at 30 °C followed by a heat ramp to 800 °C at a rate of 1 °C/min under a constant flow of nitrogen.

Nitrogen adsorption isotherms were measured by a volumetric method using a Micromeritics ASAP 2020 gas sorption analyzer. ~30 mg of sample was pre-activated at 150°C under vacuum overnight to remove all residual solvent and transferred to a pre-weighed analysis tube in a glove box. The tube containing the sample was weighed again

to determine the mass of the sample, capped with a Micromeritics TranSeal, brought out of the glove box, and transferred to the analysis port of the gas sorption analyzer. Free space correction measurements were performed using an ultra-high purity helium gas (UHP grade, Airgas) and nitrogen isotherms were measured using an ultra-high purity grade nitrogen (UHP grade, Airgas). All nitrogen analyses were performed using a liquid nitrogen bath at 77 K.

Metal content of Cr-MIL-101 and $Co(CO)_4 \subset Cr$-MIL-101 samples was quantified using Agilent 7900 inductively coupled plasma mass spectrometer (ICP-MS). ~10 mg sample was weighed in a glove box, transferred to an acid digestion vessel (Model 4749, Parr Instrument Company), and digested in ~3 mL of concentrated nitric acid (67~70% w/v %, BDH Aristar) at 150 °C overnight. Metal concentrations of the resulting solution were determined using calibration curves constructed from standard solutions (ICP-MS certified reference standards, VWR).

β-Lactone carbonylation reactions were analyzed using ^{1}H-NMR (AVANCE 400 MHz, Bruker) in $CDCl_3$ and a gas chromatograph (GC) equipped with a DB-5ms column (30 m × 0.25 mm ID × 0.25 μm, Agilent Technologies) and a flame ionization detector (FID) for quantification (Model 7890A, Agilent Technologies). Identification of the product succinic anhydrides and poly(hydroxyalkanoate) was supplemented by comparing their ^{1}H-NMR spectra to the literature spectra.

Materials

Dichloromethane (≥99%, Sigma-Aldrich), toluene (99.8% Sigma-Aldrich), 1,2-dimethoxyethane (99.5%, Sigma-Aldrich), tetrahydrofuran (ACS grade, BDH), and acetonitrile (≥99.9%, Sigma-Aldrich) were passed through two silica columns in a Glass Contour solvent purification system, degassed with a flow of argon gas for 30 min, subjected to at least three freeze-pump-thaw cycles, and dried over activated molecular sieves prior to use. β-Propiolactone (97%, Alfa Aesar), β-butyrolactone (98%, Sigma-Aldrich), and mesitylene (≥99.8% analytical standard, Sigma-Aldrich) were stirred over ≥5 w/v % calcium hydride for a minimum of three days, vacuum transferred, and degassed by at least three freeze-pump-thaw cycles prior to use. Glass beads (1 mm diameter, EMD Millipore), Silicon carbide powder (320 grit, Alfa Aesar), and quartz wool (Fine, Chemglass Inc.) were dried in a convection oven overnight at 120 °C prior to use. Succinic anhydride (≥99%, Sigma-Aldrich), Methylsuccinic anhydride (98%, Sigma-Aldrich), carbon monoxide (Research grade 4.0, Airgas), and argon (Research grade 5.7, Airgas) were used as received. The following were prepared and characterized according to literature procedure[15]: Cr-MIL-101, Na[Co(CO)$_4$], and Co(CO)$_4$⊂Cr-MIL-101 (Figures 4.S1–S5).

Experimental Details

Batch-wise β-Lactone Carbonylation Reactions with Co(CO)$_4$⊂Cr-MIL-101: A typical procedure involved charging a glass vial with the solvent (1~2 mL), β-lactone substrate (loaded at the specified concentration with respect to the solvent), Co(CO)$_4$⊂Cr-MIL-101 (loaded at the specified Co mol % with respect to the β-lactone substrate based on the ICP-MS derived cobalt content of Co(CO)$_4$⊂Cr-MIL-101), and a magnetic stir bar. The vial was then immediately transferred to a stainless-steel pressure vessel reactor (Series 4790, Parr

Instrument Company) and the reactor was sealed in an inert-atmosphere glove box. The sealed reactor was then taken out of the glove box, placed in a hood, pressurized with CO to the desired pressure, and heated to the desired temperature using a temperature controller (Digi-Sense, 68900) and an internal thermocouple probe (Omega, KQXL-18). The temperature was held constant while stirring for the specified time on a magnetic stir plate, after which the reactor was cooled in an ice bath until the pressure reached a minimum. After careful venting of CO to atmospheric pressure, the glass vial was recovered, and the product mixture was filtered through a polytetrafluoroethylene syringe filter (0.20 μm, Millex). A small sample of the filtrate was analyzed via ^{1}H-NMR and GC-FID with added mesitylene as a standard. All control reactions with Cr-MIL-101 and Na[Co(CO)$_4$] were conducted in an analogous manner as described above for Co(CO)$_4 \subset$Cr-MIL-101.

Catalyst Heterogeneity Test with Co(CO)$_4 \subset$Cr-MIL-101: A typical procedure involved conducting a standard β-lactone carbonylation reaction as outlined above for a sufficient time to reach the desired conversion of the substrate. After careful venting of CO to atmospheric pressure, the Parr reactor was refilled with nitrogen, and transferred into an inert-atmosphere glove box. The glass vial holding the reaction mixture was then taken out of the reactor and the reaction mixture was divided into two equal aliquots. One of the aliquots was passed through a polytetrafluoroethylene syringe filter to collect the filtrate in a separate vial and a small fraction of the filtrate was analyzed via ^{1}H-NMR and GC-FID. The two glass vials, one holding the collected filtrate and the other holding the unfiltered fraction of the reaction mixture, were transferred to separate stainless-steel pressure vessel reactors, and the reactors were sealed in the glove box. The two sealed reactors were then

93

taken out of the glove box, placed in a hood, and again subjected to standard reaction conditions. After the specified time, product mixtures from both reactors were recovered and analyzed via ^{1}H-NMR and GC-FID in a manner analogous to the standard β-lactone carbonylation reaction procedure outlined above and the filtered Co(CO)$_4$⊂Cr-MIL-101 catalyst was subjected to PXRD analysis.

Continuous-flow β-Lactone Carbonylation with Co(CO)$_4$⊂Cr-MIL-101: A typical procedure involved mixing the specified amount of Co(CO)$_4$⊂Cr-MIL-101 with ~500 mg of silicon carbide powder in an inert-atmosphere glove box and packing the solid mixture between two quartz wool plugs in a stainless-steel tubing segment (OD 6.35 mm, wall thickness 0.89 mm, Grainger). A thermocouple probe (KQXL-116, Omega) was mounted downstream in direct contact with the end of the catalyst bed for temperature monitoring. Void space within the tubing segment was filled with glass beads to minimize dead volume prior to isolating the packed tubing segment using valves. β-Lactone substrate and solvent were also charged into a stainless-steel sample cylinder (304L-05SF4-150, Swagelok) in the glove box and isolated using valves. Packed tubing segment and liquid feed cylinder were then transferred out of the glove box and connected to a custom-built flow reaction setup (Figure 4.S10) equipped with a CO mass flow controller (5850E, Brooks Instruments), an oxygen trap (304L-HDF4-150, Swagelok) filled with pre-reduced Cu catalyst (8 x 14 mesh Q-5, Research Catalysts), a water trap filled with CaH$_2$ (≥97%, Sigma-Aldrich), a liquid delivery pump (Series III, Scientific Systems), a single-zone furnace (Carbolite, GTF 11/50/150B) connected to a temperature controller (Digi-Sense, 68900), a single-stage gas/liquid separator (Series 20, Jerguson), a pressure gauge (PGI series, Swagelok), and a

back-pressure regulator (KPB1L, Swagelok). Headspace of the liquid feed cylinder was blanketed by a continuous flow of argon through a bubbler to maintain an inert-atmosphere throughout the reaction. The reactor setup was first pressurized to the desired pressure of CO using a back-pressure regulator and allowed to stabilize to the specified flow of CO at the desired temperature. Liquid feed was then allowed to flow through the packed catalyst bed at the specified flowrate, upon which periodic liquid-phase samples were taken from the liquid-phase outlet of the gas/liquid separator. Quantification of collected samples was carried out based on GC-FID calibration curves constructed from calibration samples with weighed amounts of β-lactone substrates, succinic anhydride products, and mesitylene standard in respective solvents (Figure 4.S11).
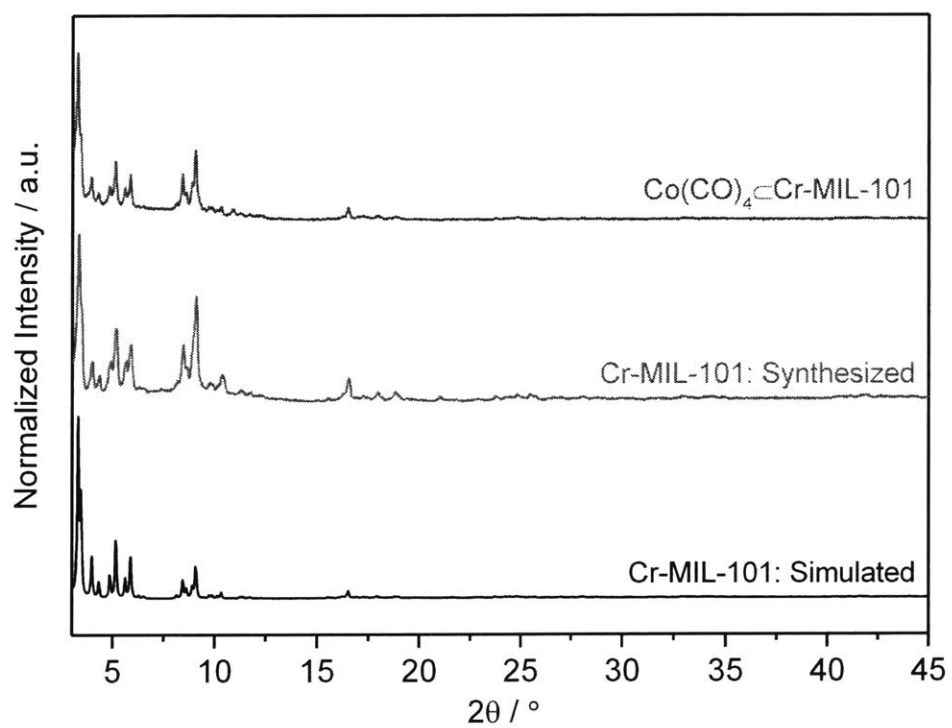
4.6. Supporting Information

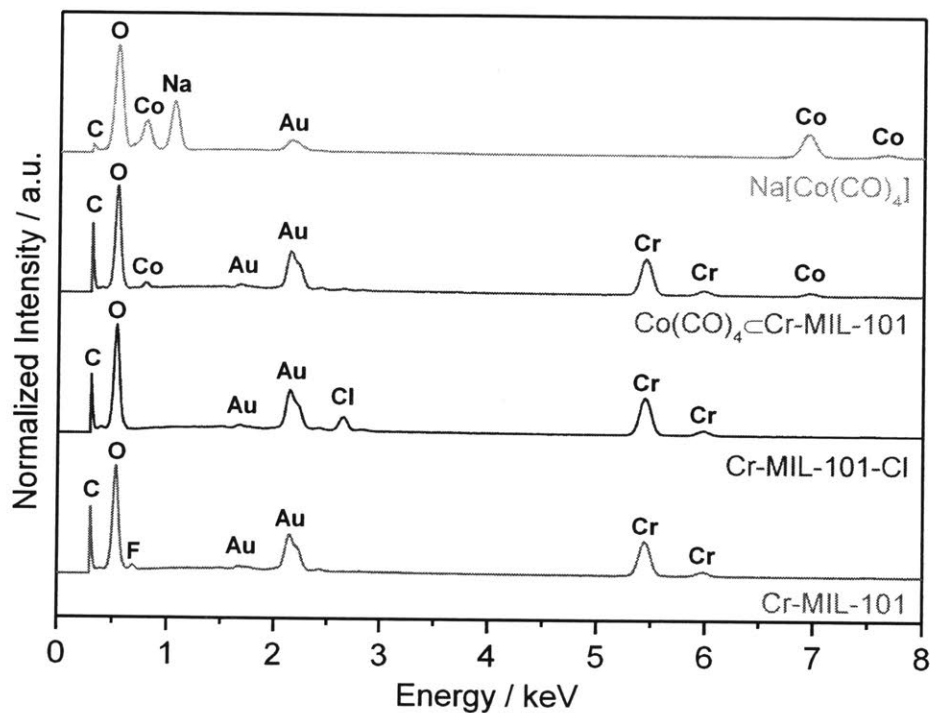**Figure 4.S1.** PXRD patterns of simulated Cr-MIL-101, synthesized Cr-MIL-101, and Co(CO)$_4$⊂Cr-MIL-101.

Figure 4.S2. EDX spectra of Cr-MIL-101, Cr-MIL-101-Cl, $Co(CO)_4 \subset Cr$-MIL-101, and $Na[Co(CO)_4]$. $Co(CO)_4 \subset Cr$-MIL-101 was prepared from $Na[Co(CO)_4]$ treatment of Cr-MIL-101-Cl, which was in turn obtained from $AlCl_3$ treatment of Cr-MIL-101. Incorporation of $Co(CO)_4^-$ into $Co(CO)_4 \subset Cr$-MIL-101 is evidenced by the presence of Co $K\alpha$ (6.92 keV) and Co $L\alpha$ (0.78 keV) peaks and the absence of Na $K\alpha$ (1.04 keV), Cl $K\alpha$ (2.62 keV), and F $K\alpha$ (0.68 keV) peaks in the spectrum of $Co(CO)_4 \subset Cr$-MIL-101. All samples were sputtered with Au prior to analysis.
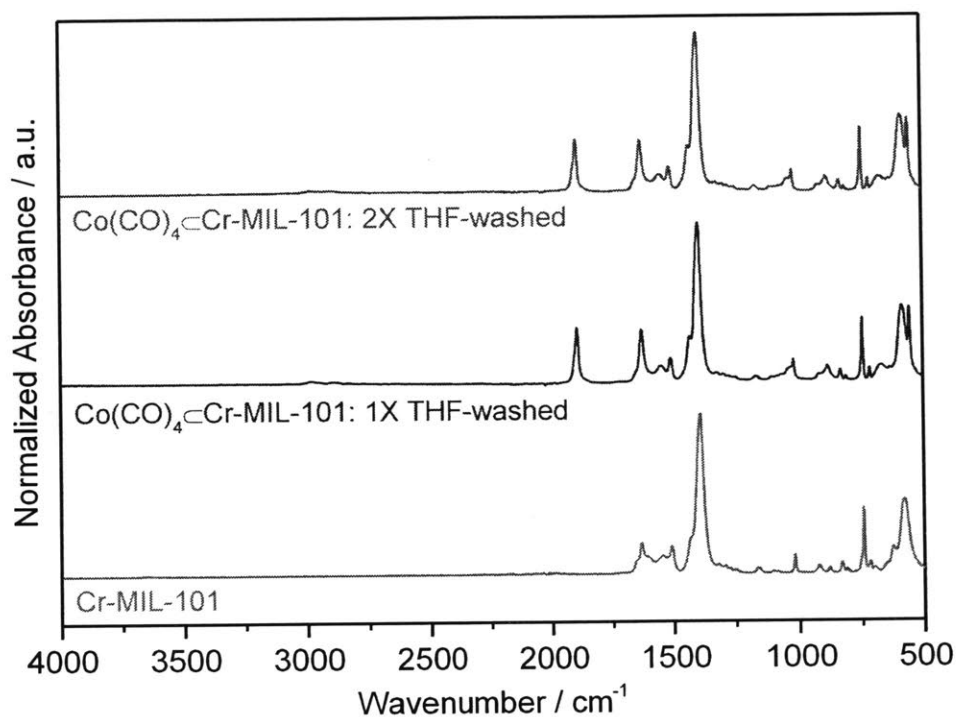
Figure 4.S3. ATR-IR spectra of Cr-MIL-101 and $Co(CO)_4 \subset Cr$-MIL-101. Single band at 1890 cm^{-1} remained after repeated overnight washes with stirring in tetrahydrofuran (50 mL per 20 mg of $Co(CO)_4 \subset Cr$-MIL-101), a solvent that readily solubilizes the $Na[Co(CO)_4]$ salt. This band corresponds well to the characteristic carbonyl stretching mode of the tetrahedral $Co(CO)_4^-$ ion in various metal complexes, including those reported for the homogeneous [Lewis acid]$^+$[Co(CO)$_4$]$^-$ carbonylation catalysts.
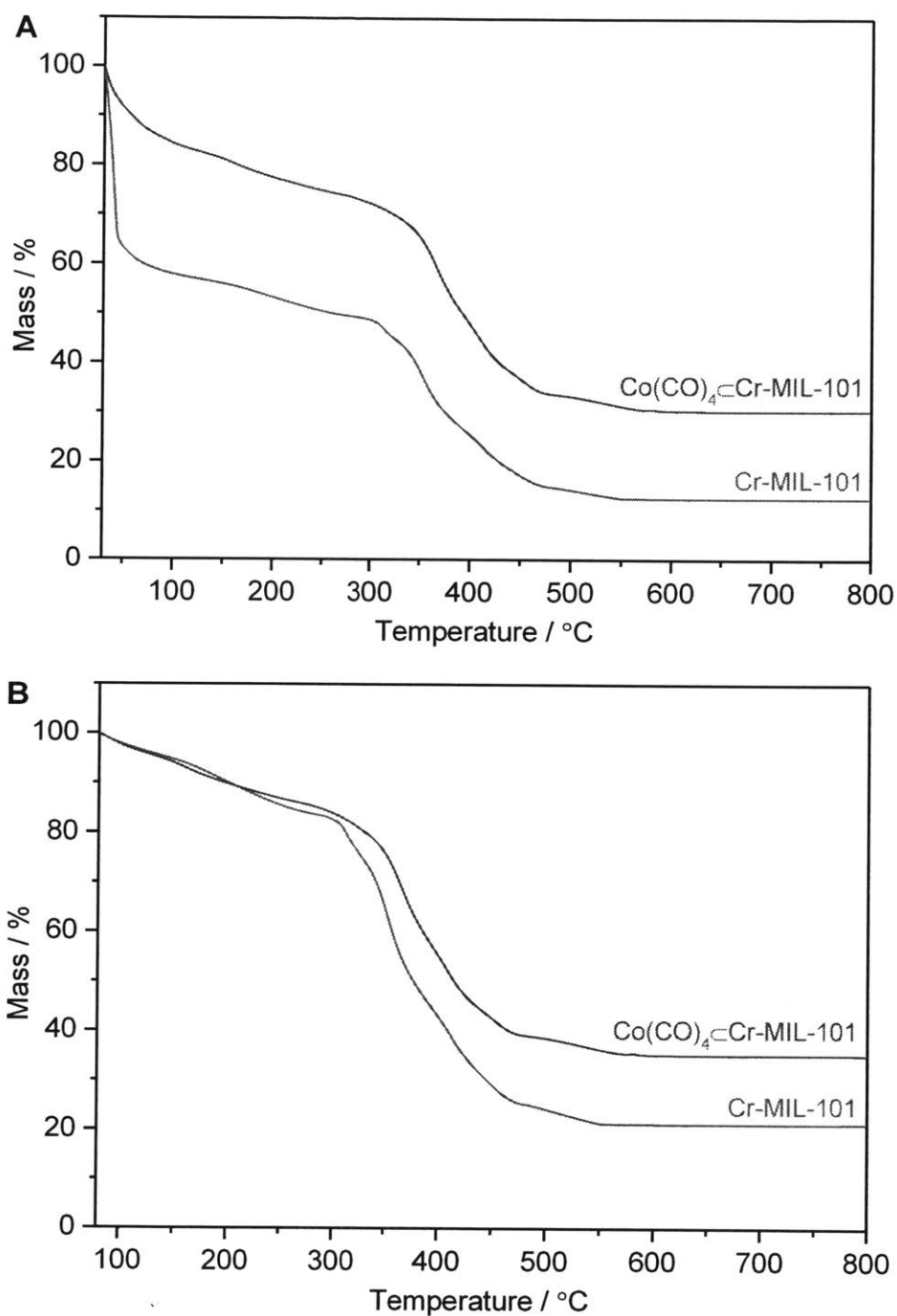
Figure 4.S4. TGA curves of Cr-MIL-101 and Co(CO)$_4$⊂Cr-MIL-101: (A) mass measurements normalized to initial mass at 30 °C and (B) mass measurements normalized to mass at 80 °C. Both samples were subjected to an overnight wash in tetrahydrofuran and subsequent filtration prior to analysis. Analysis was conducted at a heat ramp of 1 °C/min from 30 °C to 800 °C under a flow of nitrogen.
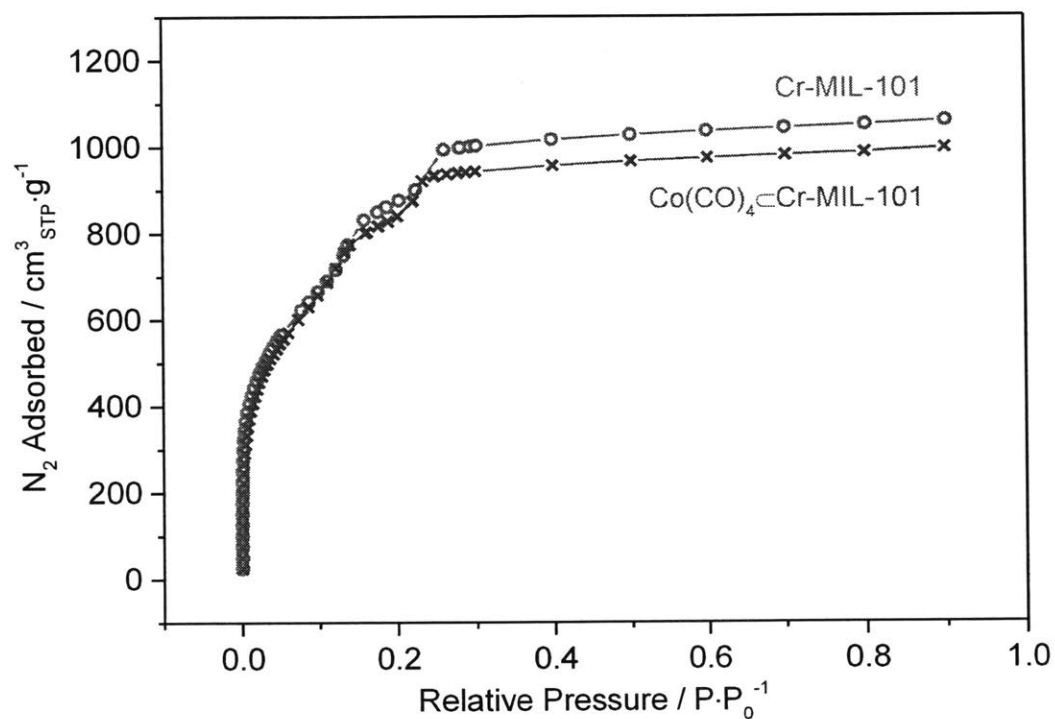
Figure 4.S5. Nitrogen adsorption isotherms of Cr-MIL-101 and Co(CO)$_4$⊂Cr-MIL-101 after outgassing under vacuum (10^{-5} torr) at 150 °C for 18 h. Calculated BET surface areas for Cr-MIL-101 and Co(CO)$_4$⊂Cr-MIL-101 were 3,450 ± 80 m^2/g and 3,270 ± 46 m^2/g, respectively. Surface areas were derived by fitting the BET equation to the acquired isotherm over the range of 0.05 ≤ P/P$_0$ ≤ 0.2.
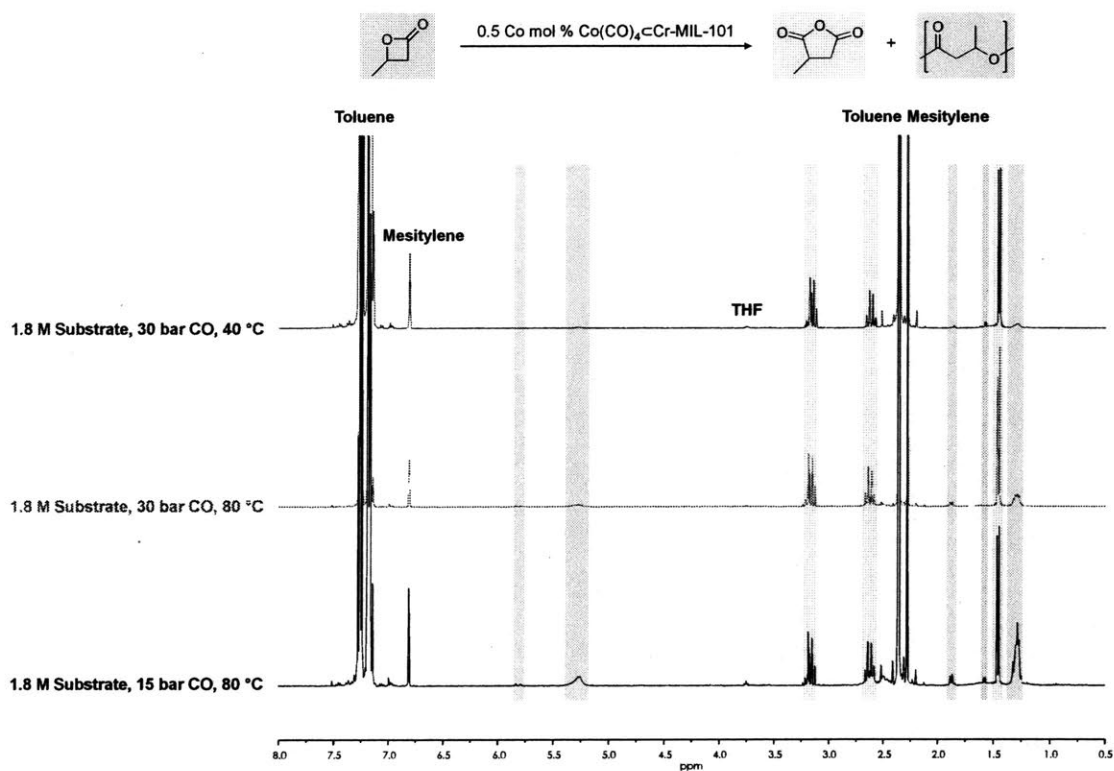
Figure 4.S6. ¹H-NMR spectra of product mixtures from batch carbonylation of β-butyrolactone by Co(CO)$_4$⊂Cr-MIL-101 under various reaction conditions. Reaction times varied to reach >75% substrate conversion under all conditions. Mesitylene used as a standard for quantification.
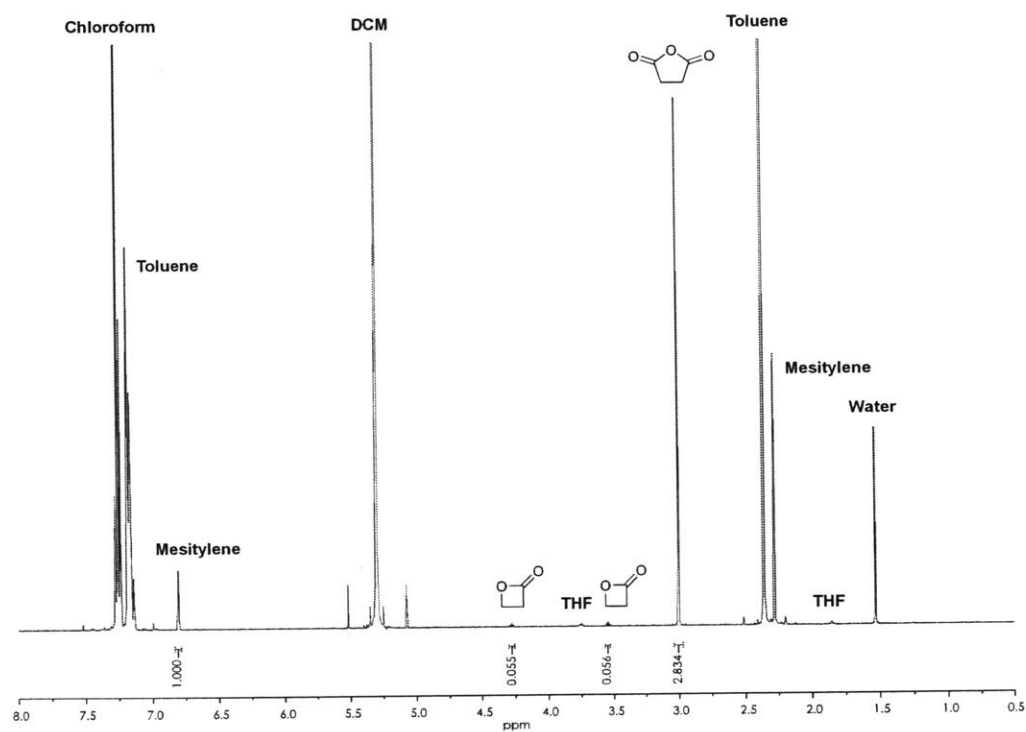
Figure 4.S7. Example ¹H-NMR spectrum of a product mixture from batch carbonylation of 1.8 M β-propiolactone in toluene by 0.3 Co mol % Co(CO)₄⊂Cr-MIL-101 at 15 bar of CO and room temperature. Dichloromethane added to the product mixture to dissolve the acquired solids for analysis and mesitylene added as a standard for quantification.
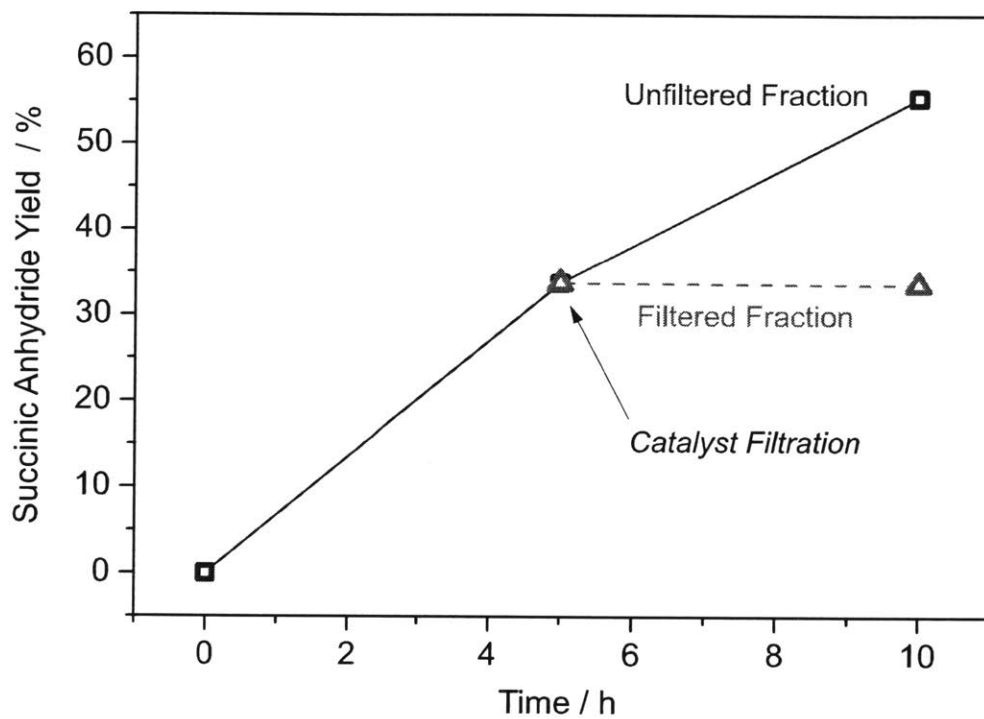
Figure 4.S8. Catalyst filtration test for batch carbonylation of β-propiolactone by Co(CO)$_4$⊂Cr-MIL-101. Reaction conditions: 0.3 Co mol % catalyst to 1.0 M β-propiolactone in dichloromethane, 15 bar of CO at 21 °C, and catalyst filtration conducted at 5 h. Lines are meant as a guide to the eye.
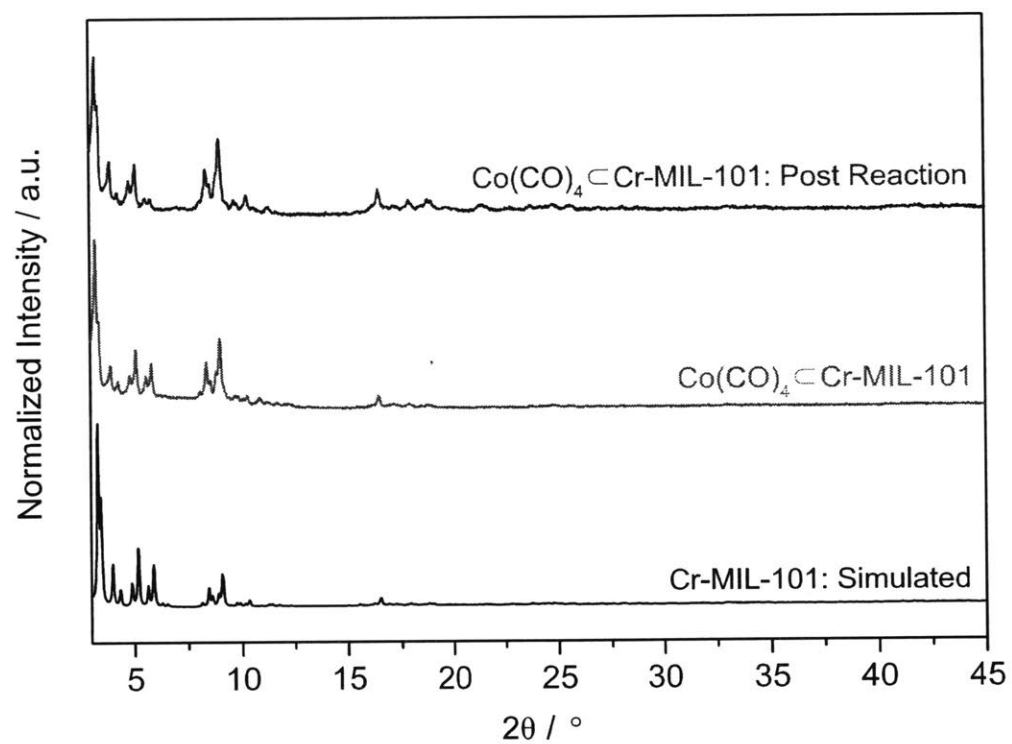
Figure 4.S9. PXRD patterns of simulated Cr-MIL-101, Co(CO)$_4$⊂Cr-MIL-101, and post-reaction Co(CO)$_4$⊂Cr-MIL-101. Reaction conditions: 0.3 Co mol % catalyst to 1.0 M β-propiolactone in dichloromethane, 15 bar of CO at 21 °C, and 10 h.
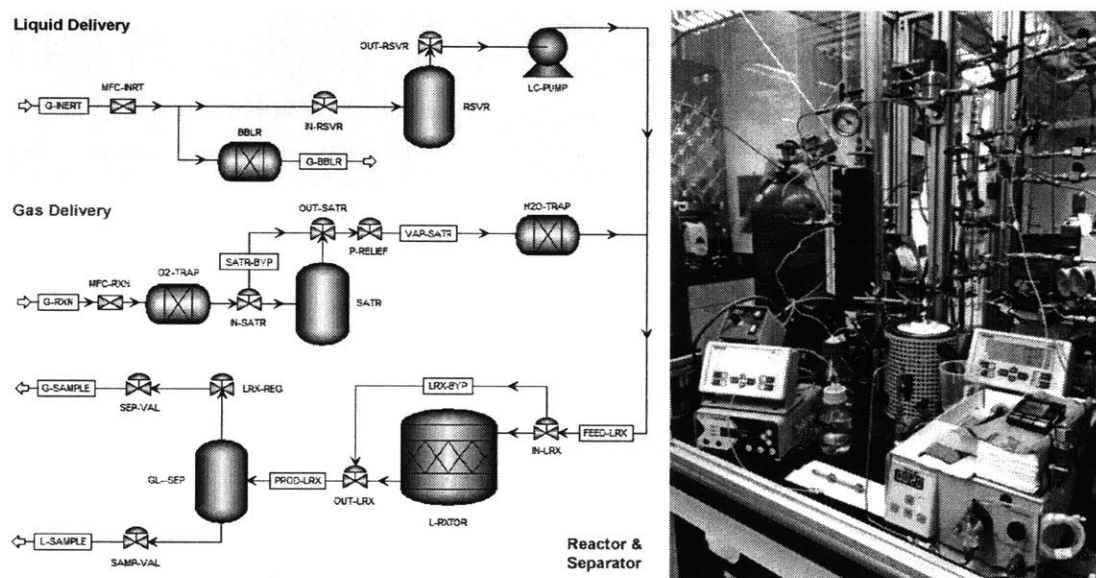
Figure 4.S10. Process flow diagram and experimental setup of the packed-bed reactor process for continuous-flow β-lactone carbonylation.
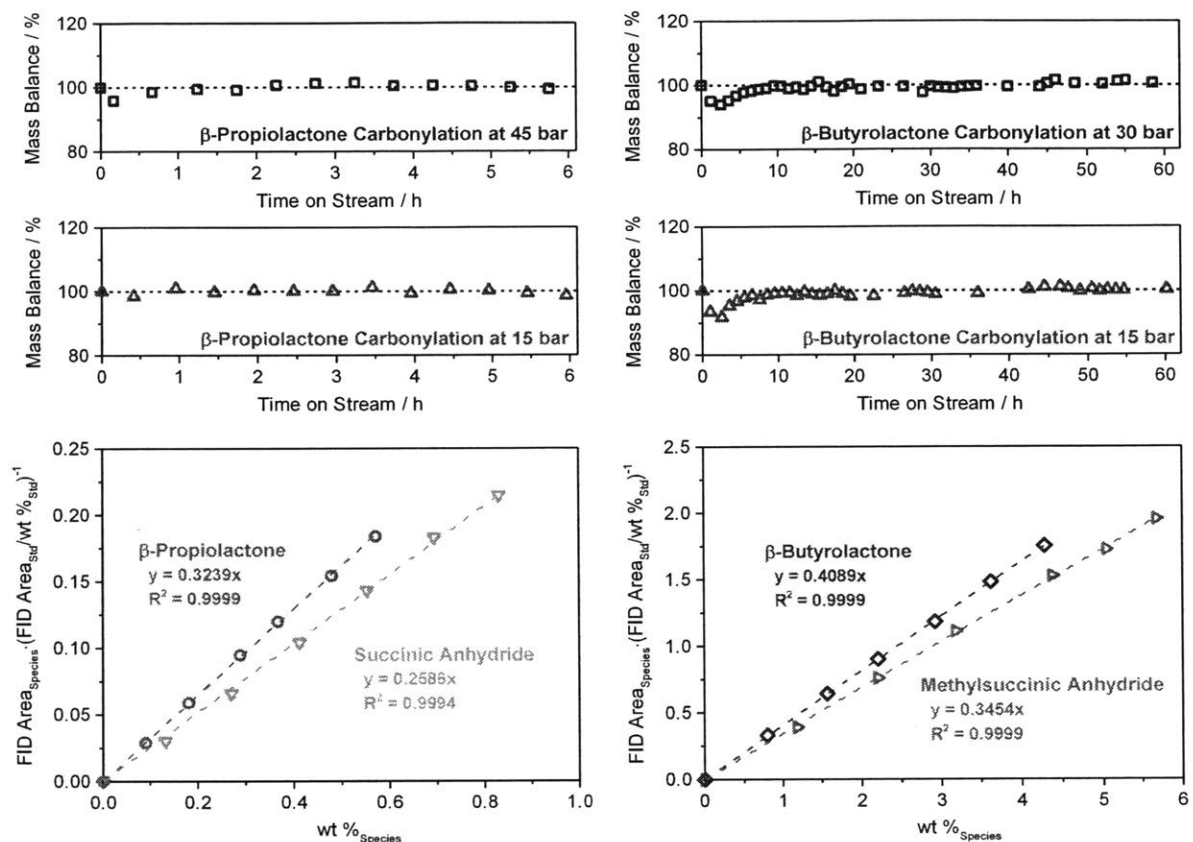
Figure 4.S11. Mass balances from continuous-flow carbonylation of β-propiolactone and β-butyrolactone by Co(CO)$_4$⊂Cr-MIL-101 (top) and GC-FID calibration curves used for quantification of the reaction species (bottom). Mass balances acquired by comparing the GC-FID-quantified amount of β-lactone and succinic anhydride in the product stream to the amount of β-lactone in the liquid feed stream. Reaction conditions: 0.1 mL/min of 0.1 M β-propiolactone in dichloromethane, 30 mL/min of CO at 45 bar or 15 bar, and 6.0 mg catalyst at 21 °C or 0.02 mL/min of 0.5 M β-butyrolactone in toluene, 30 mL/min of CO at 30 bar or 15 bar, and 130 mg catalyst at 40 °C.
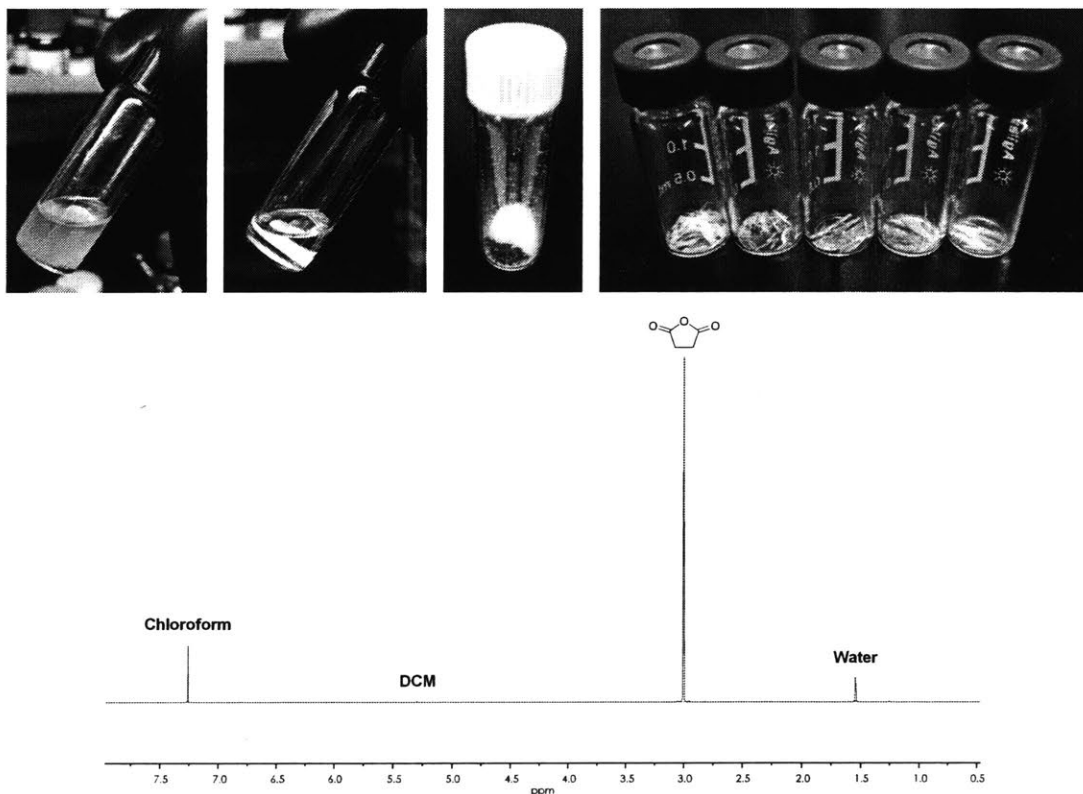
Figure 4.S12. Pictures of the batch reaction mixture, post-filtration product mixture, residual solid after evaporation of the post-filtration product mixture, residual solids after prolonged ambient air exposure of the fully-converted product stream from continuous-flow β-propiolactone carbonylation by Co(CO)$_4$⊂Cr-MIL-101 (from top left to top right), and an example ^{1}H-NMR spectrum of the acquired solids (bottom).

Table 4.S1. ICP-MS Analysis of Cr-MIL-101, Co(CO)$_4$⊂Cr-MIL-101, and Na[Co(CO)$_4$]

Sample	Cr (wt. %)	Co (wt. %)	Na (wt. %)
Cr-MIL-101[a]	22.1	Not detected	Not detected
Co(CO)$_4$⊂Cr-MIL-101[b]	14.8	3.0	0.02
Na[Co(CO)$_4$][b]	Not detected	30.4	12.2

[a] dried under vacuum at 150 °C. [b] dried under vacuum at ambient temperature.

Table 4.S2. Batch Carbonylation of β-Propiolactone by Co(CO)₄⊂Cr-MIL-101

$$O \xrightarrow{\begin{array}{c} 0.3 \text{ Co mol \% } Co(CO)_4 \subset Cr\text{-MIL-101} \\ \hline 1.8 \text{ M substrate, 15 bar CO, 24 °C, 18 h} \end{array}} O \xrightarrow{} O$$
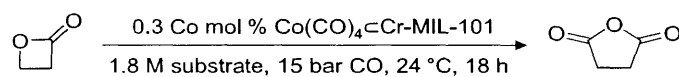
Entry	Solvent	Yield (%)[a]
1	Toluene	92
2	Dichloromethane	88
3	1,2-Dimethoxyethane	11
4	Tetrahydrofuran	7
5	Acetonitrile	6

[a] As determined by ¹H-NMR analysis against mesitylene as a standard.

4.7. References

(1)   Bechthold, I.; Bretz, K.; Kabasci, S.; Kopitzky, R.; Springer, A. Succinic Acid: A New Platform Chemical for Biobased Polymers from Renewable Resources. *Chem. Eng. Technol.* **2008**, *31*, 647–654.

(2)   Sauer, M.; Porro, D.; Mattanovich, D.; Branduardi, P. Microbial Production of Organic Acids: Expanding the Markets. *Trends Biotechnol.* **2008**, *26*, 100–108.

(3)   Cheng, K.; Zhao, X.; Zeng, J.; Zhang, J. Biotechnological Production of Succinic Acid: Current State and Perspectives. *Biofuels, Bioprod. Bioref.* **2012**, *6*, 302–318.

(4)   Schultheiss, N.; Newman, A. Pharmaceutical Cocrystals and Their Physicochemical Properties. *Cryst. Growth Des.* **2009**, *9*, 2950–2967.

(5)   Hood, D. K.; Musa, O. M. Progress in Maleic Anhydride Production. in *Handbook of Maleic Anhydride Based Materials*; Musa, O. M., Ed.; Springer International Publishing Switzerland: Cham, 2016; pp 3–54.

(6)   Trifirò, F.; Grasselli, R. K. How the Yield of Maleic Anhydride in *n*-Butane Oxidation, Using VPO Catalysts, was Improved Over the Years. *Top. Catal.* **2014**, *57*, 1188–1195.

(7)   Lohbeck, K.; Haferkorn, H.; Fuhrmann, W.; Fedtke, N. Maleic and Fumaric Acids. in *Ullmann's Encyclopedia of Industrial Chemistry*; Elvers, B., Ed.; Wiley-VCH: Weinheim, 2011; Vol. 22, pp 145–155.

(8)   *Top Value Added Chemicals from Biomass*; DOE/GO-102004-1992; U.S. Department of Energy, U.S. Department of Commerce National Technical Information Service: Alexandria, VA, 2004.

(9)   Mazière, A.; Prinsen, P.; García, A.; Luque, R.; Len, C. A Review of Progress in (Bio)catalytic Routes from/to Renewable Succinic Acid. *Biofuels, Bioprod. Bioref.* **2017**, *11*, 908–931.

(10) Ahn, J. H.; Jang, Y. S.; Lee, S. Y. Production of Succinic Acid by Metabolically Engineered Microorganisms. *Curr. Opin. Biotechnol.* **2016**, *42*, 54–66.

(11) Morales, M.; Ataman, M.; Badr, S.; Linster, S.; Kourlimpinis, I.; Papadokonstantakis, S.; Hatzimanikatis, V.; Hungerbühler, K. Sustainability Assessment of Succinic Acid Production Technologies from Biomass Using Metabolic Engineering. *Energy Environ. Sci.* **2016**, *9*, 2794–2805.

(12) Church, T. L.; Getzler, Y. D. Y. L.; Byrne, C. M.; Coates, G. W. Carbonylation of Heterocycles by Homogeneous Catalysts. *Chem. Commun.* **2007**, 657–674.

(13) Allen, S. D.; Valente, R. R.; Lee, H.; Cherian, A. E.; Bunning, D. L.; Clinton, N. A.; Fruchey, O. S.; Dombek, B. D. Process for Beta-lactone Production. U.S. 9,493,391, Nov. 15, 2016.

(14) Rowley, J. M.; Lobkovsky, E. B.; Coates, G. W. Catalytic Double Carbonylation of

Epoxides to Succinic Anhydrides: Catalyst Discovery, Reaction Scope, and Mechanism. *J. Am. Chem. Soc.* **2007**, *129*, 4948–4960.

(15) Park, H. D.; Dincă, M.; Román-Leshkov, Y. Heterogeneous Epoxide Carbonylation by Cooperative Ion-pair Catalysis in $Co(CO)_4^-$-incorporated Cr-MIL-101. *ACS Cent. Sci.* **2017**, *3*, 444–448.

(16) Hong, D. Y.; Hwang, Y. K.; Serre, C.; Férey, G.; Chang, J. S. Porous Chromium Terephthalate MIL-101 with Coordinatively Unsaturated Sites: Surface Functionalization, Encapsulation, Sorption and Catalysis. *Adv. Funct. Mater.* **2009**, *19*, 1537–1552.

(17) Getzler, Y. D. Y. L.; Kundnani, V.; Lobkovsky, E. B.; Coates, G. W. Catalytic Carbonylation of β-Lactones to Succinic Anhydrides. *J. Am. Chem. Soc.* **2004**, *126*, 6842–6843.

(18) Reichardt, R.; Vagin, S.; Reithmeier, R.; Ott, A. K.; Rieger, B. Factors Influencing the Ring-opening Polymerization of Racemic β-Butyrolactone Using Cr^{III}(salphen). *Macromolecules* **2010**, *43*, 9311–9317.

(19) Jansen, M. L. A.; van Gulik, W. M. Towards Large Scale Fermentative Production of Succinic Acid. *Curr. Opin. Biotechnol.* **2014**, *30*, 190–197.

(20) Wang, L.; Agnew, D. W.; Yu, X.; Figueroa, J. S.; Cohen, S. M. A Metal–Organic Framework with Exceptional Activity for C–H Bond Amination. *Angew. Chem. Int. Ed.* **2018**, *57*, 511–515.

(21) Stubbs, A. W.; Braglia, L.; Borfecchia, E.; Meyer, R. J.; Román-Leshkov, Y.; Lamberti, C.; Dincă, M. Selective Catalytic Olefin Epoxidation with Mn^{II}-exchanged MOF-5. *ACS Catal.* **2018**, *8*, 596–601.

(22) Ji, P.; Feng, X.; Veroneau, S. S.; Song, Y.; Lin, W. Trivalent Zirconium and Hafnium Metal–Organic Frameworks for Catalytic 1,4-Dearomative Additions of Pyridines and Quinolines. *J. Am. Chem. Soc.* **2017**, *139*, 15600–15603.

(23) Chen, X.; Peng, Y.; Han, X.; Liu, Y.; Lin, X.; Cui, Y. Sixteen Isostructural Phosphonate Metal–Organic Frameworks with Controlled Lewis Acidity and Chemical Stability for Asymmetric Catalysis. *Nat. Commun.* **2017**, *8*, 2171–2179.

(24) Ji, P.; Solomon, J. B.; Lin, Z.; Johnson, A.; Jordan, R. F.; Lin, W. Transformation of Metal–Organic Framework Secondary Building Units into Hexanuclear Zr–Alkyl Catalysts for Ethylene Polymerization. *J. Am. Chem. Soc.* **2017**, *139*, 11325–11328.

(25) Dubey, R. J. C.; Comito, R. J.; Wu, Z.; Zhang, G.; Rieth, A. J.; Hendon, C. H.; Miller, J. T.; Dincă, M. Highly Stereoselective Heterogeneous Diene Polymerization by Co-MFU-4*l*: A Single-site Catalyst Prepared by Cation Exchange. *J. Am. Chem. Soc.* **2017**, *139*, 12664–12669.

(26) Choi, K. M.; Kim, D.; Rungtaweevoranit, B.; Trickett, C. A.; Barmanbek, J. T. D.; Alshammari, A. S.; Yang, P.; Yaghi, O. M. Plasmon-enhanced Photocatalytic CO_2 Conversion within Metal–Organic Frameworks Under Visible Light. *J. Am. Chem.*

Soc. **2017**, *139*, 356–362.

(27) Li, Z.; Peters, A. W.; Platero-Prats, A. E.; Liu, J.; Kung, C. W.; Noh, H.; DeStefano, M. R.; Schweitzer, N. M.; Chapman, K. W.; Hupp, J. T.; Farha, O. K. Fine-tuning the Activity of Metal–Organic Framework-supported Cobalt Catalysts for the Oxidative Dehydrogenation of Propane. *J. Am. Chem. Soc.* **2017**, *139*, 15251–15258.

(28) Yuan, S.; Qin, J.-S.; Lollar, C. T.; Zhou, H.-C. Stable Metal–Organic Frameworks with Group 4 Metals: Current Status and Trends. *ACS Cent. Sci.* **2018**, *4*, 440–450.

Chapter 5

Gas Phase Ethylene Polymerization by AlMe$_3$-treated Cr-MFU-4l

5.1. Abstract

We report for the first time a systematic study on the catalytic gas phase polymerization of ethylene by a metal-organic framework (MOF). Cr^{3+}-exchanged MFU-4l (Cr(III)-MFU-4l, MFU-4l = Zn$_5$Cl$_4$(BTDD)$_3$, H$_2$BTDD = bis(1H-1,2,3,-triazolo[4,5-b],[4',5'-i])dibenzo[1,4]dioxin)) serves as an exemplary system to demonstrate pre-reaction treatment with alkylaluminum species as a simple method to isolate a self-activating MOF catalyst for liquid-free polymerization of ethylene. AlMe$_3$-treated Cr(III)-MFU-4l subjected to 40 bar of ethylene exhibits a polymerization activity of 52,000 mol$_{Ethylene}$·mol$_{Cr}^{-1}$·h^{-1}, one order of magnitude higher than that observed in a slurry phase reaction with Cr(III)-MFU-4l and excess alkylaluminum species. Furthermore, product polyethylene exhibits a low polydispersity index of 1.36 and a free-flowing granular morphology favorable for industrial processing, highlighting the unique advantages conferred by the single-site MOF catalysts in gas phase ethylene polymerization.

5.2. Introduction

The advent of the gas phase ethylene polymerization process, epitomized by the commercialization of the UNIPOL process by Union Carbide in 1968, transformed the

modern production of polyethylene plastics.[1] A key to its commercial success lies in the use of inexpensive fluidized bed reactors that avoid costly solvent recycling and polymer drying operations, resulting in a nearly 30% reduction in reactor construction and operation costs over conventional liquid phase processes.[2] Moreover, gas phase processes are not restricted by the inherent solubility and viscosity constraints in liquid phase processes that limit the range of producible polyethylenes and often cause complications with polymer agglomeration and reactor fouling.[3] To exploit these advantages, there has been an effort to develop heterogeneous polymerization catalysts that can reproduce the precise polymer microstructure control afforded by the molecular single-site catalysts.[4,5] This effort has largely involved chemically immobilizing the active metal species onto porous supports to achieve high dispersion of surface species available for gas phase reaction.[6-8] However, lack of precise molecular control over the immobilization process leads to variability in the final structure of the supported species, which ultimately results in numerous active site local environments with vastly differing polymerization rates.[9] Furthermore, a large number of bound sites often become inaccessible to the substrate due to multinuclear agglomeration upon immobilization.[10] These challenges are manifested in the high polydispersity of the polymer products and underutilization of the active component for various heterogeneous ethylene polymerization catalysts.[11,12] For example, Phillips chromium-oxide catalysts that currently produce the majority of commercial high-density polyethylenes (HDPE), are known to have only ~10% of their chromium centers that are active in the production of polyethylenes with polydispersity indices (PDI = M_W/M_N, M_W = weight-averaged molecular weight, M_N = number-averaged molecular weight) varying from 4.0 to 100.[11,13]

Unlike the active sites in most conventional solid catalysts, the metal sites in the inorganic nodes of metal–organic frameworks (MOFs) exhibit remarkable structural uniformity due to the intrinsic crystalline nature of the framework.[14–16] Furthermore, numerous coordination geometries afforded by the ligating organic linkers provide the node metals with unusual electronic environments that can promote desired interactions with the substrate.[17–19] Combined with the site-isolated nature of these metal ions that are affixed to a porous framework, the coordinatively unsaturated metal sites of MOFs offer opportunities for single-site catalysis uncommon to traditional solid catalysts.[20–23] Accordingly, there have been efforts to utilize these node metal centers as active sites for ethylene polymerization.[24,25] Thus far, however, MOF catalysts for this process have required alkylaluminum cocatalysts and studies have been therefore limited exclusively to slurry phase reactions. The same holds true, for instance, for our previously-reported olefin polymerization catalysts based on cation-exchanged MFU-4l (MFU-4l = $Zn_5Cl_4(BTDD)_3$, H_2BTDD = bis(1H-1,2,3,-triazolo[4,5-b],[4',5'-i])dibenzo[1,4]dioxin))[22,26,27] that feature a wide variety of active metal cations (Ti, V, Cr, or Co) replacing the peripheral tetrahedral Zn^{2+} ions of the parent framework (Figure 5.1).[28–31] Whereas these metals are placed in a tripodal coordination environment reminiscent of those found in molecular scorpionate complexes and exhibit analogous olefin polymerization activity,[32,33] the MOF catalysts are completely inactive in the absence of alkylaluminum cocatalysts. This cocatalyst dependence and consequent restriction to liquid phase operations have limited the utility of these and other MOF catalysts, since gas phase ethylene polymerization is the specific
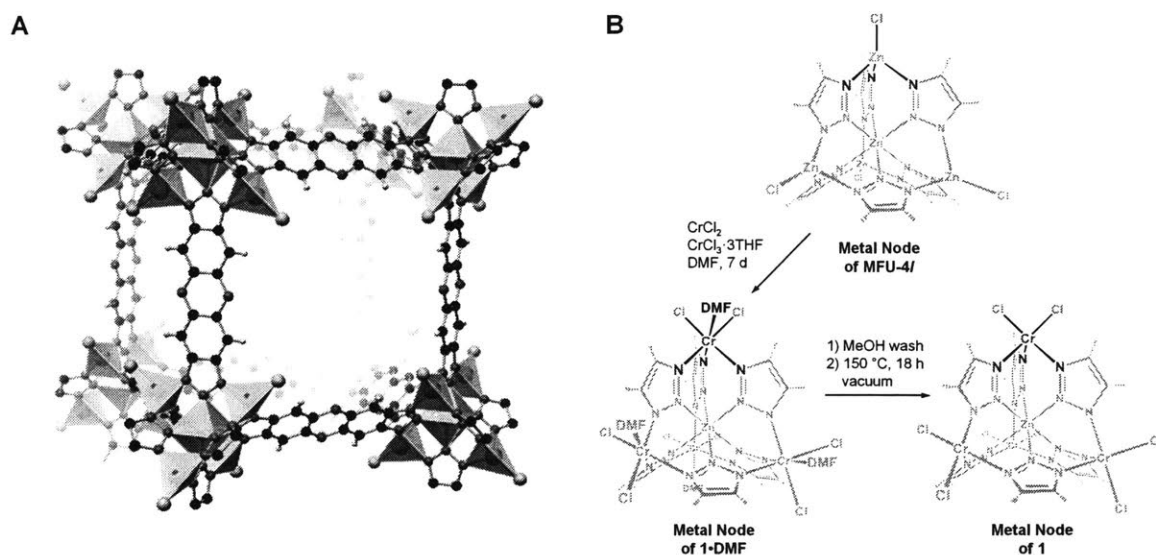
Figure 5.1. (A) Crystal structure of MFU-4*l* (B) Illustration of the inorganic nodes of MFU-4*l* and their transformation to those of Cr^{3+}-exchanged MFU-4*l* (**1**) via cation exchange and desolvation.

application for which the single-site activity and porosity of MOF catalysts can best be leveraged.

Here, we report gas phase polymerization of ethylene by Cr^{3+}-exchanged MFU-4*l* (Cr(III)-MFU-4*l*, **1**) pre-treated with AlMe$_3$. Despite the absence of excess aluminum cocatalysts during catalysis tests, the MOF catalyst shows activity for gas phase ethylene polymerization that is nearly tenfold higher than the slurry phase activity of **1**, which notably requires excess alkylaluminum under identical reaction conditions. The catalyst shows no appreciable deactivation for at least 24 h and produces dry beads of HDPE. Product polyethylene displays a low PDI of 1.36, underscoring the high degree of molecular weight control provided by our single-site MOF catalyst.

5.3. Results and Discussion

To probe the possibility of realizing gas phase polymerization with these catalysts, we prepared 1 and Cr^{2+}-exchanged MFU-4l (Cr(II)-MFU-4l, 2) as previously reported, by soaking MFU-4l in N,N-dimethylformamide (DMF) solutions of $CrCl_3$ or $CrCl_2$.[29] For 1, near-complete exchange of the tetrahedral Zn^{2+} in MFU-4l for chromium cations is achieved using 20 equivalents of $CrCl_3$ and a catalytic amount of $CrCl_2$ at room temperature (Figures 5.1 and 5.S1–S3, and Table 5.S1). In contrast, a lower extent of cation exchange at Cr_{mol}:Zn_{mol} = 2.45:2.55 was obtained with just Cr^{2+} in forming 2 (Table 5.S1). For 1, DMF in the as-synthesized material can be removed by first exchanging with methanol and drying the recovered solids under dynamic vacuum at 150 °C (Figures 5.S4). Notably, a distinct color change from forest green to a bright yellow upon solvent removal qualitatively suggests a change in the primary coordination sphere of the exchanged chromium centers.

K-edge X-ray absorption spectroscopy (XAS) provided important information on the coordination environment of chromium in 1 and 2. For comparison, a batch of Cr(III)-MFU-4l coordinated with DMF was prepared without performing the methanol exchange (1·DMF). We also analyzed $Tp_2Cr(II)$, $TpCr(III)Cl_2$·py, $Tp_2Cr(III)PF_6$, and $Tpm^*Cr(III)Cl_3$ (Tp^- = tris(pyrazolyl)borate, py = pyridine, and Tpm^* = tris(3,5-dimethylpyrazolyl)methane) as standards for Cr^{2+} and Cr^{3+} in the node of MFU-4l, having found analogous scorpionate complexes to be reliable XAS standards for nickel-, cobalt-, and vanadium-exchanged MFU-4l.[30,31,34] X-ray absorption near edge structure (XANES) analysis confirmed a chromium(III) oxidation state for 1 and a chromium(II) oxidation state for 2 (Figures 5.2A

and 5.S5); the edge energies of 1·DMF and desolvated 1 were indistinguishable at 5999.5 eV and fit among those of our chromium(III) standards, while that of 2 at 5996.1 eV was lower and much closer to the edge energies of the Cr(II) standards. Further analysis of the XANES spectrum ruled out a pseudo-tetrahedral chromium coordination geometry in 1, 1·DMF, and 2; such an arrangement is expected to produce a high-intensity pre-edge feature while 1, 1·DMF, and 2 showed pre-edge features that were similar to or smaller than those of the octahedrally coordinated chromium standards (Figure 5.S5).

The extended X-ray absorption fine structure (EXAFS) region of the XAS spectrum of dried 1 showed a first-shell peak similar in shape and position, but reduced in intensity relative to those of 1·DMF and Tpm*CrCl₃ (Figure 5.S6). This suggested similar coordination environments, but a reduced coordination number in 1, further evidence for coordinative unsaturation in 1. First-shell fits of the EXAFS data from 1 and 1·DMF (Figures 5.2B and 5.2C) and comparison with EXAFS analysis of Tp₂CrPF₆ and Tpm*CrCl₃ standards as well as computational modeling of 1 and 1·DMF by density functional theory (DFT) (Section 5.5)

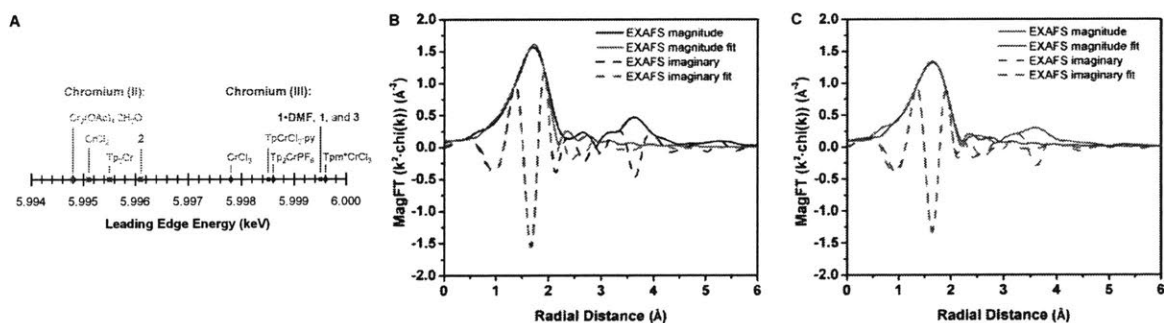**Figure 5.2.** (A) Edge energies from chromium K-edge XAS analyses of 1·DMF, 1, 2, 3, and relevant standards (Tp⁻ = tris(pyrazolyl)borate, Tpm* = tris(3,5-dimethylpyrazolyl) methane, and py = pyridine). The magnitude and imaginary parts of the Fourier-transformed k²-weighted EXAFS spectra of (B) 1·DMF and (C) 1 with their first-shell fits.

converged to primary coordination spheres consisting of 3 Cr-N and 2 Cr-Cl bonds for **1**,

and 4 Cr-N[35] and 2 Cr-Cl bonds for **1·DMF** (Table 5.1). Other coordination numbers resulted

in quantitatively worse fits, while the resulting bond lengths agreed well with those

obtained by DFT and EXAFS analyses of the standards. Furthermore, our DFT models

showed a pseudooctahedral coordination in **1·DMF** that converts to a pseudo-square

pyramidal or monovacant octahedral geometry for **1** upon removal of coordinated DMF

(Section 5.5). Indeed, these results are highly consistent with the reported structure of

other coordinatively unsaturated chromium tris(pyrazolyl)borate complexes.[36]

Unfortunately, suitable EXAFS fits were not obtained for **2**, perhaps due to disordered

solvation of chromium in both of these materials. The XAS data support a scenario wherein

cation exchange initially affords an octahedral Cr(III) center in **1·DMF** bearing one DMF

molecule (Figure 5.1B). Subsequent solvent exchange and drying results in a five-coordinate,

pseudo-square planar Cr(III) in **1**, with one open coordination site.

Table 5.1. Results of the EXAFS and DFT Analyses.[a]

Sample	Scattering Pair	CN[b]	Bond Length (Å)	S_0^2	ΔE_0 (eV)	σ^2 (Å²)
1·DMF	Cr–N	4	2.03	0.69	-5.4	0.002
	Cr–Cl	2	2.27			0.002
1	Cr–N	3	1.99	0.69	-5.4	0.002
	Cr–Cl	2	2.26			0.002
DFT-**1·DMF**	Cr–N/O[35]	4	2.058	-	-	-
	Cr–Cl	2	2.351	-	-	-
DFT-**1**	Cr–N	3	2.032	-	-	-
	Cr–Cl	2	2.290	-	-	-
Tp₂CrPF₆	Cr–N	6	2.02	0.65	-2.3	0.002
Tpm*CrCl₃	Cr–Cl	3	2.29	0.69	-1.3	0.002

[a] The average error in in bond length is 0.02 Å, in ΔE_0 is 2.3 eV, and in σ^2 is 0.001 Å². [b] CN = Coordination number.

With the presumed structure of **1** in hand, we next sought ways to convert it to a self-activating catalyst for gas phase ethylene polymerization. Although alkylchromiums are often invoked as the active species for chromium-based ethylene polymerization, their high reactivity demands rigorous site isolation to be observed experimentally.[9,36] Consequently, active chromium catalysts are conventionally generated *in situ* from precatalysts by adding excess alkylaluminum cocatalysts to the reaction medium or by subjecting the supported precatalysts to ethylene atmosphere at elevated temperatures. Given the site-isolated nature of the node metals in MOFs, we surmised that *ex situ* activation of **1** with alkylaluminums could provide a stable and isolable chromium(III) alkyl. Such a species suspended within a porous scaffold would then be accessible to incoming ethylene molecules for gas phase polymerization. To this end, **1** was treated with 0.2 M of $AlMe_3$ in hexane and vacuum-dried after filtration. The dry, $AlMe_3$-treated Cr(III)-MFU-4*l* (**3**) is crystalline and porous, as confirmed by powder X-ray diffraction XRD and N_2 sorption analyses (Figures 5.S1 and 5.S2). ICP-MS revealed a molar Cr:Al ratio of 1:1.8 for **3**, indicating some retention of aluminum species within the framework (Table 5.S1). Chromium K- edge XAS analysis of **3** showed an edge energy at 5999.5 eV that was unchanged from those of **1** and **1·**DMF, confirming the retention of chromium(III) centers following treatment with $AlMe_3$ (Figures 5.2A and 5.S7). The EXAFS region of **3** is remarkably similar to that of **1**, with the only major difference that the first shell peak displayed a significantly diminished scattering intensity (Figure 5.S7). The reduced intensity is consistent with the presumed alkylation from Cr(III)–Cl to Cr(III)–CH_3 while maintaining the node structure around the chromium centers.

The gas phase ethylene polymerization activity of **3** was probed by subjecting it to semi-batch reactions under constant ethylene pressure in the complete absence of solvent or cocatalyst. Notably, static pressurization of 2.0 mg of **3** at room temperature with 40 bar of ethylene for 1 h yielded 7.06 g polyethylene as free-flowing white granules (Figures 5.3 and 5.S8). This activity corresponds to a turnover frequency of 52,000 $mol_{Ethylene} \cdot mol_{Cr}^{-1} \cdot h^{-1}$, more than an order of magnitude higher than that observed when **1** was subjected to analogous liquid phase reactions in the presence of excess solutions of $AlMe_3$ (Table 5.2). In contrast, neither $AlMe_3$-treated MFU-4*l* nor pristine **1** polymerize ethylene under these conditions, confirming that both the cation-exchanged chromium centers in **1** and their subsequent treatment with $AlMe_3$ are required for catalysis (Table 5.2).

Differential scanning calorimetry characterization of the polyethylene product from a gas phase reaction revealed the polymer as HDPE with a high melting temperature of 130 °C and a moderate crystallinity of 66% (Figure 5.S9). Further analysis with high temperature

AlMe₃-treated Cr-MFU-4*l*   **Polyethylene Granules**
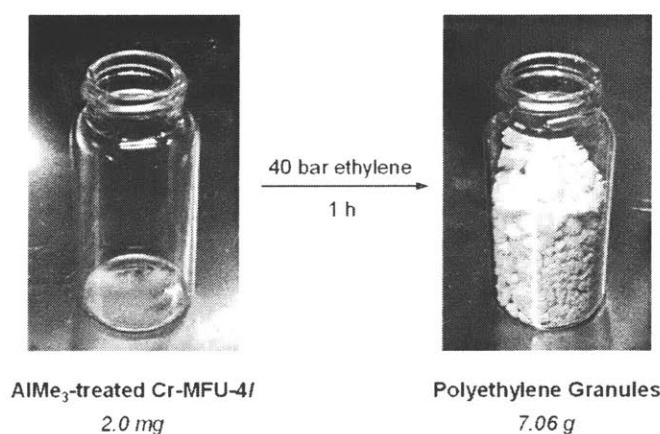2.0 mg   7.06 g

Figure 5.3. AlMe₃-treated Cr-MFU-4*l* before and after a gas phase ethylene polymerization reaction (Table 5.2, entry 1).

Table 5.2. Results of Ethylene Polymerization Reactions[a]

Entry	Catalyst	Cocatalyst	Solvent	$P_{Ethylene}$ (bar)	t (h)	TOF[b] ($mol_{Ethylene} \cdot mol_{Cr}^{-1} \cdot h^{-1}$)	T_m^c (°C)	X_C^c (%)	PDI[d]	M_N^e (kDa)
1	AlMe₃-treated Cr(III)-MFU-4l	None	None	40	1	52,000	130	66	1.36	298
2	Cr(III)-MFU-4l	AlMe₃[f]	Toluene	40	1	4,500	130	66	1.42	331
3	Cr(III)-MFU-4l	None	None	40	1	0	-	-	-	-
4	AlMe₃-treated MFU-4l	None	None	40	1	0	-	-	-	-
5[g]	Cr(III)-MFU-4l	AlMe₃[f]	Toluene	40	1	3,800	130	64	1.48	297

[a] Unless otherwise noted, reactions were conducted at room temperature without external temperature control. [b] TOF = turnover frequency. [c] Second scan percent crystallinity (X_C) and melting peak (T_m) as evaluated by differential scanning calorimetry. [d] PDI = polydispersity index [e] M_N = number-averaged molecular weight. [f] 100 molar equivalents of AlMe₃ to the ICP-MS-derived moles of chromium in Cr(III)-MFU-4l. [g] Reaction conducted at 35 °C.

gel permeation chromatography revealed a number-averaged molecular weight (M_N) of 298 kDa and a remarkably low PDI of 1.36 for the polymer product (Figure 5.S10). This exceptionally low PDI value demonstrates the structural monodispersity of the active sites in our catalyst and also suggests facile gas phase diffusion of ethylene to the active sites. Indeed, mass transport limitations are known to increase PDI through inhomogeneous local ethylene concentions.[37-39] It is also noteworthy that the polyethylene product is directly obtained in the form of free-flowing granular beads, the favored morphology for industrial processing of polyethylenes (Figure 5.3).[10]

Expectedly, when the gas phase ethylene polymerization reaction with 3 is run without external temperature control, the temperature of the reactor increases spontaneously during the course of the reaction (Figure 5.S11). We ascribe this exotherm to the high heat of reaction from ethylene polymerization ($\Delta H^\circ_{rxn} = 93.6$ kJ·mol⁻¹) that was retained in our batch reactor system.[3] In fact, this exothermic behavior caused the linear dependence of polymerization activity on ethylene pressure to deviate at higher pressures, where higher

activities were obtained (Figure 5.S11). To account for the exothermicity, we conducted a control reaction where **1** and excess AlMe$_3$ in toluene were subjected to 40 bar of ethylene for 1 h at 35 °C, the average temperature measured from a gas phase reaction with **3** (Table 5.2, entry 5). Surprisingly, the liquid phase reaction with **1** and AlMe$_3$ at elevated temperature resulted in activity even lower than that of the identical reaction conducted without heating. We attribute this behavior to the thermally-accelerated deactivation of **1** in the presence of excess AlMe$_3$ and solvent: under these conditions, alkylaluminums are known to exchange the active sites in the nodes of MFU-4*l* and cause subsequent reduction, aggregation, and formation of transition metal nanoparticles.[40] Importantly, these deactivation pathways are inaccessible to **3**, whose catalytic activity does not require liquid medium or additional alkylaluminum. Indeed, not only does **3** retain its activity despite autogenous heating, but its activity persists and no appreciable deactivation is observed even for prolonged reaction times of 24 h (Figure 5.4).
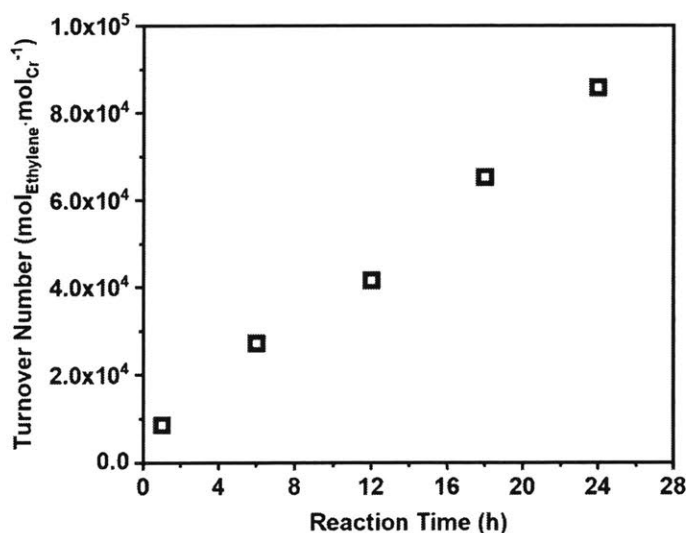

Figure 5.4. Gas phase ethylene polymerization with AlMe$_3$-treated Cr-MFU-4*l*. Reaction conditions: 2.0 mg catalyst, 10 bar ethylene, and room temperature.

5.4. Conclusion

In summary, we show for the first time that MOFs are capable catalysts for gas phase ethylene polymerization, with activity and lifetime surpassing those of the liquid-phase process. Isolation of Cr-alkyl species prior to catalytic tests affords active MOFs that do not require solvent or the presence of *in situ* alkylaluminum cocatalyst. HDPE produced by this catalyst in the gas phase presents as free-flowing granules with exceptionally low polydispersity. We attribute this favorable performance of the catalyst to the site accessibility and structural uniformity unique to the isolated single sites in the MOF platform. We believe these intrinsic structural advantages could be further utilized to develop improved MOF catalysts for the commercially-important gas phase ethylene polymerization reaction.

5.5. Experimental Information

General Considerations

All manipulations of air/water-sensitive compounds were conducted using standard inert-atmosphere glove box and Schlenk line techniques.

Powder X-ray diffraction (PXRD) patterns were recorded on a Bruker Advance II diffractometer equipped with $\theta/2\theta$ Bragg-Brentano geometry and Ni-filtered Cu Kα radiation (Kα_1 = 1.5406 Å). The tube voltage and current were 40 kV and 40 mA, respectively. Dry powdered sample was placed in a polyimide capillary tube or on a rotating zero-background silicon crystal plate for analysis.

Nitrogen adsorption isotherms were measured by a volumetric method using a Micromeritics ASAP 2020 gas sorption analyzer. ~30 mg of sample was pre-activated under vacuum overnight to remove all residual solvent and transferred to a pre-weighed analysis tube in a glove box. The tube containing the sample was weighed again to determine the mass of the sample, capped with a Micromeritics TranSeal, brought out of the glove box, and transferred to the analysis port of the gas sorption analyzer. Free space correction measurements were performed using an ultra-high purity helium gas (UHP grade, Airgas) and nitrogen isotherms were measured using an ultra-high purity grade nitrogen (UHP grade, Airgas). All nitrogen analyses were performed using a liquid nitrogen bath at 77 K.

Metal content of samples was quantified using Agilent 7900 inductively coupled plasma mass spectrometer (ICP-MS). ~10 mg sample was weighed in a glove box, transferred to an acid digestion vessel (Model 4749, Parr Instrument Company), and digested in ~3 mL of concentrated nitric acid (67~70% w/v %, BDH Aristar) at 150 °C overnight. Metal concentrations of the resulting solution were determined using calibration curves constructed from standard solutions (ICP-MS certified reference standards, VWR).

Energy dispersive X-ray spectroscopy (EDX) analyses were conducted using a JEOL 6010LA analytical scanning electron microscope at 15 keV and a working distance of 10 mm. Dry powdered samples were mounted onto a stage using carbon tape and sputtered with Au prior to analysis.

X-ray absorption spectroscopy (XAS) measurements at the chromium K-edge (5.9892 keV) were performed on the 10-ID beamline of the Materials Research Collaborative Access Team at the Advanced Photon Source, Argonne National Laboratory. Data was acquired in transmission and step-scan mode using ionization chambers optimized for the maximum current with linear response ($\sim$1010 photons detected/sec). A chromium foil spectrum was acquired simultaneously with each sample measurement for energy calibration. Analytes were pressed in a N_2 glovebox into a cylindrical sample holder consisting of six wells, forming a self-supporting wafer which was then placed in a quartz tube (2.5 cm OD, 10.0 cm length) sealed with Kapton windows by two Ultra-Torr fittings.

First-shell fits of the extended X-ray absorption fine structure (EXAFS) analysis were performed using the Artemis software.[41] Initial bond lengths and coordination numbers were determined from a proposed structural model whereas the closeness between simulated data and experimental data were evaluated using S_0^2, ΔE_0, ΔR, and $\Delta\sigma^2$ parameters. A good fit was obtained by adjusting the coordination number and bond distances of the model until reasonable parameters were obtained. When comparing multiple samples, the S_0^2 value was typically determined by fitting reference compounds.

Attenuated total reflectance infrared (ATR-IR) absorption spectra were acquired using either a Bruker Tensor 37 instrument with a germanium tip ATR sample holder in air or a Bruker Alpha instrument with a diamond tip ATR sample holder under an inert atmosphere.

Differential scanning calorimetry (DSC) analyses were conducted on a Texas Instruments Q100 using a crimped standard sample pan. A double-scan method was used in order to eliminate inconsistencies due to variation in the thermal or mechanical history of individual samples. This method is summarized as follows: 1) Equilibrate at 0 °C. 2) Heat at a rate of 10 °C per minute until 200 °C. 3) Maintain 200 °C for two minutes. 4) Cool the sample at a rate of 10 °C per minute until 0 °C. 5) Heat at a rate of 10 °C per minute until 200 °C. 6) Maintain 200 °C for two minutes. 7) Cool the sample at a rate of 10 °C per minute until 0 °C. Thermal parameters (heat of fusion (ΔH_f) and melting temperature maxima (T_M)) were taken from the second heating cycle (step 5).

High temperature gel permeation chromatography (HT-GPC) analyses were conducted on an Agilent PL-GPC220.

Materials

N,N-Dimethylformamide (DMF, 99.5%, Sigma-Aldrich), toluene (99.8% Sigma-Aldrich), hexane (≥99%, Sigma-Aldrich), ethanol (99.9%, Sigma-Aldrich), methanol (99.9%, VWR), and diethyl ether (≥99%, Sigma-Aldrich) were passed through two silica columns in a Glass Contour solvent purification system, degassed with a flow of argon gas for 30 min, subjected to at least three freeze-pump-thaw cycles, and dried over activated molecular sieves prior to use. Pyridine (anhydrous, 99.8%, Sigma-Aldrich) was subjected to at least three freeze-pump-thaw cycles, and dried over activated molecular sieves prior to use. Ethylene (UHP, Airgas) was passed through an oxygen trap (304L-HDF4-150, Swagelok) filled with activated molecular sieves and pre-reduced Cu catalyst (8 x 14 mesh Q-5, Research Catalysts) prior

to use. MFU-4*l* was prepared and characterized according to literature procedure[42].

Chromium (II) chloride (99.99%, Strem Chemicals), chromium (III) chloride

tetrahydrofuran adduct (98%, Strem Chemicals), chromium (III) chloride hexahydrate

(>99.5%, Alfa Aesar), potassium hydrotris(pyrazol-1-yl)borate (98%, Strem Chemicals),

lithium hexafluorophosphate (98%, Sigma-Aldrich), zinc dust (≥98%, Sigma-Aldrich),

sodium acetate (≥99.0 %, Fisher Scientific) hydrochloric acid (99.999% metals basis, Alfa

Aesar), and trimethylaluminum (2.0 M in hexanes and 2.0 M in toluene, Sigma-Aldrich)

were used as received.

Experimental Details

Preparation of Cr(III)-MFU-4*l* (1 and 1·DMF): A typical procedure involved charging a

bottle containing a suspension of MFU-4*l* (500 mg, 0.396 mmol) and DMF (100 mL) with a

DMF (100 mL) solution of $CrCl_2$ (97.3 mg, 0.792 mmol, 2.0 equivalents), and $CrCl_3(THF)_3$

(2.95 g, 7.92 mmol, 20 equivalents) in an inert-atmosphere glove box. The resulting

suspension was maintained under these conditions at ambient temperature for seven days,

after which the solids were filtered off. For the preparation of 1·DMF, the resulting solid

was then soaked in dry DMF twice for 24 h each, followed by CH_2Cl_2 twice for 24 h each.

The solid was then dried under vacuum at 100°C for 18 h until the overhead pressure

reached $<10^{-5}$ torr. For the preparation of 1, the obtained solid from the initial cation

exchange in DMF was re-suspended in methanol (200 mL) and heated at 60 °C for 24 h in

a sealed bottle. This hot soaking procedure was repeated two times. The resulting material

was then dried under vacuum at 150 °C for 18 h until the overhead pressure reached $<10^{-5}$

torr. *Heating at higher temperatures under vacuum, without performing the methanol soak first, resulted in loss of crystallinity before loss of DMF as determined by IR and PXRD analysis.*

Preparation of Cr(II)-MFU-4l (2): A typical procedure involved charging a bottle containing a suspension of MFU-4l (500 mg, 0.396 mmol) and DMF (100 mL) with a DMF (100 mL) solution of $CrCl_2$ (2.43g, 19.8 mmol, 50 equivalents) in an inert-atmosphere glove box. The resulting green suspension was maintained under these conditions at ambient temperature for seven days, after which the solids were filtered off. The obtained solid was then soaked in *DMF* for three days, removing the solvent by filtration every 24 h. The product was then soaked in hot tetrahydrofuran (60 °C) under air free conditions for three days, changing the supernatant every 24 h. The resulting material was then dried under vacuum at 150 °C for 18 h until the overhead pressure reached $<10^{-5}$ torr.

Preparation of AlMe$_3$-treated Cr(III)-MFU-4l (3): A typical procedure involved charging a glass vial containing 1 (50.0 mg, 37.0 μmol) with a hexane solution of 0.2 M AlMe$_3$ (1.5 mL, 0.294 mmol, 8 equivalents) in an inert-atmosphere glove box. The resulting suspension was maintained under these conditions at ambient temperature for 3 h, after which the solids were filtered off. The obtained solid was then re-suspended in hexane (3.0 mL) and maintained at ambient temperature overnight. This washing procedure was repeated two times. The resulting material was then dried under vacuum for 18 h.

Preparation of TpCrCl₂·pyridine: TpCrCl₂·pyridine was prepared and characterized according to literature procedure.[43]

Preparation of Tpm*CrCl₃: Tpm*CrCl₃ was prepared and characterized according to literature procedure.[44]

Preparation of Chromium(II) acetate hydrate ($Cr_2(OAc)_4$·2H_2O):[45] The reaction was set up in a three-neck round bottom flask, containing a suspension of $CrCl_3$·6H_2O (10.0 g, 38 mmol), zinc dust (8.0 g, 122 mmol), water (34 mL) and a magnetic stir bar, and degassed by sparging with nitrogen. Concentrated HCl (17 mL) was then added via an addition funnel at such a rate as to avoid overfoaming of the reaction. After gas evolution had ceased, a deep blue solution was observed over a suspension of unreacted zinc. This suspension was allowed to settle and then the solution was transferred by syringe (without transferring the zinc) to a flask containing sodium acetate (36 g, 439 mmol) and water (55 mL, degassed by three cycles of freeze-pump thaw). The resulting red suspension was then filtered, working quickly to minimize exposure of the product to air. After rinsing with 150 mL water, 75 mL ethanol, and 50 mL diethyl *ether (all degassed by sparging with nitrogen), the resulting brick red solid was transferred to a Schlenk flask. The resulting brick red powder was dried under vacuum and transferred to a nitrogen glovebox for handling and storage. 5.93 g, 15.7 mmol, 83% yield. Note that samples of $Cr_2(OAc)_4$·2H_2O start to visibly discolor after one hour of exposure to air, and turn totally grey after overnight exposure to air. Samples could be removed from the glovebox and immediately analyzed without significant decomposition. No decomposition was apparent, however, after four years of storage in a nitrogen glovebox. IR*

(diamond ATR, nitrogen glovebox): 3481, 3367, 3269, 2987, 1568, 1450, 1418, 1354, 1030, 679, 625, 542, 406 cm^{-1}. UV-Vis (H$_2$O, 23 °C): λ_{max} = 408, 568 nm.[46] Elemental analysis: C (24.68% found, 25.54% theory, −0.86% difference), H (3.74% found, 4.29% theory, −0.55% difference), and N (<0.02% found, 0% theory).
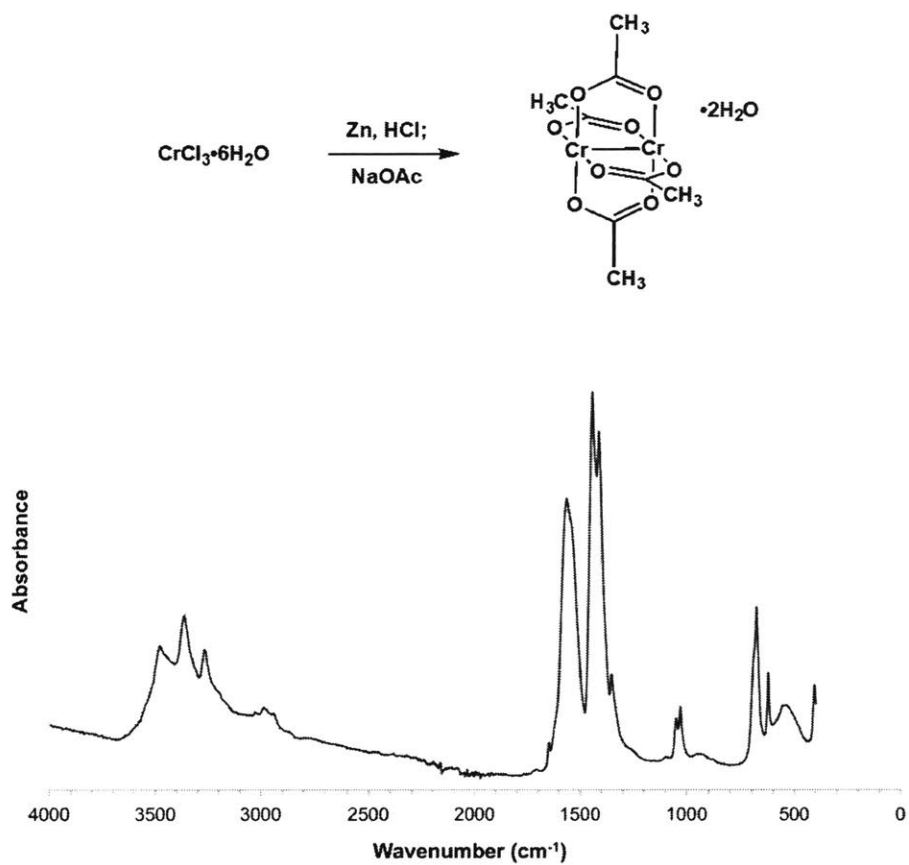

Figure 5.S-A. IR spectrum of Cr$_2$(OAc)$_4$·2H$_2$O. Diamond ATR, nitrogen atmosphere.

Preparation of CrCl$_2$·2 pyridine:[47,48] A suspension of CrCl$_2$ (500 mg, 4.07 mmol) and pyridine (10.0 mL, 124 mmol) was heated to reflux under nitrogen atmosphere with magnetic stirring in a Schlenk flask equipped with a condenser for one hour. The reaction

was then allowed to cool to room temperature, and then continue to stirring for 14 h. In a nitrogen glovebox, a bright green solid was isolated by vacuum filtration, leaving an olive colored mother liquor. The solid was rinsed with pyridine (5 mL), toluene (10 ml) and hexane (10 mL) and then dried under vacuum. 925 mg, 3.29 mmol, 80 % yield. *Although no significant color change was observed after one hour of exposure to air, after over 12 h the solid turned dark green. The solid was stored and handled in a nitrogen glovebox, but could be briefly exposed to air for analysis.* Elemental analysis: C (42.72% found, 42.73% theory, 0.01% difference), H (3.71% found, 3.59% theory, 0.12% difference), N (9.84% found, 9.97% theory, 0.13% difference). IR (Ge ATR, briefly exposed to air): 3115, 3067, 3044, 3006, 1660, 1608, 1575, 1492, 1448, 1367, 1241, 1222, 1156, 1080, 1044, 1015, 760, 690, 641 cm^{-1}.
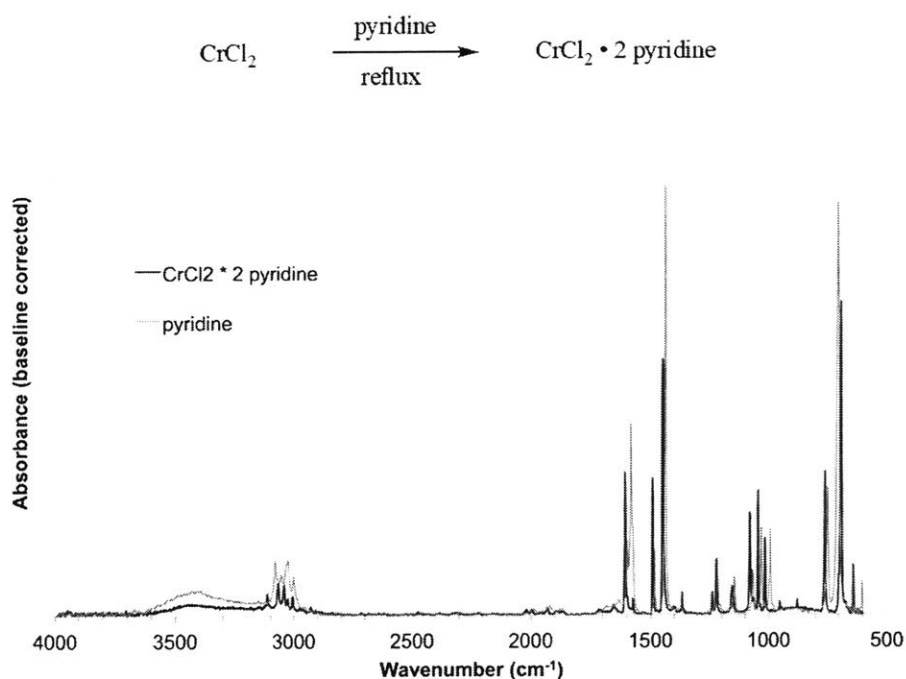
$$CrCl_2 \quad \xrightarrow[\text{reflux}]{\text{pyridine}} \quad CrCl_2 \cdot 2\ \text{pyridine}$$

Figure 5.S-B. IR spectrum of $CrCl_2\cdot$2pyridine. Ge ATR, exposed briefly to air.

Preparation of Tp₂Cr·2KCl: In a nitrogen glovebox, a homogeneous solution of $CrCl_2$ (122 mg, 0.992 mmol) and methanol (10 mL) was added in drops to a solution of potassium hydrotris(pyrazol-1-yl)borate (KTp, 500 mg, 1.98 mmol) and methanol (10 mL). After stirring for 40 minutes, an olive colored powder was filtered from a rose-colored mother liquor. The product was then rinsed with methanol and then dried under vacuum. 444 mg, 0.708 mmol, 71% yield. *Exposure of the solid to air leads to an immediate color change to dark brown.* The product was stored and analyzed in a nitrogen glovebox only. Elemental analysis: C (32.27% found, 34.47% theory, difference 2.2%), H (2.83% found, 3.22% theory, 0.39% found), N (24.64% found, 26.80% theory, 2.16% difference). IR (diamond ATR, nitrogen glovebox) 3117, 2472 (v_{B-H}), 1498, 1403, 1295, 1204, 1112, 1054, 1040, 983, 960, 752, 715, 660, 617 cm⁻¹.

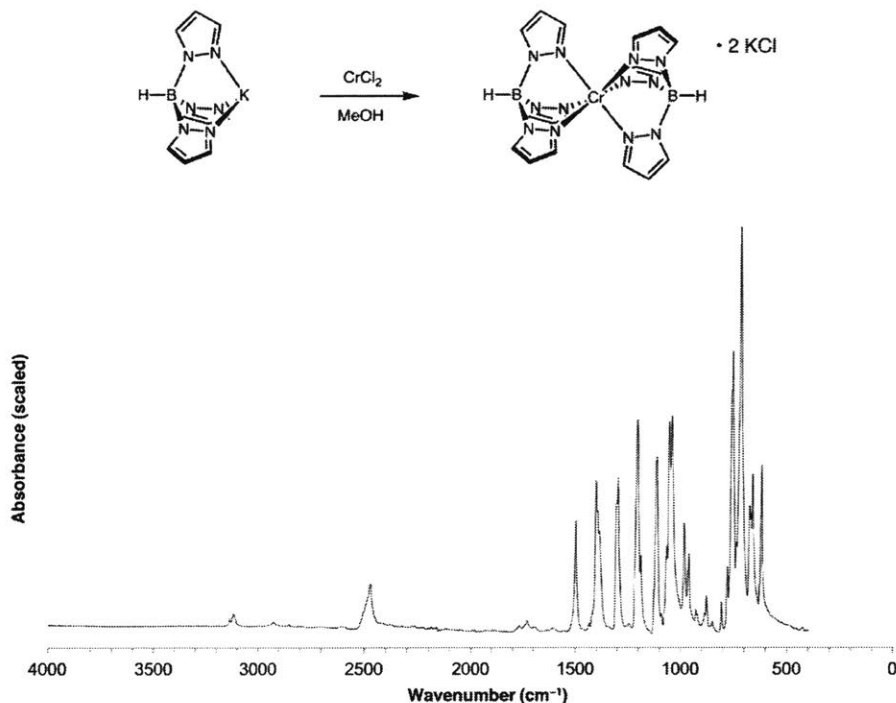**Figure 5.S-C**. IR spectrum of Tp₂Cr·2KCl. Diamond ATR, nitrogen atmosphere.

Preparation of Tp₂CrPF₆: In a nitrogen glovebox, a solution of $CrCl_2$ (122 mg, 0.992 mmol) and methanol (10 mL) was added to a stirring solution of potassium hydrotris(pyrazol-1-yl)borate (KTp, 500 mg, 1.98 mmol) and methanol (10 mL). The addition resulted in a suspension consisting of a tan solid underneath a green solution. The reaction was then removed from the glovebox, and stirred open to the air for one hour, during which the tan solid slowly dissolved resulting in a burgundy solution. This solution was then transferred dropwise to s stirring solution of lithium hexafluorophosphate (300.8 mg, 1.98 mmol, 2.0 equiv.) and water (10 mL), resulting in the precipitation of a yellow solid. This suspension was diluted by 20 mL water and then the yellow solid was obtained by filtration, rinsing several times with water and then drying under vacuum. 300 mg, 0.482 mmol, 49% yield. Yellow, block shaped crystals could be produced by vapor diffusion of water into a dilute methanol solution of Tp₂CrPF₆. Elemental Analysis: C (34.52% found, 34.70% theory, 0.18% difference), H (3.06% found, 3.24% theory, 0.18% difference), N (26.64% found, 26.98% theory, 0.34% found). IR (Ge ATR, benchtop): 3155, 2513 (v_{B-H}), 1505, 1407, 1390, 1311, 1205, 1191, 1115, 1076, 1053, 989, 882, 843, 771, 709 cm⁻¹.
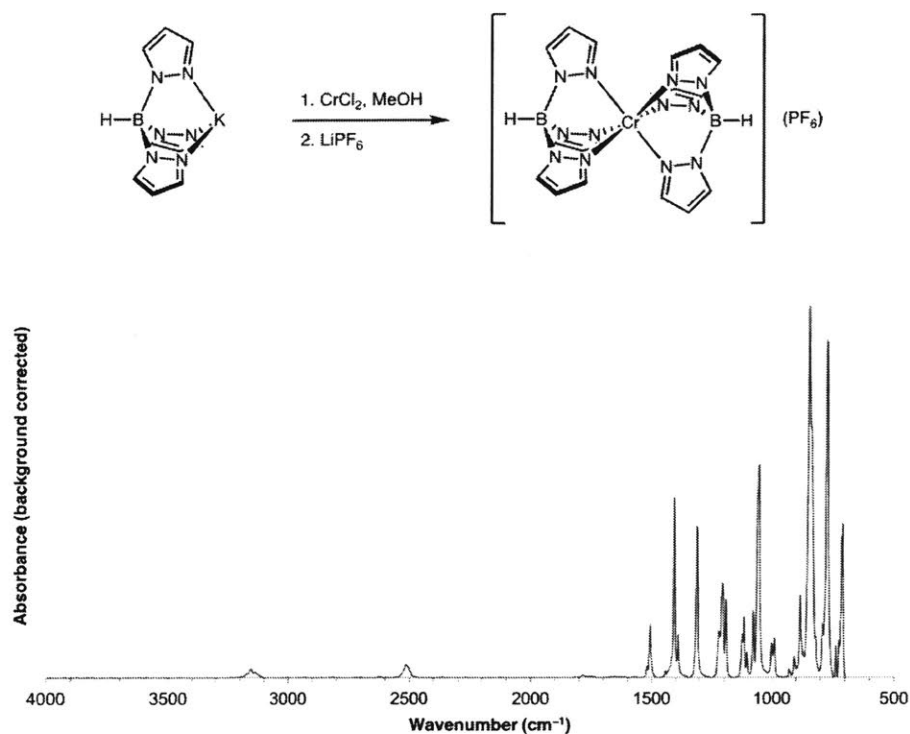
Figure 5.S-D. IR spectrum of Tp$_2$CrPF$_6$. Ge ATR, background corrected.

Gas Phase Polymerization of Ethylene with AlMe$_3$-treated Cr(III)-MFU-4*l* (3): A typical procedure involved charging a glass vial with **3** (2.0 mg, 0.80 µmol) and transferring the vial to a 50 mL stainless-steel pressure vessel reactor (Series 4790, Parr Instrument Company) in an inert-atmosphere glove box. The sealed reactor was then taken out of the glove box, placed in a hood, and slowly pressurized with ethylene to the desired pressure, after which the pressure was maintained by keeping the reactor connected to the ethylene cylinder. Temperature of the reactor was monitored using a temperature controller (Digi-Sense, 68900) and an internal thermocouple probe (Omega, KQXL-18) that was suspended ~0.5 cm above the bottom of the glass vial in the reactor. After the specified time, the reactor was slowly vented and opened to recover the solid product in the glass vial. The

obtained free-flowing granular beads were later subjected to ATR-IR, DSC, and HT-GPC analyses.

Slurry Phase Polymerization of Ethylene with Cr(III)-MFU-4*l* and AlMe₃: A typical procedure involved charging a glass vial with **1** (2.0 mg, 1.5 µmol), a toluene solution of 75 mM AlMe₃ (2.0 ml, 0.150 mmol, 100 equivalents), and a magnetic stir bar, then transferring the vial to a 50 mL stainless-steel pressure vessel reactor (Series 4790, Parr Instrument Company) in an inert-atmosphere glove box. The sealed reactor was then taken out of the glove box, placed in a hood, and slowly pressurized with ethylene to the desired pressure, after which magnetic stirring was started and pressure was maintained by keeping the reactor connected to the ethylene cylinder. Temperature of the reactor was monitored and controlled using a temperature controller (Digi-Sense, 68900) and an internal thermocouple probe (Omega, KQXL-18) that was suspended ~0.5 cm above the bottom of the glass vial in the reactor. After the specified time, the reactor was slowly vented, opened to air, and then quenched with methanol. The resulting suspension was transferred to a round bottom flask using excess methanol and the solvent was removed under vacuum. The resulting solid was treated with 100 mL of methanol and 10 mL HCl, sonicated for 30 min, and then filtered off and dried in vacuo. The obtained solids were later subjected to ATR-IR, DSC, and HT-GPC analyses.

DFT Analysis Method: A truncated model of **1** was prepared by focusing on one Cr₄ZnCl₈(benzotriazolate)₆ cluster, assuming coordination of chromium by three nitrogens and two extraframework chlorides. Benzotriazolate ligands were substituted for the

BTDD^{2-} ligands in MFU-4l. We optimized the geometry for three MOF fragments using Density Functional Theory (DFT)[49,50], using the software packaged Q-Chem 5.0.[51] For these calculations, we used the functional PBE[52] and a 6-31g[53,54] basis set. We set the total energy convergence threshold for the geometry optimization to 5.0*10^{-8}. For both 1 and 1·DMF, we calculated a range of spin multiplicities in order to ascertain the likely ground electronic state for the cluster. For both Cr(III)-MFU-4l clusters, the two lowest energy spin states were m_s = 1 and m_s = 2, with energy differences of less than 0.02 eV and thereby indistinguishable in DFT. For simplicity we discuss the high-spin state m_s = 2.

DFT Analysis of Unsolvated 1: Figure 5.S-E depicts the structure of DFT-1. Each of the chromium centers is mono-vacant octahedral/square pyramidal in geometry, with two equatorial Cr-Cl bonds, two equatorial Cr-N bonds, and one axial Cr-N bond. The average Cr-Cl bond length is 2.290 Å and the average Cr-N bond length is 2.032 Å (Table 5.S-A), consistent with the distances of 2.26 and 1.99 obtained by EXAFS fitting. Averages of 1.961 Å and 2.067 Å were obtained for axial and equatorial Cr-N bond lengths displaying a significant trans effect. The average Cl-Cr-N bond angles are 163.8° (*trans*-equatorial) and 97.8° (*cis*-axial). These average dimensions are summarized in Figure 5.S-E.
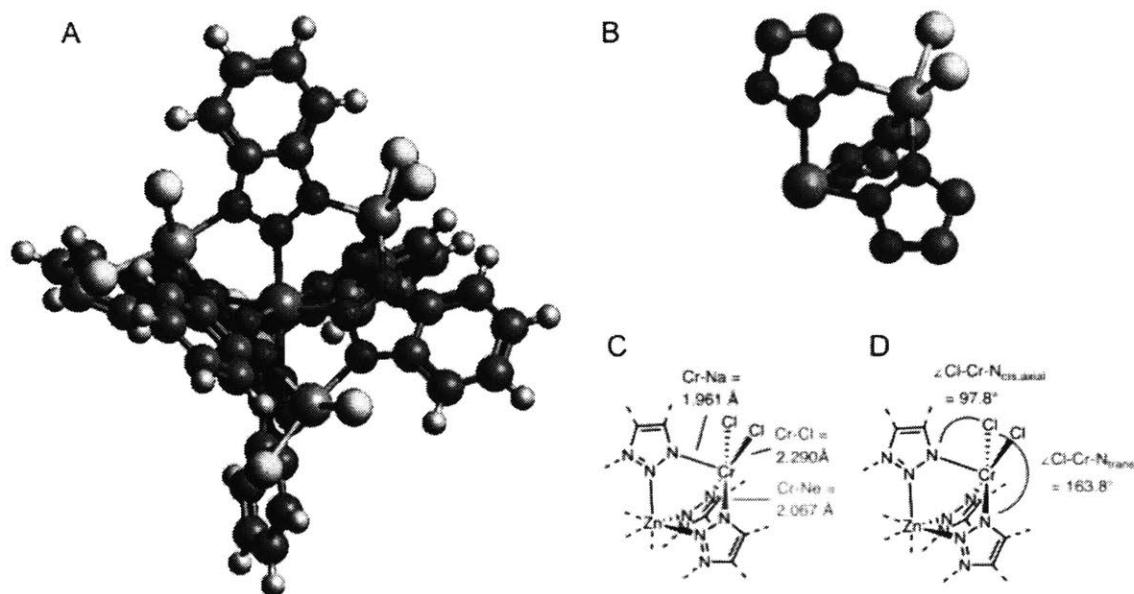
Figure 5.S-E Structure of DFT-1 A) full structure of model. B) Truncated structure of DFT-1 highlighting the primary coordination structure of chromium in this material. C) Selected average bond lengths. D) Selected average bond angles.

Table 5.S-A. Selected bond lengths and bond angles extracted from DFT-1.

Dimension	Cr1	Cr2	Cr3	Cr4
Cr–N$_{equatorial}$(1)	2.085 Å	2.077 Å	2.077 Å	2.060 Å
Cr–N$_{equatorial}$(2)	2.067 Å	2.054 Å	2.067 Å	2.050 Å
Cr–N$_{axial}$	1.970 Å	1.969 Å	1.963 Å	1.940 Å
Cr–Cl(1)	2.297 Å	2.285 Å	2.299 Å	2.276 Å
Cr–Cl(2)	2.298 Å	2.294 Å	2.293 Å	2.281 Å
<Cl-Cr-N$_{trans}$(1)	169.3°	166.1°	169.7°	168.6°
<Cl-Cr-N$_{trans}$(2)	160.3°	156.7°	160.4°	159.8°
<Cl-Cr-N$_{axial}$(1)	101.3°	100.9°	99.5°	95.0°
<Cl-Cr-N$_{axial}$(2)	93.8°	97.2°	93.7°	100.7°

DFT Analysis of 1·DMF: Figure 5.S-F depicts the structure of DFT-1·DMF. Each of the chromium centers is pseudo-octahedral in the primary coordination sphere, with two equatorial Cr-Cl bonds, three Cr-N bonds, and one Cr-O bond. The average Cr-Cl bond length is 2.351 Å, compared with the value of 2.27 Å resulting from the EXAFS fit. The average Cr-N bond length is 2.063 Å and the average Cr-O bond length is 2.044 Å (Table 5.S-B), but our XAS method does not distinguish between N and O scatterers. So we use an average Cr-N/O bond length of 2.058 Å to compare with the value of 2.03 Å obtained by the XAS fit (Table 5.1). Averages of 2.036 Å and 2.077 Å were obtained for Cr-N bond lengths trans to DMF and trans to chloride respectively displaying a much smaller trans effect than in unsolvated 1.
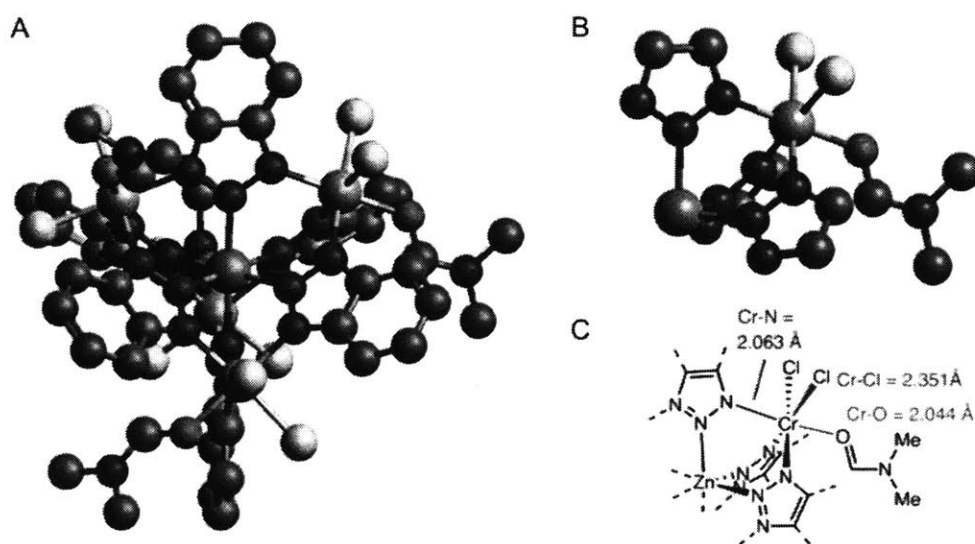

Figure 5.S-F Structure of DFT-1·DMF A) full structure of model, hydrogens omitted for clarity. B) Truncated structure of DFT-1·DMF highlighting the primary coordination structure of chromium in this material. C) Selected average bond lengths.

Table 5.S-B. Selected bond lengths extracted from DFT-1·DMF.

Bond Length	Cr1	Cr2	Cr3	Cr4
Cr-N_{Cl} (1)[a]	2.098	2.070	2.086	2.056
Cr-N_{Cl} (2)[a]	2.087	2.069	2.075	2.071
Cr-N_{DMF}[b]	2.040	2.031	2.044	2.028
Cr-O(DMF)	2.050	2.048	2.030	2.046
Cr-Cl (1)	2.350	2.333	2.372	2.341
Cr-Cl (2)	2.349	2.346	2.378	2.340

[a]Cr-N bond trans to chloride. [b]Cr-N bond trans to DMF.
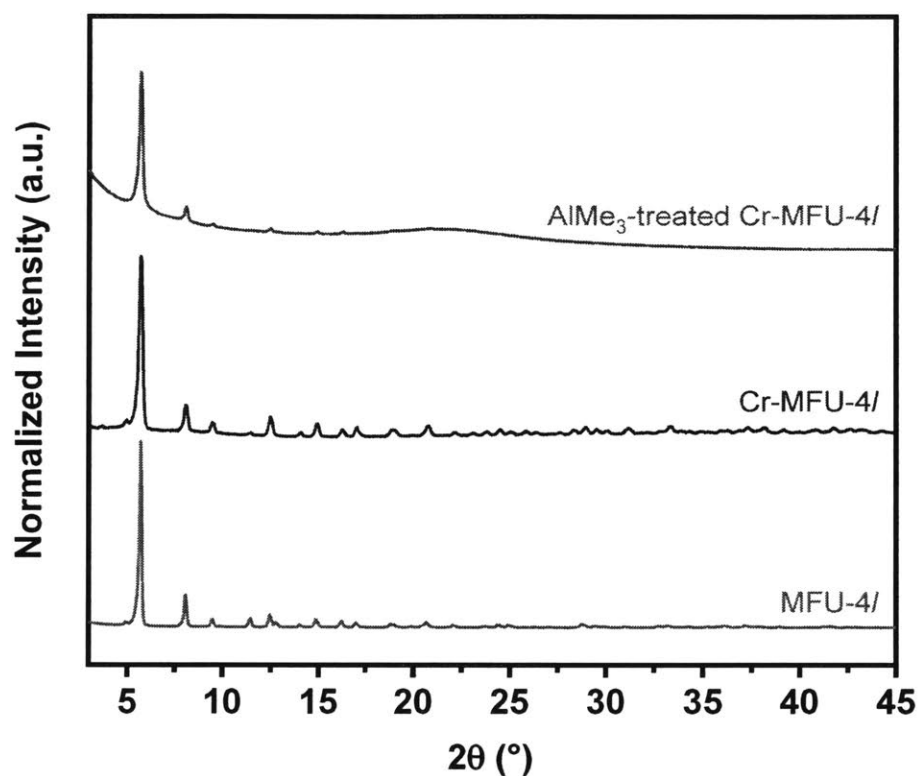
Figure 5.S1. PXRD patterns of MFU-4*l*, Cr-MFU-4*l* and AlMe₃-treated MFU-4*l*. MFU-4*l* and Cr-MFU-4*l* samples were prepared by placing a thin layer of the appropriate material on a zero-background silicon crystal plate whereas the AlMe₃-treated Cr-MFU-4*l* sample was prepared by placing a small amount of material within a sealed polyimide capillary tube under an inert atmosphere.
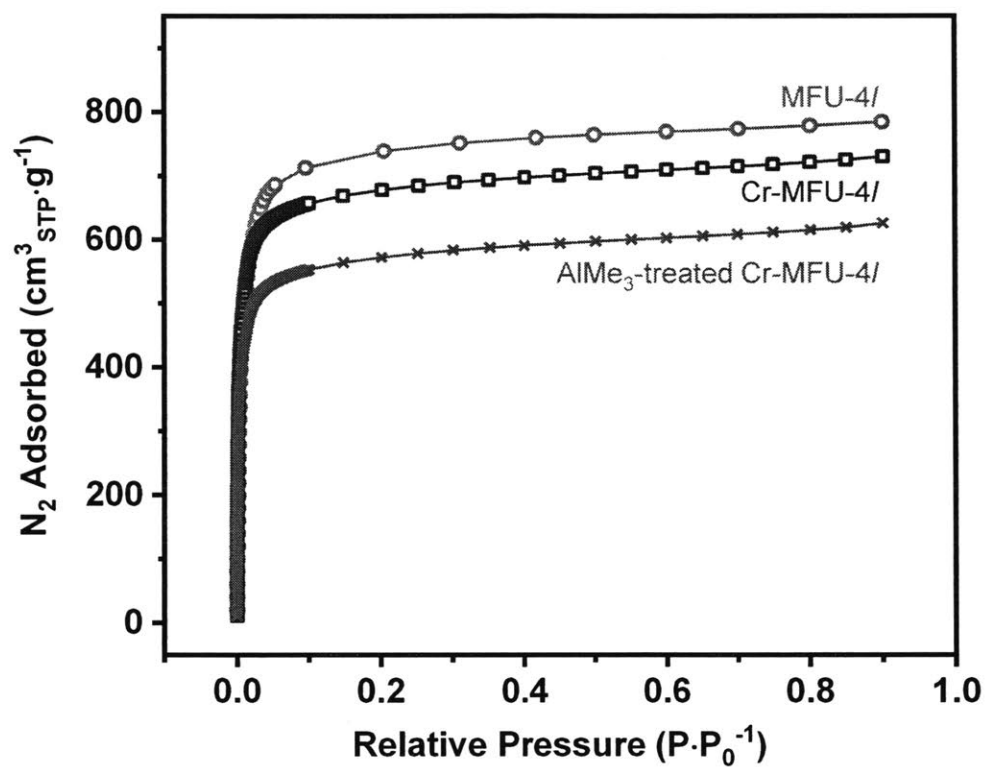
Figure 5.S2. Nitrogen adsorption isotherms of MFU-4*l*, Cr-MFU-4*l* and AlMe₃-treated MFU-4*l* after outgassing under vacuum (10⁻⁵ torr) for 18 h. Calculated BET surface areas for MFU-4*l*, Cr-MFU-4*l* and AlMe₃-treated MFU-4*l* were 3,150 ± 20 m²/g, 2,830 ± 10 m²/g, and 2,360 ± 4 m²/g, respectively.
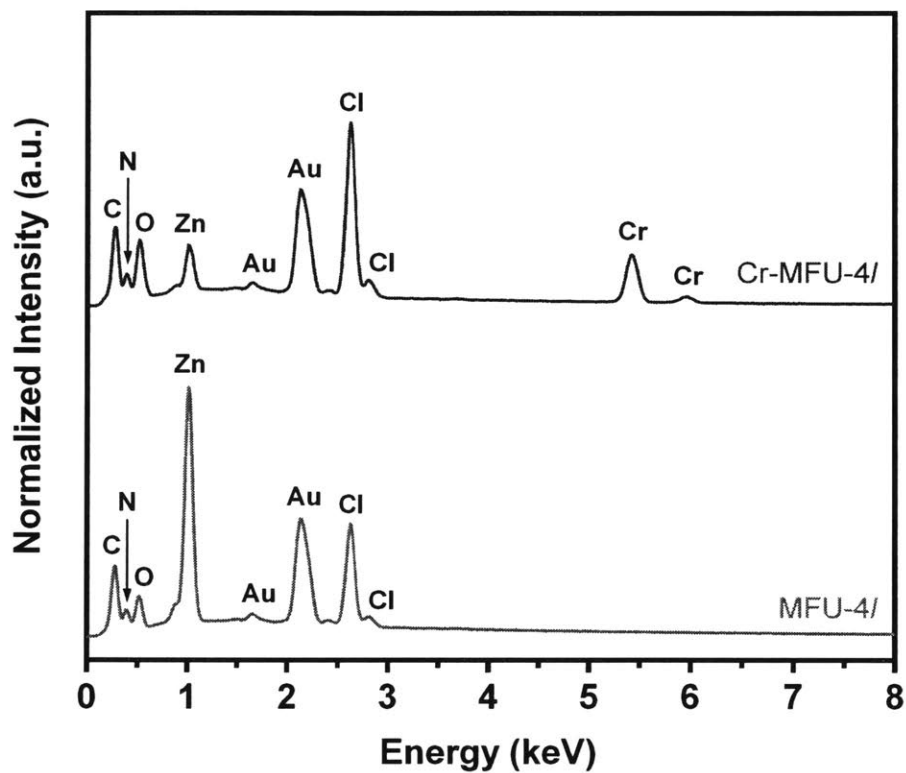
Figure 5.S3. EDX spectra of MFU-4*l* and Cr-MFU-4*l*. Both samples were subjected to identical Au sputtering procedure prior to analysis to avoid charging effects. Acquired EDX intensities were normalized with respect to the Au Mα signal at 2.12 keV.

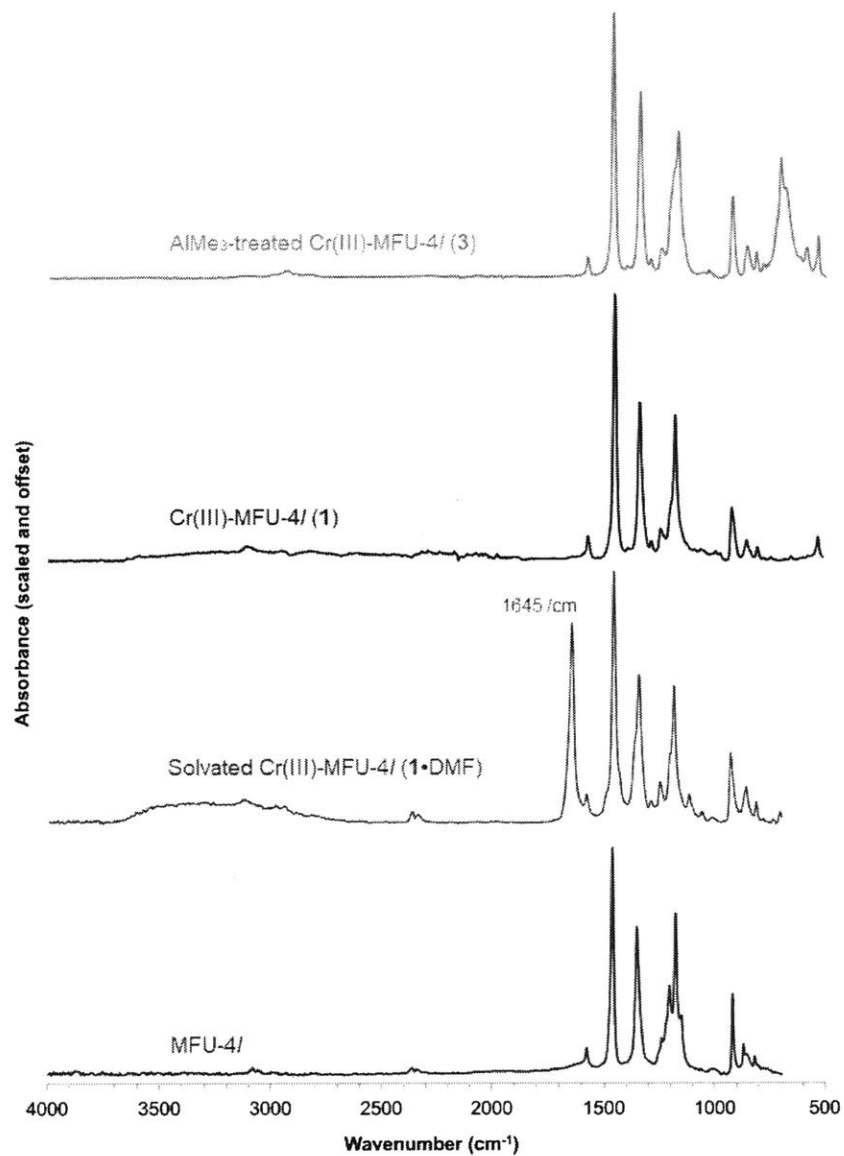**Figure 5.S4.** ATR-IR spectra of MFU-4*l*, DMF-solvated Cr(III)-MFU-4*l* (1•DMF), Cr(III)-MFU-4*l* (1), and AlMe$_3$-treated Cr(III)-MFU-4*l* (3). 1 and 3 were analyzed on a diamond tip ATR in a nitrogen glovebox. 1•DMF and MFU-4*l* were analyzed on a Ge ATR exposed to ambient air.
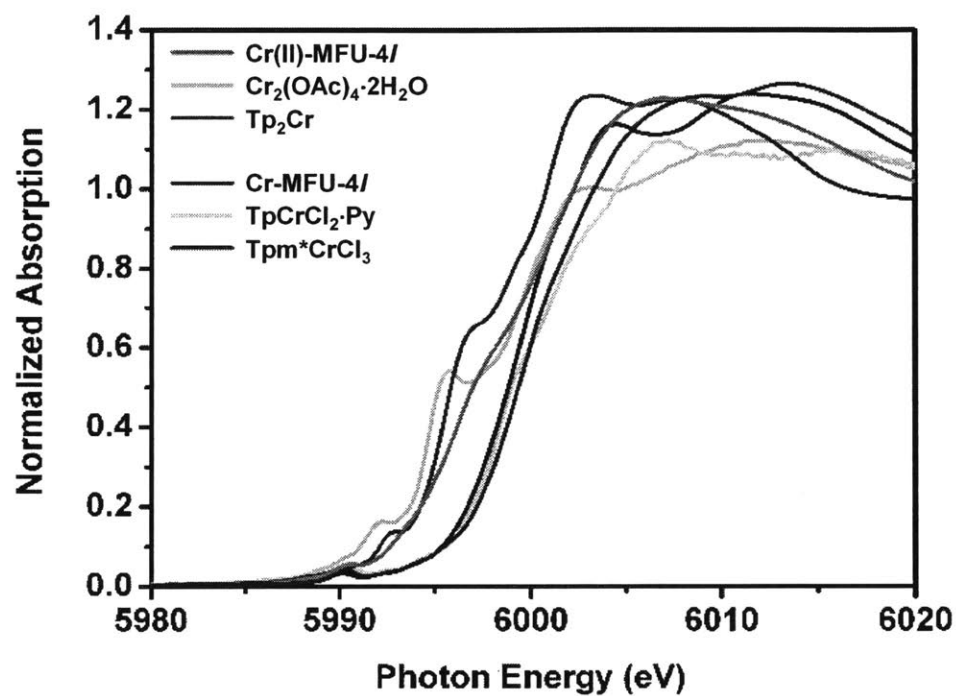
Figure 5.S5. X-ray absorption spectra of Cr-MFU-4*l* and relevant standards. Cr(II)-MFU-4*l* was prepared via cation-exchange from MFU-4*l* using CrCl₂.
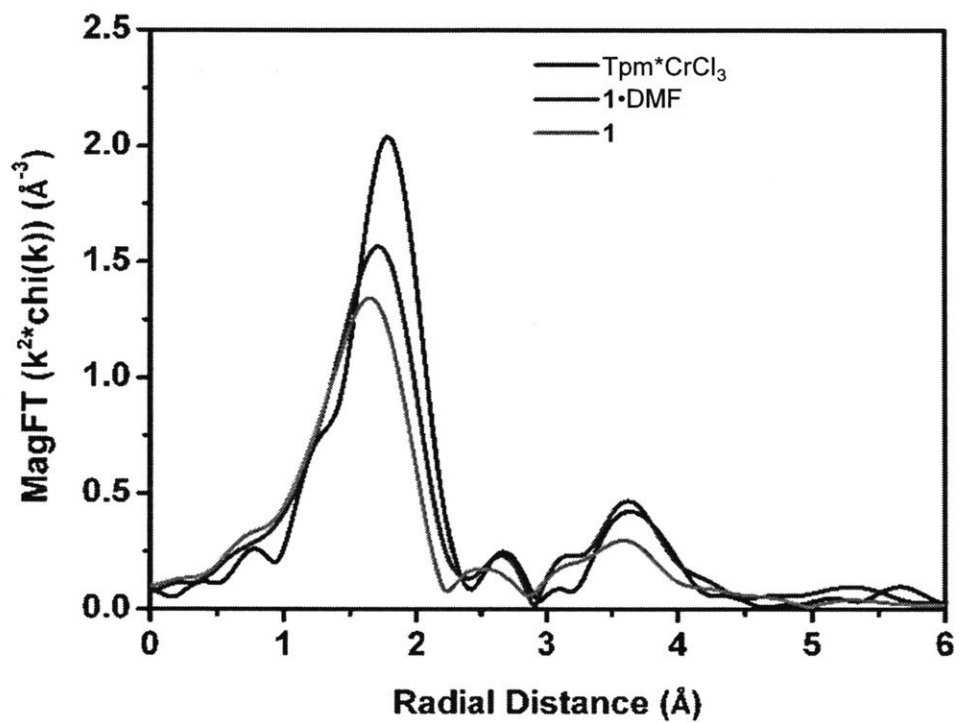
Figure 5.S6. EXAFS plots of Tpm*CrCl$_3$, DMF-solvated Cr(III)-MFU-4*l* (1·DMF), and desolvated Cr(III)-MFU-4*l* (1).
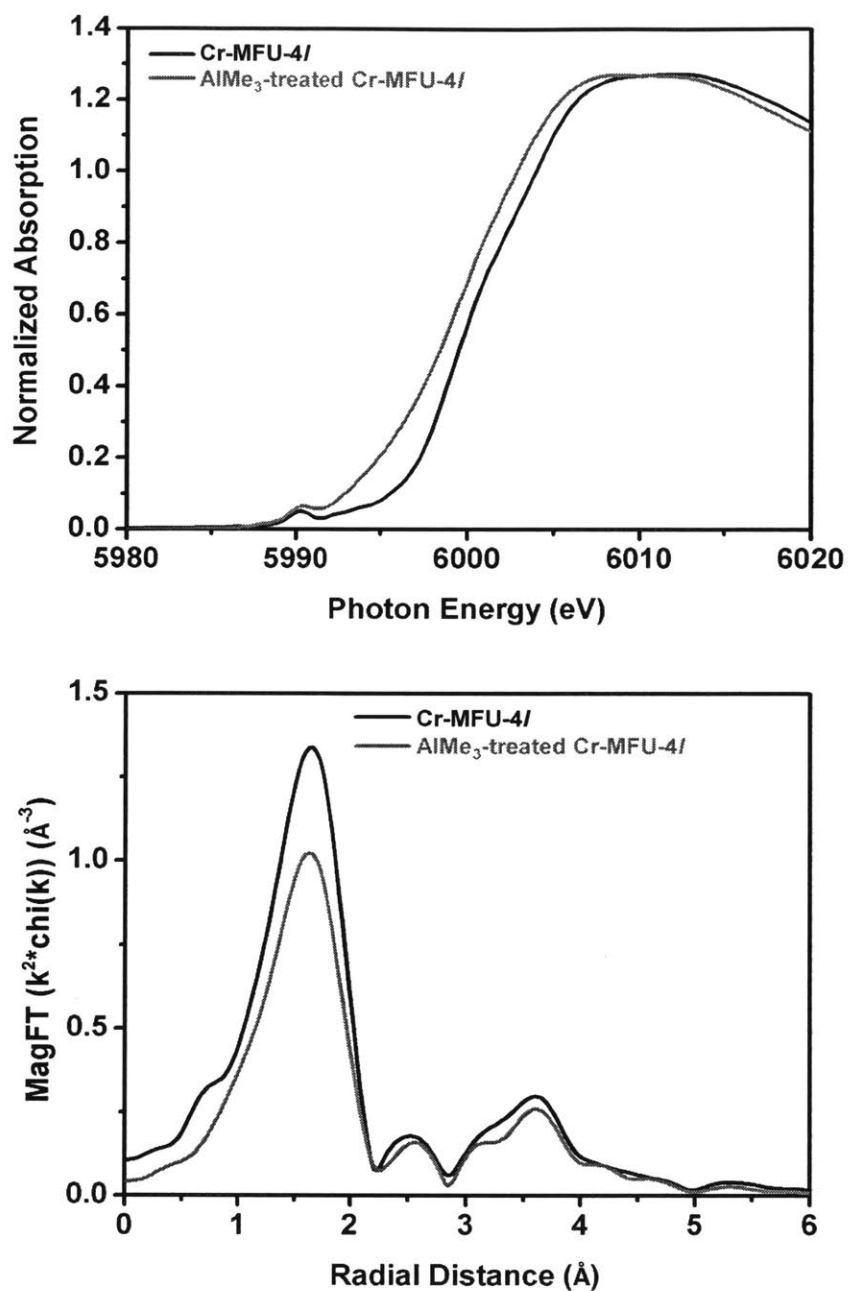
Figure 5.S7. XAS (Top) and EXAFS (Bottom) analyses of Cr-MFU-4*l* and AlMe₃-treated Cr-MFU-4*l*. The edge energy value, as defined by the inflection point of the leading edge, was 5999.5 eV for both samples.
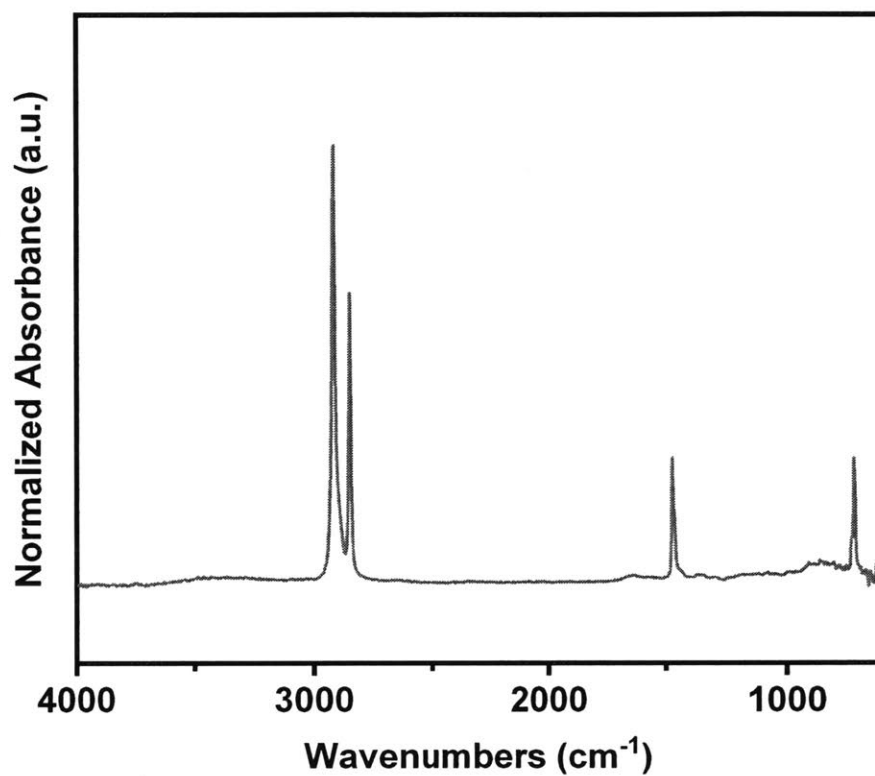
Figure 5.S8. Attenuated total reflectance infrared spectroscopy analysis of the solid product from a gas phase ethylene polymerization reaction with AlMe$_3$-treated Cr-MFU-4l (Table 5.2, entry 1). Characteristic polyethylene bands at 2920 cm^{-1}, 2850 cm^{-1}, 1470 cm^{-1}, 1460 cm^{-1}, 730 cm^{-1}, and 720 cm^{-1} are clearly present.[55]

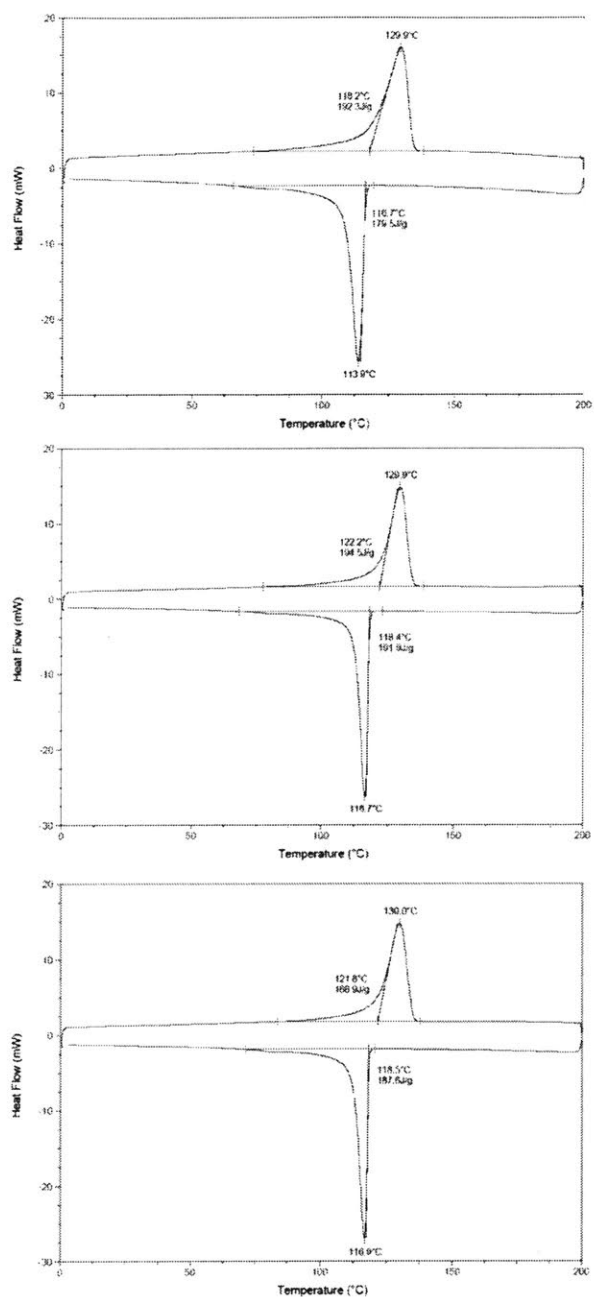**Figure 5.S9.** Second heat-cool scan from differential scanning calorimetry analysis of polyethylene products from ethylene polymerization reactions with AlMe$_3$-treated Cr-MFU-4l (top), Cr-MFU-4l and AlMe$_3$ in toluene (middle), and Cr-MFU-4l and AlMe$_3$ in toluene at 35 °C (bottom). Percent crystallinities of samples were derived using 293 J/g as a theoretical heat of fusion for polyethylene with 100% crystallinity.[56]
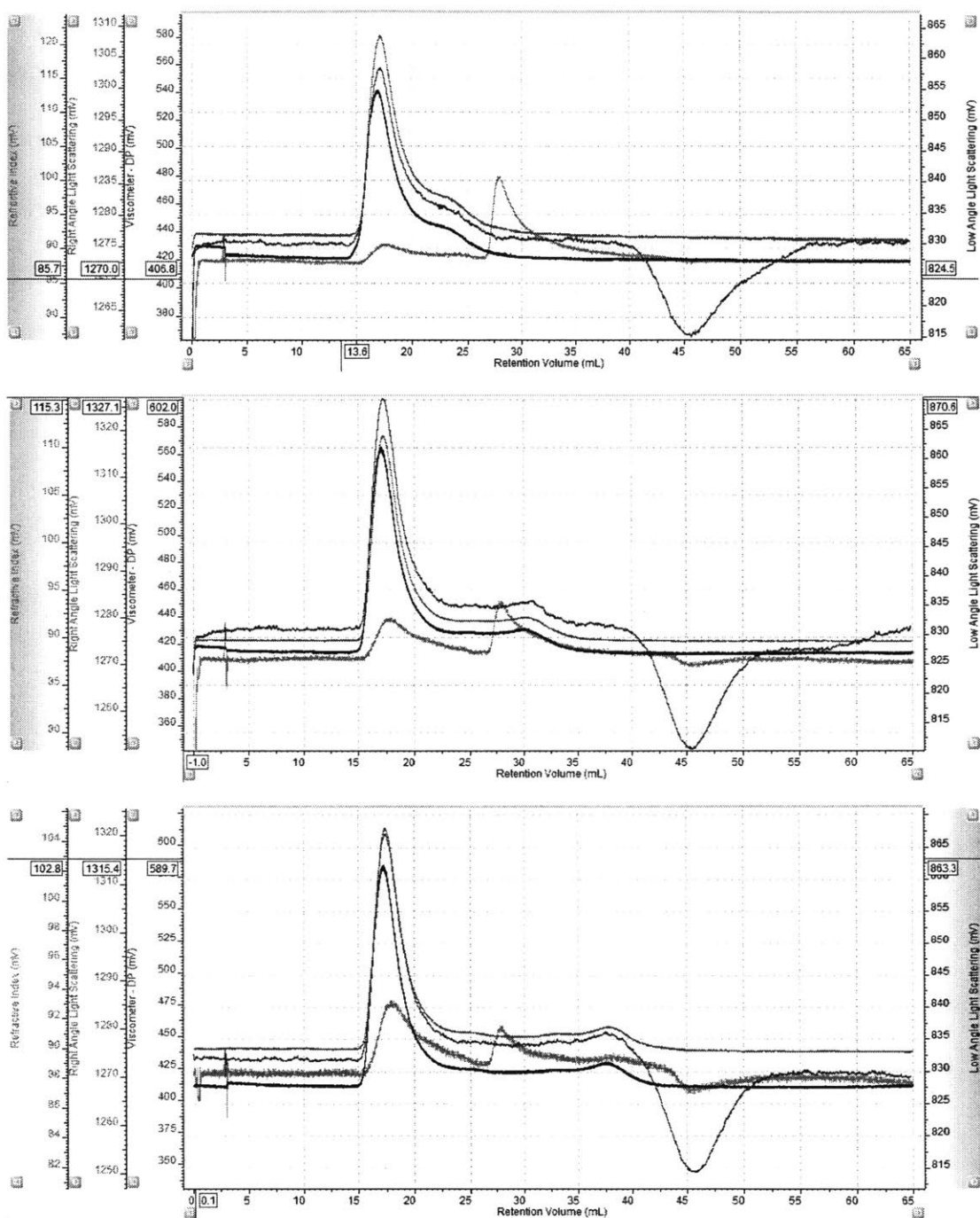
Figure 5.S10. HT-GPC chromatograms from analyses of product polyethylenes obtained from gas phase reaction of AlMe$_3$-treated Cr(III)-MFU-4*l* (top, table 5.2 entry 1), slurry phase reaction of Cr(III)-MFU-4*l* and excess AlMe$_3$ (middle, table 5.2 entry 2), and slurry phase reaction of Cr(III)-MFU-4*l* and excess AlMe$_3$ at 35 °C (bottom, table 5.2 entry 5).
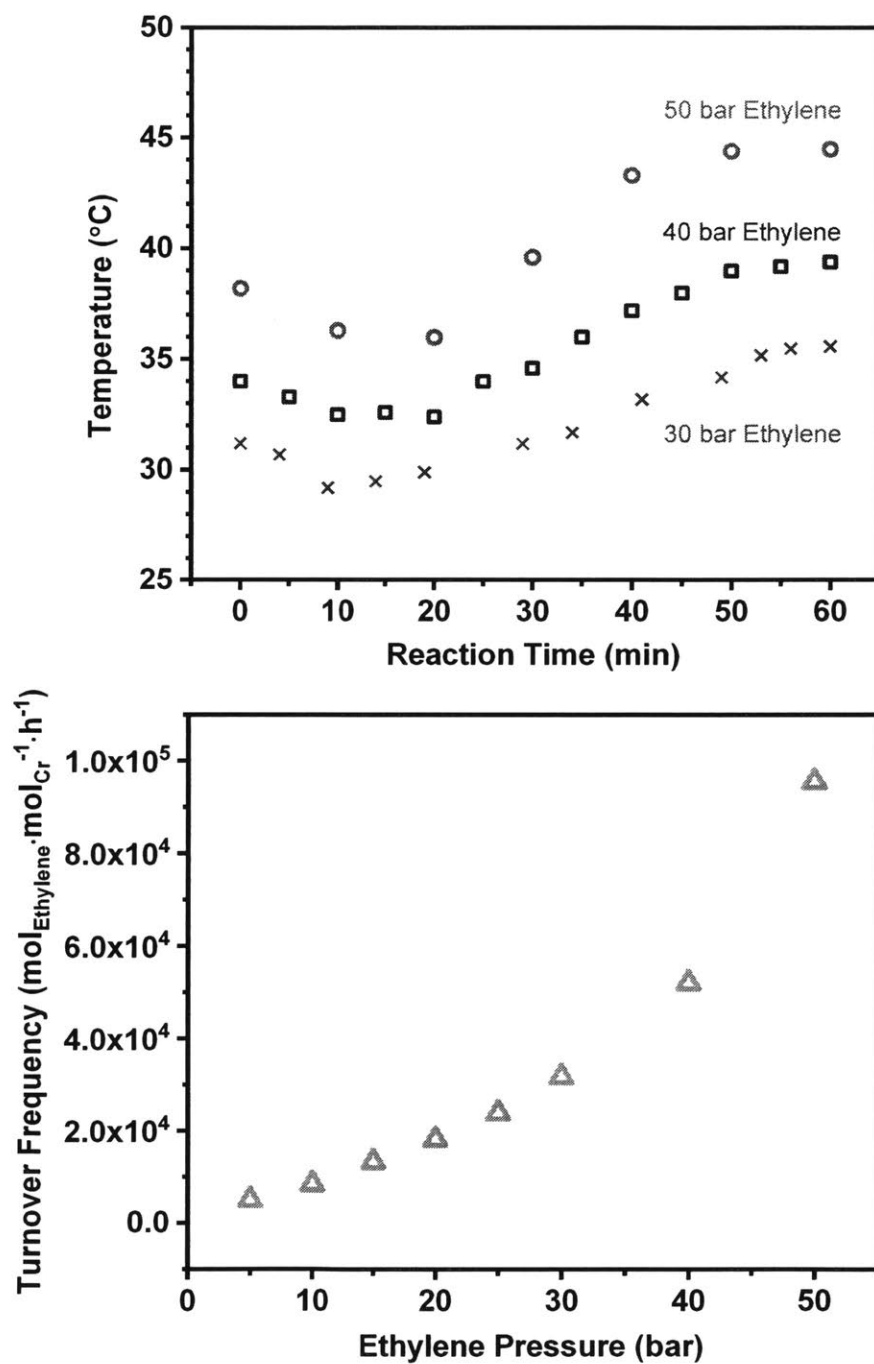
Figure 5.S11. Reactor temperature as a function of reaction time (top) and polymerization activity as a function of ethylene pressure (bottom) for gas phase ethylene polymerization reactions with AlMe$_3$-treated Cr-MFU-4l at various ethylene pressures.

Table 5.S1. ICP-MS Analyses of MFU-4*l*, Cr-MFU-4*l*, and AlMe₃-treated Cr-MFU-4*l*.[a]

Sample	Zn	Cr	Al
MFU-4*l*	5.0	Not detected	Not detected
Cr-MFU-4*l*	1.12	3.88	Not detected
AlMe₃-treated Cr-MFU-4*l*	1.15	3.85	6.84

[a] Relative metal ratios for Zn and Cr normalized to add up to 5.0, as each node of MFU-4*l* contains 5 metal sites.

5.7. References

(1)   Karol, F. J. Catalysis and the UNIPOL® Process in the 1990's. *Macromol. Symp.* **1995**, *89*, 563–575.

(2)   Xie, T.; McAuley, K. B.; Hsu, J. C. C.; Bacon, D. W. Gas Phase Ethylene Polymerization: Production Processes, Polymer Properties, and Reactor Modeling. *Ind. Eng. Chem. Res.* **1994**, *33*, 449–479.

(3)   Whiteley, K. S. Polyethylene. in *Ullmann's Encyclopedia of Industrial Chemistry*; Elvers, B., Ed.; Wiley-VCH: Weinheim, 2012; Vol. 29, pp 1–38.

(4)   Hlatky, G. G. Heterogeneous Single-Site Catalysts for Olefin Polymerization. *Chem. Rev.* **2000**, *100*, 1347–1376.

(5)   Harrison, D.; Coulter, I. M.; Wang, S.; Nistala, S.; Kuntz, B. A.; Pigeon, M.; Tian, J.; Collins, S. Olefin Polymerization Using Supported Metallocene Catalysts: Development of High Activity Catalysts for Use in Slurry and Gas Phase Ethylene Polymerizations. *J. Mol. Catal. A Chem.* **1998**, *128*, 65–77.

(6)   Stalzer, M. M.; Delferro, M.; Marks, T. J. Supported Single-Site Organometallic Catalysts for the Synthesis of High-Performance Polyolefins. *Catal. Letters* **2015**, *145*, 3–14.

(7)   Kumkaew, P.; Wanke, S. E.; Praserthdam, P.; Danumah, C.; Kaliaguine, S. Gas-Phase Ethylene Polymerization Using Zirconocene Supported on Mesoporous Molecular Sieves. *J. Appl. Polym. Sci.* **2003**, *87*, 1161–1177.

(8)   Kim, S. H.; Somorjai, G. A. Surface Science of Single-Site Heterogeneous Olefin Polymerization Catalysts. *Proc. Natl. Acad. Sci.* **2006**, *103*, 15289–15294.

(9)   Copéret, C.; Allouche, F.; Chan, K. W.; Conley, M. P.; Delley, M. F.; Fedorov, A.; Moroz, I. B.; Mougel, V.; Pucino, M.; Searles, K.; Yamamoto, K.; Zhizhko, P. A. Bridging the Gap Between Industrial and Well-Defined Supported Catalysts. *Angew. Chem. Int. Ed.* **2018**, *57*, 2–45.

(10) Severn, J. R.; Chadwick, J. C.; Duchateau, R.; Friederichs, N. "Bound but Not Gagged" - Immobilizing Single-Site α-Olefin Polymerization Catalysts. *Chem. Rev.* **2005**, *105*, 4073–4147.

(11) Copéret, C.; Comas-Vives, A.; Conley, M. P.; Estes, D. P.; Fedorov, A.; Mougel, V.; Nagae, H.; Núñez-Zarur, F.; Zhizhko, P. A. Surface Organometallic and Coordination Chemistry toward Single-Site Heterogeneous Catalysts: Strategies, Methods, Structures, and Activities. *Chem. Rev.* **2016**, *116*, 323–421.

(12) Severn, J. R.; Chadwick, J. C. Immobilisation of Homogeneous Olefin Polymerisation Catalysts. Factors Influencing Activity and Stability. *Dalt. Trans.* **2013**, *42*, 8979–8987.

(13) McDaniel, M. P. A Review of the Phillips Supported Chromium Catalyst and Its

Commercial Use for Ethylene Polymerization. In *Advances in Catalysis*; Gates, B. C. and Knözinger, H. Eds.; Elsevier Inc.: Oxford, 2010; Vol. 53; pp 123–606.

(14) Yaghi, O. M.; Kalmutzki, M. J.; Diercks, C. S. *Introduction to Reticular Chemistry*; Wiley-VCH: Weinheim, 2019.

(15) Song, Y.; Li, Z.; Ji, P.; Kaufmann, M.; Feng, X.; Chen, J. S.; Wang, C.; Lin, W. Metal–Organic Framework Nodes Support Single-Site Nickel(II) Hydride Catalysts for the Hydrogenolysis of Aryl Ethers. *ACS Catal.* **2019**, *9*, 1578–1583.

(16) Otake, K.; Ye, J.; Mandal, M.; Islamoglu, T.; Buru, C. T.; Hupp, J. T.; Delferro, M.; Truhlar, D. G.; Cramer, C. J.; Farha, O. K. Enhanced Activity of Heterogeneous Pd(II) Catalysts on Acid-Functionalized Metal–Organic Frameworks. *ACS Catal.* **2019**, *9*, 5383–5390.

(17) Park, H. D.; Dincă, M.; Román-Leshkov, Y. Continuous-Flow Production of Succinic Anhydrides via Catalytic β-Lactone Carbonylation by $Co(CO)_4 \subset Cr$-MIL-101. *J. Am. Chem. Soc.* **2018**, *140*, 10669–10672.

(18) Yuan, S.; Qin, J.; Xu, H.; Su, J.; Rossi, D.; Chen, Y.; Zhang, L.; Lollar, C.; Wang, Q.; Jiang, H.; Son, D. H.; Xu, H.; Huang, Z.; Zou, X.; Zhou, H. $[Ti_8Zr_2O_{12}(COO)_{16}]$ Cluster: An Ideal Inorganic Building Unit for Photoactive Metal–Organic Frameworks. *ACS Cent. Sci.* **2018**, *4*, 105–111.

(19) Ji, P.; Drake, T.; Murakami, A.; Oliveres, P.; Skone, J. H.; Lin, W. Tuning Lewis Acidity of Metal–Organic Frameworks via Perfluorination of Bridging Ligands: Spectroscopic, Theoretical, and Catalytic Studies. *J. Am. Chem. Soc.* **2018**, *140*, 10553–10561.

(20) Kalmutzki, M. J.; Hanikel, N.; Yaghi, O. M. Secondary Building Units as the Turning Point in the Development of the Reticular Chemistry of MOFs. *Sci. Adv.* **2018**, *4*, eaat9180.

(21) Vitillo, J. G.; Bhan, A.; Cramer, C. J.; Lu, C. C.; Gagliardi, L. Quantum Chemical Characterization of Structural Single Fe(II) Sites in MIL-Type Metal–Organic Frameworks for the Oxidation of Methane to Methanol and Ethane to Ethanol. *ACS Catal.* **2019**, *9*, 2870–2879.

(22) Denysenko, D.; Jelic, J.; Reuter, K.; Volkmer, D. Postsynthetic Metal and Ligand Exchange in MFU-4*l*: A Screening Approach toward Functional Metal–Organic Frameworks Comprising Single-Site Active Centers. *Chem. Eur. J.* **2015**, *21*, 8188–8199.

(23) Park, H. D.; Dincă, M.; Román-Leshkov, Y. Heterogeneous Epoxide Carbonylation by Cooperative Ion-Pair Catalysis in $Co(CO)_4^-$-Incorporated Cr-MIL-101. *ACS Cent. Sci.* **2017**, *3*, 444–448.

(24) Rivera-Torrente, M.; Pletcher, P. D.; Jongkind, M. K.; Nikolopoulos, N.; Weckhuysen, B. M. Ethylene Polymerization Over Metal–Organic Framework Crystallites and the Influence of Linkers on Their Fracturing Process. *ACS Catal.*

2019, 9, 3059–3069.

(25) Ji, P.; Solomon, J. B.; Lin, Z.; Johnson, A.; Jordan, R. F.; Lin, W. Transformation of Metal–Organic Framework Secondary Building Units into Hexanuclear Zr–Alkyl Catalysts for Ethylene Polymerization. *J. Am. Chem. Soc.* **2017**, *139*, 11325–11328.

(26) Denysenko, D.; Grzywa, M.; Jelic, J.; Reuter, K.; Volkmer, D. Scorpionate-Type Coordination in MFU-4*l* Metal–Organic Frameworks: Small-Molecule Binding and Activation upon the Thermally Activated Formation of Open Metal Sites. *Angew. Chem. Int. Ed.* **2014**, *53*, 5832–5836.

(27) Denysenko, D.; Werner, T.; Grzywa, M.; Puls, A.; Hagen, V.; Eickerling, G.; Jelic, J.; Reuter, K.; Volkmer, D. Reversible Gas-Phase Redox Processes Catalyzed by Co-Exchanged MFU-4*l*(arge). *Chem. Commun.* **2012**, *48*, 1236–1238.

(28) Brozek, C. K.; Bellarosa, L.; Soejima, T.; Clark, T. V.; López, N.; Dincă, M. Solvent-Dependent Cation Exchange in Metal–Organic Frameworks. *Chem. Eur. J.* **2014**, *20*, 6871–6874.

(29) Comito, R. J.; Fritzsching, K. J.; Sundell, B. J.; Schmidt-Rohr, K.; Dincă, M. Single-Site Heterogeneous Catalysts for Olefin Polymerization Enabled by Cation Exchange in a Metal–Organic Framework. *J. Am. Chem. Soc.* **2016**, *138*, 10232–10237.

(30) Dubey, R. J. C.; Comito, R. J.; Wu, Z.; Zhang, G.; Rieth, A. J.; Hendon, C. H.; Miller, J. T.; Dincă, M. Highly Stereoselective Heterogeneous Diene Polymerization by Co-MFU-4*l*: A Single-Site Catalyst Prepared by Cation Exchange. *J. Am. Chem. Soc.* **2017**, *139*, 12664–12669.

(31) Comito, R.; Wu, Z.; Zhang, G.; Lawrence, J.; Korzyński, M.; Kehl, J. A.; Miller, J.; Dincă, M. Stabilized Vanadium Catalyst for Olefin Polymerization by Site Isolation in a Metal–Organic Framework. *Angew. Chem. Int. Ed.* **2018**, *57*, 1–6.

(32) Rojas, R.; Valderrama, M.; Wu, G. Synthesis, Structural Characterization and Ethylene Polymerization Behavior of Complex [Ph$_4$P][CrCl$_3$\{HB(pz)$_3$\}] [HB(pz)$_3$ = Hydrotris(1-pyrazolyl)Borate]. *Inorg. Chem. Commun.* **2004**, *7*, 1295–1297.

(33) García-Orozco, I.; Quijada, R.; Vera, K.; Valderrama, M. Tris(pyrazolyl)methane-chromium(III) Complexes as Highly Active Catalysts for Ethylene Polymerization. *J. Mol. Catal. A: Chem.* **2006**, *260*, 70–76.

(34) Comito, R. J.; Metzger, E. D.; Wu, Z.; Zhang, G.; Hendon, C. H.; Miller, J. T.; Dincă, M. Selective Dimerization of Propylene with Ni-MFU-4*l*. *Organometallics* **2017**, *36*, 1681–1683.

(35) Our DFT model treats **1**·DMF as having three nitrogen, two chlorine, and one oxygen atom in the primary coordination sphere of chromium as a result of DMF coordination. However, it is very difficult to distinguish nitrogen and oxygen scattering points by our EXAFS method so we treated these elements as the same for the sake of simplicity. A reasonably good fit is still obtained despite this assumption.

(36) Kersten, J. L.; Kucharczyk, R. R.; Yap, G. P. A.; Rheingold, A. L.; Theopold, K. H. [(Tp$^{(tBu,Me)}$)CrR]: A New Class of Mononuclear, Coordinatively Unsaturated Chromium(II) Alkyls with *cis*-Divacant Octahedral Structure. *Chem. Eur. J.* **1997**, *3*, 1668–1674.

(37) Nagel, E. J.; Kirillov, V. A.; Ray, W. H. Prediction of Molecular Weight Distributions for High-Density Polyolefins. *Ind. Eng. Chem. Prod. Res. Dev.* **1980**, *19*, 372–379.

(38) Bhagwat, M. S.; Bhagwat, S. S.; Sharma, M. M. Mathematical Modeling of the Slurry Polymerization of Ethylene: Gas-Liquid Mass Transfer Limitations. *Ind. Eng. Chem. Res.* **1994**, *33*, 2322–2330.

(39) Klet, R. C.; Tussupbayev, S.; Borycz, J.; Gallagher, J. R.; Stalzer, M. M.; Miller, J. T.; Gagliardi, L.; Hupp, J. T.; Marks, T. J.; Cramer, C. J.; Delferro, M.; Farha, O. K. Single-Site Organozirconium Catalyst Embedded in a Metal–Organic Framework. *J. Am. Chem. Soc.* **2015**, *137*, 15680–15683.

(40) Metzger, E. D.; Comito, R. J.; Wu, Z.; Zhang, G.; Dubey, R. C.; Xu, W.; Miller, J. T.; Dincă, M. Highly Selective Heterogeneous Ethylene Dimerization with a Scalable and Chemically Robust MOF Catalyst. *ACS Sustain. Chem. Eng.* **2019**, *7*, 6654–6661.

(41) Ravel, B.; Newville, M. *J. Synchrotron Radiat.* **2005**, *12*, 537–541.

(42) Denysenko, D.; Grzywa, M.; Tonigold, M.; Streppel, B.; Krkljus, I.; Hirscher, M.; Mugnaioli, E.; Kolb, U.; Hanss, J.; Volkmer, D. *Chem. Eur. J.* **2011**, *17*, 1837–1848.

(43) Abrams, M. J.; Faggiani, R.; Lock, C. S. *Inorganica Chim. Acta* **1985**, *106*, 69–74.

(44) Toshida, T.; Yamamoto, T.; Okada, H.; Murakita, H. Catalyst for Trimerization of Ethylene and Process for Trimerizing Ethylene Using the Catalyst. US6900152, May 31, 2005.

(45) Jolly, W. *The Synthesis and Characterization of Inorganic Compounds*; Prentice Hall: Englewood Ciffs, NJ, 1970. p 443.

(46) Reported: λ_{max} = 410 nm and 568 nm in Vargas-Vasquez, S; Romero-Zerón, L. B.; MacMillan, B. *Chem. Eng. Comm.* **2010**, *197*, 491–505.

(47) Chatelet, M. *Compt. Rend.* **1934**, *199*, 290.

(48) Lux, H.; Eberle, L.; Sarre, D. *Chem. Ber.* **1964**, *97*, 503–509.

(49) Hohenberg, P.; Kohn, W. *Phys. Rev.* **1964**, *136*, B864–B871.

(50) Kohn, W.; Sham, L. J. *Phys. Rev.* **1965**, *140*, A1133–A1138.

(51) Shao Y. et al. *Mol. Phys.* **2015**, *113*, 184–215.

(52) Perdue, J.; Burke, K.; Ernzerhof, M. *Phys. Rev. Lett.* **1996**, *77*, 3865.

(53) Ditchfield, R.; Hehre, W. J.; Pople, J. A. *J. Chem. Phys.* **1971**, *54*, 724–728.

(54) Hehre, W. J.; Ditchfield, R.; Pople, J. a. *J. Chem. Phys.* **1972**, *56*, 2257–2261.

(55) Krimm, S.; Liang, C. Y.; Sutherland, G. B. B. M. *J. Chem. Phys.* 1956, 25, 549–562.

(56) Mathot, V. B. F.; Pijpers, M. F. J. *J. Therm. Anal.* 1983, 28, 349–358.